ANGULAR CORRELATIONS OF PROMPT GAMMA-RAYS FROM THE SPONTANEOUS FISSION OF ^{252}Cf

By

Christopher Goodin

Dissertation

Submitted to the Faculty of the

Graduate School of Vanderbilt University

in partial fulfillment of the requirements

for the degree of

DOCTOR OF PHILOSOPHY

in

Physics

August 2008

Nashville, Tennessee

Approved:

Professor Joseph H. Hamilton

Professor Akunuri V. Ramayya

Professor Volker E. Oberacker

Professor Thomas W. Kephart

Professor Robert A. Weller

DEDICATION

To Katy

ACKNOWLEDGMENTS

It has been an honor and a pleasure to work under the direction of Professor Hamilton and Professor Ramayya, who have taught me so much. They have been my advisors in the truest sense.

I would like to thank those individuals at Oak Ridge National Laboratory who have taken the time from their demanding schedules to teach me and assist me in my research. I would especially like to thank Ken Carter and Dan Stracener for giving me the opportunity to have hands on experience with ion sources, and Krzysztof Rykaczewski, Jon Batchelder, and Sean Liddick for their lessons in nuclear spectroscopy.

Nick and Jirina Stone have provided me with essential help in conducting the research presented in this work. Nick has freely shared with me his many years of experience in measuring g-factors, and Jirina has done the same with her encyclopedic knowledge of nuclear models.

I would also like to acknowledge the work of Andrey Daniel in helping develop the software used for the analysis presented in this thesis.

Finally, I would like to thank my wife Katy for her love and support. She has been there for me at every step.

TABLE OF CONTENTS

LIST OF TABLES

LIST OF FIGURES

CHAPTER I

INTRODUCTION

1.1 The structure of neutron rich nuclei

The ground state properties of stable nuclei with N or Z near a spherical closed shell are well understood from the spherical shell model [1]. The shell model prediction of closed shells at N,Z=2, 8, 20, 28, 50, 82 is confirmed experimentally in these nuclei. The order and spacing of the single-particle states of protons and neutrons near spherical closed shells of stable nuclei are well reproduced in modern shell model calculations. Nuclei with N and Z well removed from the spherical closed shells take on a deformed shape [2].

Neutron rich nuclei may be spherical or deformed, with the latter case leading to a reordering of the single particle states. This reordering can sometimes lead to the appearance of new closed shells [3], differing from those predicted by the spherical shell model. Neutron rich nuclei can also take on exotic shapes, such as octupole deformed or triaxial. One of the most exciting recent developments in nuclear physics is the discovery of nuclear chirality, or mirror symmetry, which will be discussed in this work for neutron rich ruthenium isotopes.

Studies of the prompt gamma-rays emitted by the neutron rich fragments produced in spontaneous or induced fission have yielded many new insights over the years [4]. In particular, the neutron rich nuclei populated in the spontaneous fission of ^{252}Cf range from the superdeformed doubly closed subshell at Z=38, N=60,62 to

the spherical double shell closure at ^{132}Sn shell closure, to the region of octupole deformation around Z=56, N=88 ^{144}Ba, and to the deformed midshell Nd and Sm nuclei. Therefore, the study of these nuclei allows access to a wide range of nuclear properties such as shape-coexistence, nuclear shell structure, and rotation-vibration interactions. Furthermore, fission fragments are often highly excited and allow the study of these nuclei at high spin and excitation energy. The nuclei discussed in this work are studied by using the angular correlations between the radiation emitted from excited states. These angular correlations between gamma-rays can give information about the spins of nuclear excited states, as well as the multipolarities of the emitted radiations. These transition multipolarities can be used to infer the parities of the nuclear states. Information on spins of nuclear levels is critical in extracting the nature of the single particle levels and of collective bands in deformed nuclei. For the experiment discussed in this work, the angular correlations can also be used to measure the g-factors of certain excited states.

1.2 The Magnetic Properties of the Nucleus

The most accessible magnetic property of a nucleus is its' dipole moment. The scale of nuclear magnetism is the nuclear magneton, μ_N=0.315 MeV/T. An MeV is a relatively small amount of energy in macroscopic terms, and a Tesla is a very large unit of magnetic field. Therefore, the magnetic moment of a nucleus is very small and quite difficult to measure directly. A very strong magnetic field is required to produce a measurable interaction with a nucleus. In this work, the magnetic field used to probe the nucleus is the hyperfine field of an iron lattice. This interaction

will be discussed in detail in the "Method" section.

A dimensionless quantity which is often used to compare the magnetic moments of different excited states in the nucleus is the g-factor, defined by

$$g = \frac{\mu}{\mu_N I} \tag{1.1}$$

where I is the spin of the nuclear state and μ is the magnetic moment of the nucleus. The g-factors of excited states are measured for many neutron rich fission fragments in this work. Depending on the type of nucleus, there are several different models which can be used to calculate g-factors, and the applicability of each model to the particular cases measured in this work will be discussed.

The magnetic dipole moment of a nucleus can be seen as having two distinct contributions. One is the motion of charge within the nucleus. This can be understood in the classical sense as being similar to the magnetic moment of a current carrying loop of wire. The second contribution comes from the intrinsic magnetic moment of each nucleon related to its intrinsic spin motion. This is sometimes called the spin magnetic moment, and it has no classical analog. Both these contributions can be taken into account in the shell model by the equation [5]

$$\vec{\mu} = \mu_N \sum_{k=1}^{A} (\vec{g}_k^{(l)} \mathbf{l_k} + \vec{g}_k^{(s)} \mathbf{s_k}) \tag{1.2}$$

where the g$^(l, s)$'s for a proton (p) and neutron (n) are

$$g_p^{(l)} = 1,\ g_n^{(l)} = 0,\ g_p^{(s)} = 5.586,\ g_n^{(s)} = -3.826 \tag{1.3}$$

The g^l factors take into account the motion of charge, while the g^s factors account for the contribution of the intrinsic magnetic moment of each particle. This equation is not practically useful for predicting the g-factors of excited states in heavy nuclei because the shell model neglects the important effects caused by the interaction between nucleons. This difficulty gives an indication as to why it is important to study g-factors; they give information not only about the single-particle and collective behavior of a nucleus, but also about the interaction between nucleons. Nuclear g-factors can be measured by studying the perturbation of angular correlations of gamma-rays emitted by nuclei which are experiencing strong magnetic fields. Methods for predicting and interpreting g-factors, as well as other nuclear properties, are discussed in the next chapter.

CHAPTER II

THEORETICAL MODELS

2.1 Collective models

The properties of even-even nuclei well removed from closed shells are in general related to the coherent motion of the nucleons. The simplest form of collective motion is rotational motion, where the coherent motion of the nucleons in a deformed potential gives rise to a band with energies

$$E(I) = I(I+1)\frac{\hbar^2}{2J} \tag{2.1}$$

where I is the angular momentum of each state and J is the moment of inertia of the nucleus. In this model, known as the rigid rotor model, the g-factors of the rotational states are simply g=Z/A where Z is the number of protons and A is the number of total nucleons. Most of the states in rotational even-even nuclei measured in this work agree with this simple estimate. However, for some measurements in this work and for past measurements, a downward deviation from g=Z/A has been observed. This has been explained as the result of non-coherent motion from the protons and neutrons in the nucleus. Specifically, if the protons and neutrons have different deformations, then the g-factor of a rotational state is lowered by a correction factor, f, given by [6]

$$g = \frac{Z}{A}(1-2f) \tag{2.2}$$

where f is defined as

$$f = \frac{\beta_2 - \beta_2(p)}{\beta_2} = 1 - \frac{A}{N\frac{\beta_2(n)}{\beta_2(p)} + Z} \tag{2.3}$$

and β_2, $\beta_2(p)$, and $\beta_2(n)$ are the nuclear, proton, and neutron quadrupole deformations, respectively.

Another simple type of coherent motion is nuclear vibration. In the ideal case, the energy spectrum of the nucleus is composed of evenly spaced groups of degenerate states, corresponding to one or more vibrational phonons. The g-factors of these states are still given in the simplest estimate by Z/A. However, the experimental g-factors of excited states in vibrational nuclei are often somewhat different than the g-factors of states in rotational nuclei. The ^{140,142}Xe nuclei discussed later in this work can be seen as transitional nuclei between vibrational ^{138}Xe and more rotational ^{144,146}Ba. If differing proton and neutron deformations are considered for vibrational nuclei, then the correction of the g-factor is given by [6]

$$g = \frac{Z}{A}(1 - \frac{4}{3}f) \tag{2.4}$$

The rotation-vibration model is the most commonly used model for the interpretation of the structure of even-even nuclei [2]. In this model, the collective motion of the nucleons is calculated from a deformed, axially symmetric nuclear potential, and rotations and vibrations give rise to excited states. The resulting excited state spectrum is given by

$$E_{|I,K,n_\beta,n_\gamma>} = \frac{\hbar^2}{2J}[I(I+1) - K^2] + n_\beta\hbar\omega_\beta + \hbar\omega_\gamma(2n_\gamma + \frac{K}{2}) \tag{2.5}$$

where I and J are the same as above, n_β and n_γ are the quantum numbers associated with axial and triaxial vibrations, respectively, and K is the quantum number related to the rotational alignment of the nucleus with the intrinsic symmetry axis. In this model, states of differing quantum numbers are given by $|IKn_\beta n_\gamma>$. The factors $\hbar\omega_\beta$ and $\hbar\omega_\gamma$ are the β- and γ-vibrational zero point energies, respectively. The A$\sim$110 nuclei studied in this work have rotational bands built on the $|0200>$ state. This band is called the K=2 or γ-band, and the mixing ratios of transitions from the γ-band to the ground-band are studied in this work. There are various models for predicting these mixing ratios, but none have been successful in fully reproducing the data measured in this work. A detailed discussion on mixing ratios is given later in this chapter.

2.2 The spherical shell model

Several nuclei discussed in this work are best understood in terms of the spherical shell model. The $^{134}_{52}$Te nucleus, with two protons outside doubly closed $^{132}_{50}$Sn, has properties which are almost completely determined by the valence protons. Furthermore, the heavy $^{93-95}$Sr nuclei discussed in this work have been interpreted as having structure dominated by particles or holes interacting with a ^{94}Sr core. The surprisingly strong closure of the f5/2 and d5/2 spherical subshells at Z=38 and N=56, respectively, indicate the shifting of the single particle orbitals that make these nuclei unique.

The basic recipe for calculating magnetic moments in the shell model is given by equation 1.2. However, recent shell model calculations also take into account the

interactions of the valence nucleons with each other and the core. Equation 1.2 is then modified by

$$\mu = \mu_0 \sum_{k=1}^{A} (g_k^{(l)}(eff)\mathbf{l_k} + g_k^{(s)}(eff)\mathbf{s_k}) + g_k^{(p)}(eff)[Y_2, \mathbf{s_k}] \tag{2.6}$$

Here $g_k^{(s)}$(eff) and $g_k^{(l)}$(eff) and $g_k^{(p)}$(eff) are the "effective" g-factors which must be calculated by using an effective interaction such as the CD-Bonn interaction [7] and Y_2 is the l=2 spherical harmonic. The $g_k^{(p)}$(eff) term takes into account core polarization, which is caused by the electromagnetic interaction of the valence protons with the core protons. Calculations of this type are commonly used to predict g-factors near closed shells [8]. In the chapter on ^{134}Te, a calculation based on the CD-Bonn interaction is discussed in detail.

2.3 The particle-axial rotor model

For deformed odd-A nuclei, the excited levels can be understood in terms of rotational, ΔI=1 bands built on single particle orbitals. The particle-axial rotor model predicts excited states based on the single particle levels predicted by the Nilsson model for deformed nuclei. These single particle states are coupled to a rotating, deformed, even-even core. The ^{101}Zr, ^{103,105,107}Mo, and ^{109,111}Ru nuclei studied in this work are best understood in terms of this model. It should be noted that the basic assumption of axial symmetry in this model is not correct for these nuclei, as the ruthenium nuclei are known to be triaxial. However, even with the approximation of axial symmetry, the properties such as the g-factors and mixing ratios are well

reproduced by this model.

Following the procedure outlined in [9], mixing ratios of ΔI=1 transitions within a rotational band are given by

$$\delta = \sqrt{\frac{5}{12}} \frac{1}{K} \frac{E_\gamma}{1.2 \times 10^3} \frac{Q_0}{g_K - g_R} \frac{< I_f K 20 | I_i K >}{< I_f K 10 | I_i K >} \tag{2.7}$$

where E_γ is in keV. For these calculations, $g_R = \frac{1}{2} Z/A$, the quadrupole moment Q_0 is taken from experiment, and g_K can be calculated by using the M1 matrix elements tabulated by [10] for the various single particle configurations by

$$g_K = g_l + \frac{g_s - g_l}{2K} \sum (\alpha^2_{l,K-1/2} + \alpha^2_{l,K+1/2}) \tag{2.8}$$

where the α's are the Nilsson coefficients [11] and $g_{l,s}$ are the orbital and spin g-factors given in equation 1.3. In many cases, by comparing the mixing ratios calculated for several available single particle states to the experimental value, the most likely single particle configuration can be determined. It should be noted that the matrix elements are tabulated in [10] as a function of the deformation parameter β, which can be determined from the quadrupole moment by $\beta = 64.95 \frac{Q_0}{ZA^{2/3}}$. If both the mixing ratio of a transition in a given band and the g-factor of a state in the band are measured, then the g_R value can be determined explicitly by using equation 2.7 and

$$g = g_K + (g_K - g_R) \frac{K^2}{I(I+1)} \tag{2.9}$$

2.4 The IBM-2

The interacting boson model (IBM-1) [12] describes the fermions in an even-even nucleus as coupling pairwise to form A/2 bosons. The nucleus is then described by its algebraic, rather than geometric, properties. This model is somewhat successful in reproducing the energies of low lying states. However, the IBM-1 has the limitation that it cannot predict magnetic properties such as M1 transitions and E2/M1 mixing ratios. These properties arise from the independence of proton and neutron degrees of freedom. In the IBM-2, the protons and neutrons are considered independently. Therefore, the IBM-2 is the algebraic equivalent to the geometric collective model with independent proton and neutron deformations [6] discussed above. The IBM-2 predicts the g-factor of the 2^+ state to be

$$g_{2^+} = g_\pi \frac{N_\pi}{N} + g_\nu \frac{N_\nu}{N} \tag{2.10}$$

where $N_{\pi(\nu)}$is the number of proton (neutron) bosons or boson holes outside the nearest closed shell and $N=N_\pi+N_\nu$. The parameters g_π and g_ν are the effective proton and neutron boson g-factors, respectively. Microscopic calculations indicate $g_\pi=1$ and $g_\nu=0$. For neutron rich nuclei above ^{132}Sn, effective boson g-factors of $g_\pi=0.65(5)$ and $g_\nu=0.05(5)$ have long been used and reproduce the experimental data reasonably well [13]. The applicability of this choice of parameters for nuclei with $N_\pi/N_\nu \leq 1$ is tested in this work for ^{140,142}Xe. A new determination of the effective boson g-factors with the inclusion of these g-factors is given in the chapter on ^{140,142}Xe.

2.5 E2/M1 Mixing Ratios

Transitions between states with ΔI=1 and like parity can in general have multipolarity M1, E2, M3... where M1 is the magnetic dipole, E2 is the electric quadrupole, and so on. Assuming that only the lowest two multipolarities dominate, these transitions will be mixed E2/M1. The E2/M1 mixing ratio is defined as

$$\delta^2(E2/M1; J_1 \rightarrow J_2) = \frac{T(E2; J_1 \rightarrow J_2)}{T(M1; J_1 \rightarrow J_2)} \tag{2.11}$$

where the T(E2),T(M1) are the probabilities for an E2 or M1 transition, respectively. From the definition, it is clear that the choice of sign of the mixing ratio is a matter of convention only. The sign convention of Krane and Steffen is adopted in this work [14], and the mixing ratio is given by the E2 and M1 matrix elements between states.

$$\delta(E2/M1; J_1 \rightarrow J_2) = 0.835 E_\gamma \frac{< J_2||E2||J_1 >}{< J_2||M1||J_1 >} \tag{2.12}$$

where E_γ is in MeV. Therefore, the mixing ratio is a measure of the ratio of the M1 and E2 transition matrix elements. Since the mixing ratio is dependent on both the electric quadrupole operator and the magnetic dipole operator, it contains information about both the shape and magnetic properties of the nucleus.

The Weisskopf single particle estimate for mixing ratios is

$$\delta(E2/M1) = 1.521 \times 10^{-3} E_\gamma A^{2/3} \tag{2.13}$$

For the transitions between 2^+ states in this work, this estimate drastically under-

predicts the mixing ratio. This is because there is enhanced E2 transition probability related to the collectivity of these levels. The simple rotational-model prediction for the mixing ratio is

$$\delta(E2/M1) = 3.56 \times 10^{-3} E_\gamma A^{5/3} \tag{2.14}$$

Both of these simple estimates are independent of nuclear shape. While the rotational estimate is closer to the mixing ratios measured in this work, most of the values fall in between the single-particle and collective estimate.

Greiner's rotation-vibration model with independent proton and neutron deformations [6] predicts the mixing ratio for gamma-band to ground band transitions in rotational nuclei to be

$$\left(\frac{\delta}{E}\right)_{I_i \to I_f} = \left(8.6 \times 10^{-6} \frac{\beta_p^2 (1 - 0.72\beta_p)^2}{f^2(1-2f)^2} A^{\frac{10}{3}} \times \frac{< I_f 2 I_i | 022 >}{< I_f 1 I_i | 112 >} \frac{1}{I_f(I_f+1)}\right)^{1/2} MeV^{-1} \tag{2.15}$$

while for vibrational nuclei, the mixing ratio is given as

$$\left(\frac{\delta}{E}\right)_{2^+_\gamma \to 2^+} = 8.6 \times 10^{-4} \frac{A^{5/3}\beta_0}{(1-2f)f} \tag{2.16}$$

where β_0 is the "effective deformation" of the vibrating nucleus. These predictions will be compared to the experimental values measured for gamma-band to ground band transitions in ^{102,104,106,108}Mo, ^{108,110,112}Ru, and ^{112,114,116}Pd.

2.6 Theoretical A_2 and A_4 coefficients for angular correlations

For an angular correlation between two transitions $\gamma_1(L_1, L_1')$ and $\gamma_2(L_2, L_2')$ with initial state I_1, intermediate state I_2, and final state I_3, the theoretical values for the A_2, A_4 coefficients can be calculated from the equation

$$\begin{aligned} A_k(\delta_1, \delta_2) =& \frac{1}{1+\delta_1^2}(F_k(L_1, L_1, I_1, I_2) + (-1)^{(L_1 - L_1')} 2\delta_1 F_k(L_1, L_1', I_1, I_2) + \delta_1^2 F_k(L_1', L_1', I_1, I_2)) \\ & \times \frac{1}{1+\delta_2^2}(F_k(L_2, L_2, I_3, I_2) + 2\delta_2 F_k(L_2, L_2', I_3, I_2) + \delta_2^2 F_k(L_2', L_2', I_3, I_2)) \end{aligned}$$

where δ_1 and δ_2 are the multipole mixing ratios of the first and second transitions, respectively, and the $L_{1,2}$ are the multipolarities under consideration. F_k is defined by

$$F_k(L, L', I_i, I) = (-1)^{I_1 + I - 1}[(2L+1)(2L'+1)(2I+1)(2k+1)]^{\frac{1}{2}} \begin{pmatrix} L & L' & k \\ 1 & -1 & 0 \end{pmatrix} \begin{Bmatrix} L & L' & k \\ I & I & I_i \end{Bmatrix} \tag{2.17}$$

The array in parentheses is the Wigner 3-j symbol and the array in curly brackets is the Wigner 6j symbol. These can be calculated explicitly via [15]

$$\begin{pmatrix} j_1 & j_2 & j_3 \\ m_1 & m_2 & m_3 \end{pmatrix} = (-1)^{j_1 - J_2 - m_3}$$

$$\times \left(\frac{(j_1+j_2-j_3)!(j_1-j_2+j_3)!(-j_1+j_2+j_3)!(j_1+m_1)!(j_1-m_1)!(j_2+m_2)!(j_2-m_2)!(j_3+m_3)!(j_3-m_3)!}{(j_1+j_2+j_3+1)!}\right)^{1/2}$$

$$\sum_k \frac{(-1)^k}{k!(j_1+j_2-j_3-k)!(j_1-m_1-k)!(j_2+m_2-k)!(j_3-j_2+m_1+k)!(j_3-j_1-m_2+k)!}$$

and

$$\left\{ \begin{array}{ccc} j_1 & j_2 & j_3 \\ & & \\ l_2 & l_3 & l_3 \end{array} \right\} = (-1)^{j_1+j_2+l_1+l_2} \Delta(j_1 j_2 j_3) \Delta(l_1 l_2 j_3) \Delta(l_1 j_2 l_3) \Delta(j_1 j_2 l_3) \times$$

$$\sum_k \frac{(-1)^k (j_1+j_2+l_1+l_2+1-k)!}{k!(j_1+j_2-j_3-k)!(l_1+l_2-j_3-k)!(j_1+l_2-l_3-k)!(l_1+j_2-l_3-k)!(-j_1-l_1+j_3+l_3+k)!(-j_2-l_2+j_3+l_3+k)!}$$

where

$$\Delta(abc) = \left[\frac{(a+b-c)!(a-b+c)!(-a+b+c)!}{(a+b+c+1)!} \right]^{1/2} \tag{2.18}$$

where j, l, m, are integer or half-integer and a, b, and c are integers. There are several tabulations of A_2 and A_4 for various spin sequences and mixing ratios. The A_2 and A_4 parameters in this work were calculated by using the code "Delta" [16] available from the National Nuclear Data Center.

CHAPTER III

EXPERIMENT AND ANGULAR CORRELATION METHOD

3.1 Experiment

The data for this thesis come from an experiment performed in November of 2000 for two weeks with the Gammasphere detector array located at Lawrence Berkeley National Laboratory. For this experiment, a thick ^{252}Cf fission source with an α activity of 62 μCi was placed between two 13 μm thick unmagnetized iron foils. The fission fragments were fully stopped in the iron foils and the gamma-rays emitted from the fission fragments were not Doppler-shifted. The source was put inside a 7.62 cm polyethylene ball and placed in Gammasphere, which had 101 functioning detectors. The detectors were high-purity germanium detectors with BGO scintillators for Compton suppression. The detector faces were 25.4 cm from the source with a face diameter of 10 cm. The total solid angle coverage of Gammasphere was 45% of 4π, the time resolution was 8 ns, the energy resolution was 2.3 keV, and the average total γ efficiency was about 8%. The trigger for the experiement was a "hit" in any three detectors. A total of $\sim 4\times10^{11}$ $\gamma-\gamma-\gamma$ events were recorded.

The γ transitions studied in this experiment are the de-excitations of the secondary fragments from the spontaneous fission of ^{252}Cf. In spontaneous fission, the nucleus splits into two primary fragments, with the mass of the fragments following the well known asymetric distribution in fission. These primary fragments have high excitation energy and will emit neutrons on a time scale of roughly 10^{-20} seconds. It has been

shown that each fission event produces about three or four of these prompt neutrons [17]. The neutron evaporation leaves the resulting nuclei in a state of high spin and excitation energy, and these secondary fragments will emit prompt γ rays on the time scale of 10^{-14} seconds. The angular correlations between these γ rays are the focus of this work.

As mentioned earlier, the fission fragments in this experiment were fully stopped in the iron foils. Therefore, the implanted fission fragments were subject to the hyperfine fields (HFFs) caused by their implantation in substitutional sites in the iron lattice and the interaction of the nucleus with the foil. The strength of these fields can be quite high; >100 T in some cases. Since the hyperfine field depends on the interaction of the nucleus with the electrons surrounding it and the interaction of those electrons with the medium, the fields vary depending on the isotope, the type of foil, and the temperature. The hyperfine fields for iron have been tabulated by [18], and this reference has been found to be correct in most cases.

The time window for each event in this experiment was 1024 ns, and most events recorded have more than three coincident gamma transitions. This allows for the use of four-fold coincidences in some cases. Furthermore, the data can be sorted into a matrix of coincidences in which each set of two coincident gamma rays is placed once. For example, an event with three energies, $\gamma_1, \gamma_2, \gamma_3$, would be placed into the matrix as three separate events, $\gamma_1 - \gamma_2$, $\gamma_1 - \gamma_3$, and $\gamma_2 - \gamma_3$. In this work, "doubles" or "double coincidence" refers to this type of sorting of the triple coincidence data.

When the experiment was performed in November of 2000, the data were never intended to be used for angular correlations or g-factor measurements. However,

the fact that the fission fragments were implanted in a ferromagnetic material made g-factor measurements possible by using the integral perturbed angular correlation (IPAC) technique. To use the IPAC technique, it was necessary to develop a data analysis method to take full advantage of the angular information in the data, which previously had been ignored. The IPAC technique and the method for angular correlations with Gammasphere are discussed in this chapter.

3.2 Angular Correlations and The Integral Perturbed Angular Correlation (IPAC) Method

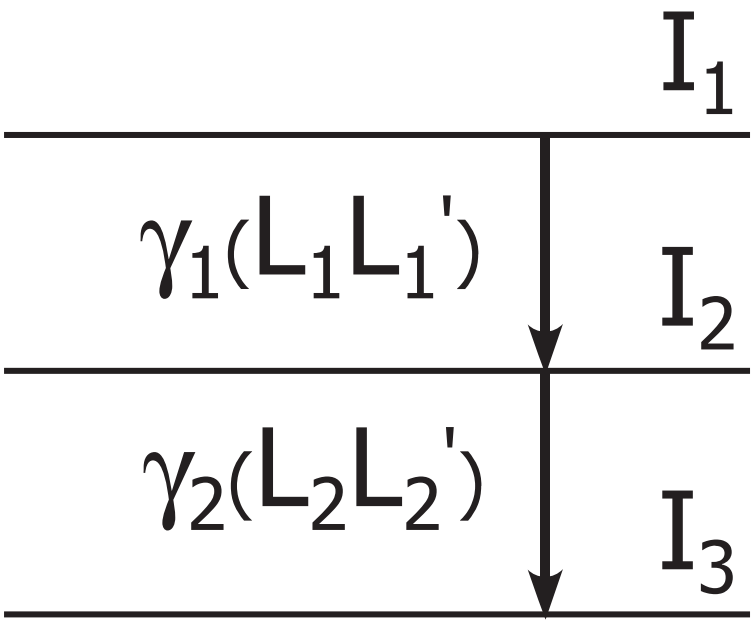

Figure 3.1: A cascade of two gamma rays.

For a cascade of two γ-rays as shown in figure 3.1, the angular correlation between the gamma rays is defined as the probability of γ_2 being emitted at a certain angle

relative to γ_1. Therefore, the detection of γ_1 in a detector at a fixed position defines an axis, and the relative angle to that axis of γ_2 defines the angle between the two. For many such measurements, the probability of detecting γ_2 at an angle of θ with respect to γ_1 is given by the angular correlation function, which is traditionally written as a sum of Legendre polynomials, P_k, by

$$W(\theta) = 1 + A_2 P_2(cos\theta) + A_4 P_4(cos\theta) \tag{3.1}$$

where the A_2 and A_4 depend on the spins of the levels and the multipolarities of the transitions and can be calculated theoretically or can be free parameters in a fit of experimental data.

If the intermediate state in figure 3.1 interacts with a magnetic field of sufficient strength for a sufficient length of time, then the experimentally observed angular correlation will be attenuated. Specifically, for a constant magnetic field, B, a nucleus with a magnetic moment μ will precess about the direction of B with the Larmor precession frequency given by

$$\omega_L = -\frac{\mu_N g B}{\hbar} \tag{3.2}$$

Taking $\omega_L = \frac{\phi}{\tau}$, where τ is the lifetime of the intermediate state and ϕ is the angle subtended by the precession of the nucleus in the time τ, the precession angle can be written in terms of the g-factor by

$$\phi = -\frac{\mu_N g B \tau}{\hbar} \tag{3.3}$$

Since the directions of the magnetic domains in an un-magnetized, un-cooled iron foil are random, the direction of this precession is random. This random rotation produces a de-orientation over the lifetime of the state, attenuating the correlation. In this case, "attenuation" implies that the absolute value of the angular correlation coefficients will decrease.

In practice, the experimental angular distribution function is given by

$$N(\theta_n) = A_0^{exp}(1 + A_2^{exp}P_2(cos\theta_n) + A_4^{exp}P_4(cos\theta_n)) \tag{3.4}$$

for some set of discrete angles, θ_n where A_0 is a normalization constant and depends only on the source strength and counting time. The attenuation of the angular correlation is then measured by the attenuation factors, G_2 and G_4, defined by

$$G_k = \frac{A_k^{exp}}{A_k^{theory}} \tag{3.5}$$

From the attenuation factor G_k, the average precession angle ϕ can then be found by solving [19]

$$G_k = \frac{1}{2k+1}(1 + 2\sum_{q>0}^{k} \frac{1}{1+q^2\phi^2}) \tag{3.6}$$

This method of measuring a perturbed angular correlation (PAC) to deduce the g-factor of an excited state has some inherent limitations. Figure 3.2 shows the dependence of G_k and the inverse of its derivative on the precession angle. This plot shows how, as ϕ gets large, the uncertainty in the measurement, which depends on $\mid \frac{d\phi}{dG_{2,4}} \mid$, also gets very large. The same is true if ϕ is very small. This places

a fundamental limitation on the sensitivity of this type of g-factor measurement. Typically, the errors in A_2 and A_4 are small for states with lifetimes between a few hundred picoseconds and a few nanoseconds and for fields between 10 and 100 T. Also, it should be clear from equation 3.6 that the PAC method can only determine the magnitude, and not the sign, of the g-factor. This is in contrast to the method employed by [20], in which the HFFs were aligned by an external magnetic field. Despite these limitations , there are still many cases where this method can be applied.

3.3 Details of the Method: IPAC with Gammasphere

3.3.1 Angular Properties of Gammasphere

At its full capacity, Gammasphere consists of 110 germanium detectors, corresponding to 5995 unique detector pairs. The detectors are placed at 17 different azimuthal angles and 60 various polar angles. For each azimuthal angle, there are 5 to 10 detectors placed symmetrically with respect to the polar angle. Because of the symmetries of Gammasphere, the angle between any two detectors will be one of only 64 possible values, and each of these 64 angle bins has many pairs of detectors. For this experiment, only 101 detectors were present, so the number of detectors in each bin is slightly less than if Gammasphere were at full capacity. The angle bin information for this experiment is given in table III.1.

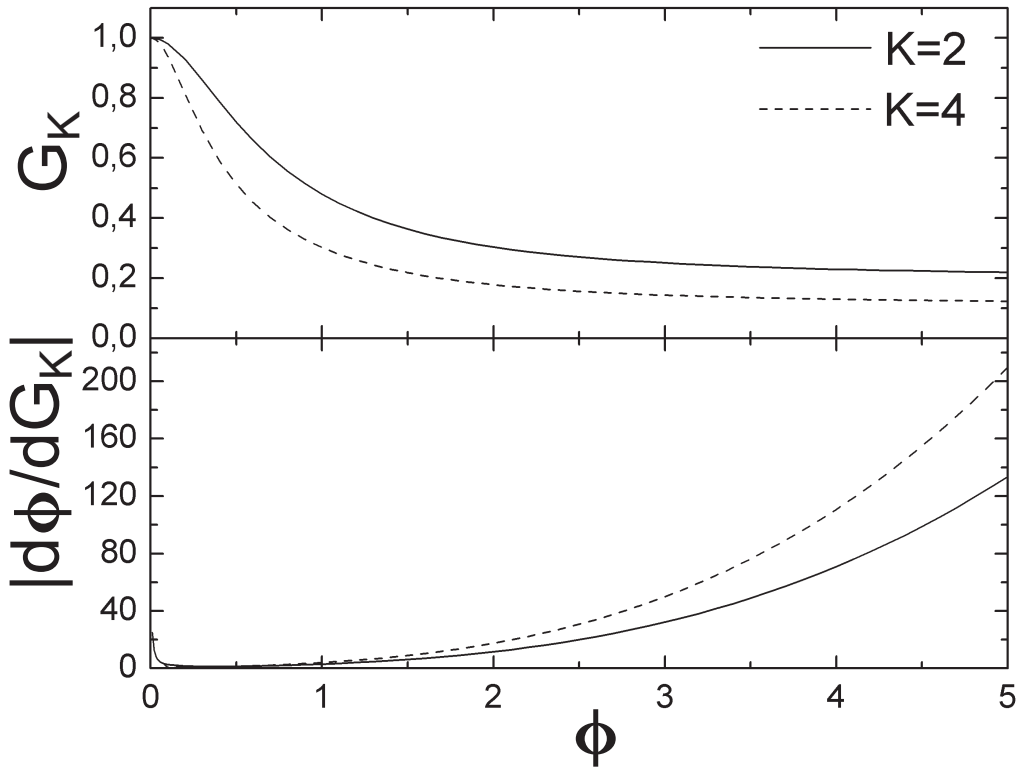

Figure 3.2: Dependence of the attenuation factors $G_{2,4}$ and $|\frac{d\phi}{dG_{2,4}}|$ on the precession angle ϕ.

3.3.2 Angular Binning

The 64 angle bins shown in table III.1 are comprised of detector pairs sharing the same central angle. After the relative intensity of each angle bin is found, the A_2 and A_4 parameters can be found by fitting the distribution to the function given by equation 3.1. However, 64 data points is more than sufficient to determine a fourth order polynomial, so the bins can be further combined into 17 angle bins. After each of the 64 histograms has been fit to find the intensity of the peak in question, the data can be further binned by properly adding these numbers, taking into account the response function of each bin. This procedure will be discussed in the following sections.

3.3.3 Data Sorting

To measure the angular correlation, the triple coincidence data were sorted into 64 two dimensional histograms corresponding to the 64 angle bins. An example of some of these histograms is shown in figure 3.3. The histograms were produced by reading the full data set event by event. For each $\gamma-\gamma$ coincidence, the angle between the detectors which detected γ_1 and γ_2 was calculated and the event was added to the appropriate histogram. For each bin, n, the histogram was then fit to find the number of coincidences of the cascade of interest, N_n. This N_n must be corrected for relative detector efficiency, the number of detectors in the particular bin, and the detector response functions. The value for the corrected N_n is given by

$$N_n = \epsilon_n(E_1, E_2) \int_0^\pi W(\theta) R_n(\theta, E_1, E_2) sin(\theta) d\theta \tag{3.7}$$

Table III.1: Angle bins in Gammasphere with the 101 detectors used in the November 2000 experiment.

Bin	Cos(θ)	Num. Pairs	Bin	Cos(θ)	Num. Pairs	Bin	Cos(θ)	Num. Pairs
1	0.939	203	23	0.309	56	45	-0.391	90
2	0.934	58	24	0.298	100	46	-0.471	52
3	0.840	47	25	0.282	101	47	-0.495	89
4	0.823	45	26	0.269	104	48	-0.500	56
5	0.815	104	27	0.175	100	49	-0.577	116
6	0.809	56	28	0.168	44	50	-0.580	101
7	0.764	100	29	0.139	23	51	-0.594	90
8	0.762	45	30	0.064	92	52	-0.613	104
9	0.755	50	31	0.057	104	53	-0.656	50
10	0.745	30	32	0.000	273	54	-0.745	30
11	0.656	50	33	-0.057	104	55	-0.755	50
12	0.613	104	34	-0.064	90	56	-0.762	45
13	0.594	88	35	-0.139	23	57	-0.764	100
14	0.580	100	36	-0.168	44	58	-0.809	56
15	0.577	116	37	-0.175	101	59	-0.815	104
16	0.500	56	38	-0.269	104	60	-0.823	44
17	0.495	88	39	-0.282	101	61	-0.840	44
18	0.471	52	40	-0.298	100	62	-0.934	58
19	0.391	91	41	-0.309	56	63	-0.939	196
20	0.357	58	42	-0.327	46	64	-1.000	46
21	0.333	60	43	-0.333	60			
22	0.327	44	44	-0.357	58			

where $\epsilon_n(E_1, E_2)$ is the function describing the relative efficiency of the pair, $R_n(\theta, E_1, E_2)$ is the response function of the pair, and W(θ) is given in equation 3.1.

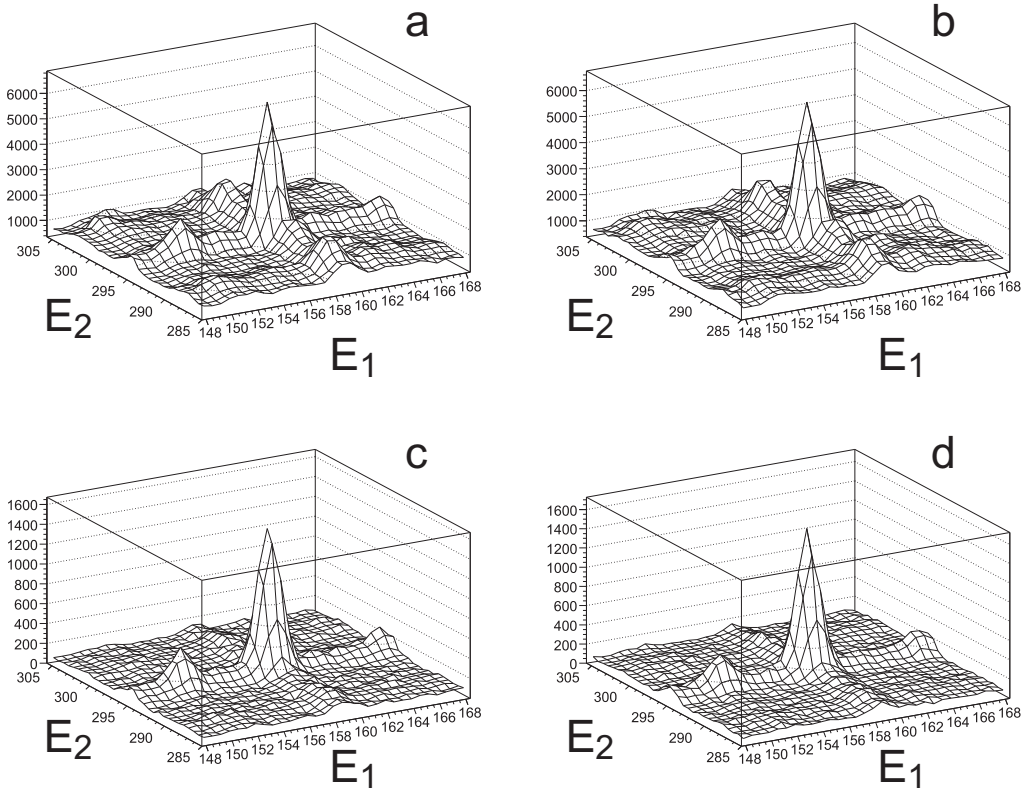

Figure 3.3: Two-dimensional histograms constructed for the $4^+ \rightarrow 2^+ \rightarrow 0^+$cascade in ^{148}Ce. **a** and **c** represent bin number 5, while **b** and **d** show bin 31. **a** and **b** are ungated histograms, while **c** and **d** are required to be in coincidence with at least one of 9 γ-rays corresponding to coincident transitions in ^{148}Ce or in partner nuclei ^{100,102}Zr.

The 64 histograms can also be made with additional gates, making full use of our triple coincidence data. For example, when considering the $4^+ \rightarrow 2^+ \rightarrow 0^+$ cascade in ^{110}Ru, the events in each histogram might be required to be in coincidence with the $2^+ \rightarrow 0^+$ transitions in it's fission partners ^{138,140}Xe. This is useful when added selectivity is necessary. The histograms with additional gates (triple coincidences) are

typically 20×20 keV, with the center corresponding to the energies of the two γs of interest. When only doubles are necessary, we used 64 large histograms (4096×4096, 0.666 keV per channel) which include the entire energy surface.

3.3.4 Bin Efficiency

The number of coincidences in each angle bin must be corrected for the relative efficiencies of the detector pairs. It was shown [21] that the efficiencies of the individual detectors of Gammasphere may vary greatly compared to the mean efficiency. If the detector pairs *i,j* belong to bin *n*, the efficiency of the bin is given by

$$\epsilon_n(E_1, E_2) = \frac{1}{2}\sum_{i,j}[\epsilon_i(E_1)\epsilon_j(E_2) + \epsilon_i(E_2)\epsilon_j(E_1)] \tag{3.8}$$

To calculate the $\epsilon_{i,j}(E)$'s, a singles γ spectrum was constructed for each detector. A separate singles spectrum was constructed for the sum of all detectors. The summed spectrum was divided by the number of working detectors (101) and then the individual detector spectra were divided by the normalized sum spectrum. The resulting spectra give the relative efficiency curve for each detector. Examples of spectra produced in this manner are given in figure 3.4, which shows how the relative efficiency varies greatly for some detectors, but only slightly for others. However, the relative efficiencies of *all* detectors fluctuate outside statistical errors, making the relative efficiency correction a necessity.

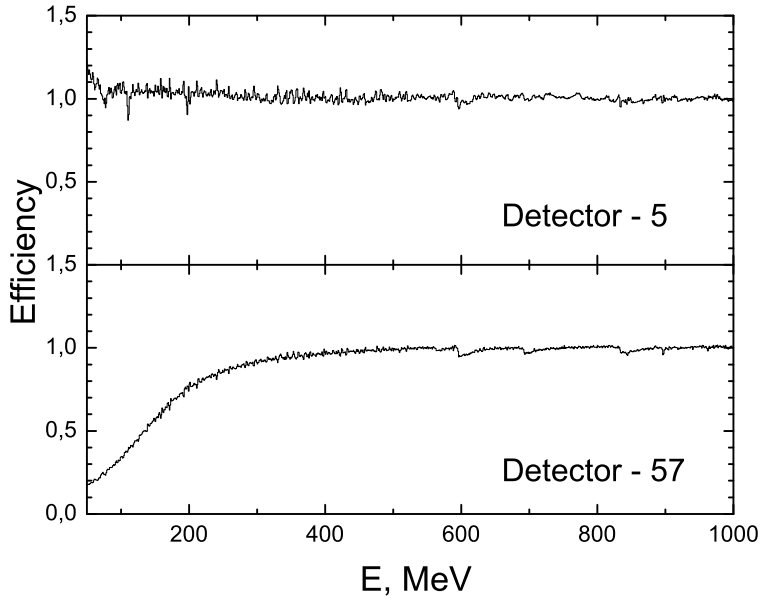

Figure 3.4: Relative efficiencies of detectors 5 and 57.

3.3.5 The Response Function

The response function was calculated by using a simple Monte Carlo simulation, with the γ ray transport simulated up to the first collision. This is equivalent to the traditional calculation of Q_k [22]. The mean free path, λ(E), of γ-rays was calculated by using the known Gammasphere detector properties. The energy dependence of $R_n(\theta,E_1,E_2)$ is negligible, as discussed below, so only $R_n(\theta)$ was is used in the angular correlation analysis.

The energy dependence of the solid angle correction factor, which is equivalent to the energy dependence of the response function, is given by

$$Q_\lambda = J_\lambda / J_0 \tag{3.9}$$

and

$$J_\lambda = \int P_k(cos(\theta)) \times \epsilon(\alpha, E) \times sin(\alpha) d\alpha \tag{3.10}$$

where

$$\epsilon(\alpha, E) = 1 - e^{-\tau(E)\rho x} \tag{3.11}$$

Here τ(E) is the energy dependent absorption coefficient, ρ is the density, and x is the path length through the detector, which depends on the angle with the center, α. By using the known values for τ(E) in germanium, the energy dependence of the solid angle correction factor can be calculated, and is shown in figure 3.5. The variation of A_2 with γ energy is less than 0.5%, and the energy dependence of the solid angle correction was therefore ignored in our analysis.

3.3.6 Fitting Procedure

To determine the angular correlation, each of the 64 histograms was fit to find the intensity of the peak of interest, N_n. This fitting method is based on the analysis of two dimensional $\gamma - \gamma$ coincidence spectra given in [23]. To fit a given histogram, a window within the histogram is selected. Within this window, the positions of the peaks are defined by using projections of the histogram on the two axes. The surface is then approximated by three types of background and the sum of the two dimensional γ peaks found in the projections. The three types of background consist

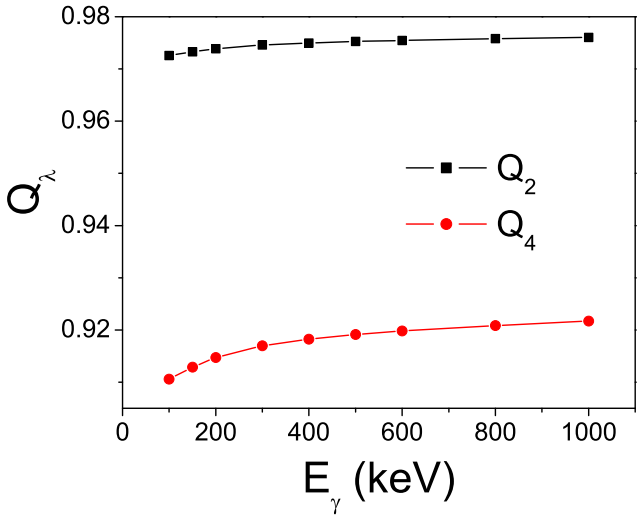

Figure 3.5: The energy dependence of the solid angle correction factors.

of a smooth two-dimensional background and two series of ridges parallel to the axes corresponding to γ lines in the x and y direction. The last part of the fitting procedure is to solve a well known NNLS (Non-Negative Least Square) problem [24].

By using the N_n^{exp} found from fitting the histograms, the two parameters A_2 and A_4 are fit by using the minimization expression

$$min \sum_n \frac{(N^{exp}(\theta_n) - N(\theta_n))^2}{\delta_{n,exp}^2 + \delta_{n,model}^2} \tag{3.12}$$

The experimental uncertainty in the γ peak intensity is always much greater than the model error, so δ_{model} was neglected. Once the experimental A_2 and A_4 are found, the g-factor can be calculated.

In practice, a set of 64 experimental points is more than adequate to estimate the three parameters in equation 3.4, and it is therefore convenient to further combine

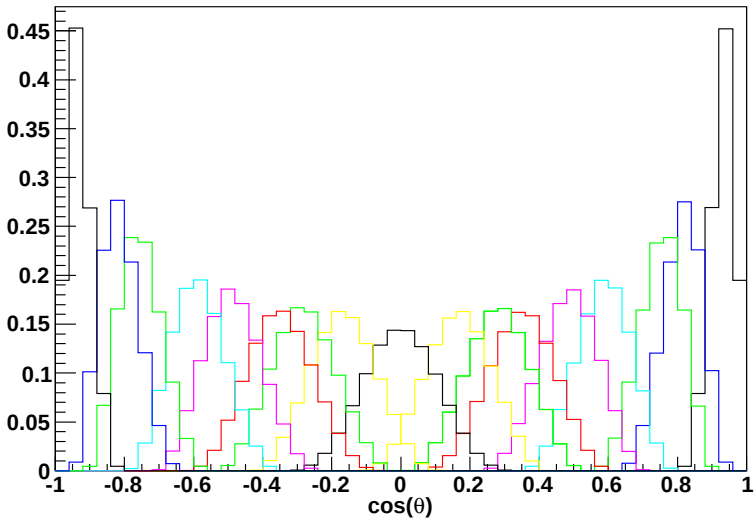

Figure 3.6: The response functions of the 17 groups in the ideal case when all 110 detectors are present and have the same efficiency.

angle bins, thereby increasing the statistics of each bin. Note that the minimization approach did not assume that all the pairs of a group must have the same angle. This means the angle bins can be combined into even larger groups by using the equation

$$N_{gr_\alpha} = \sum_n \epsilon_n(E_1, E_2) \int_0^\pi W(\theta) \frac{\sum_n \epsilon_n(E_1, E_2) R_n(\theta, E_1, E_2)}{\sum_n \epsilon_n(E_1, E_2)} sin(\theta) d\theta \tag{3.13}$$

where the index n is summed over the elements of each group α. The N_{gr_α} can be obtained by summing the N_n values given by equation 9 for some grouping. The 64 angle bins are then grouped into 17 larger bins. The response function for each of the 17 groups is presented in figure 3.6, which shows the angular position and resolution of the bins.

CHAPTER IV

STRUCTURE OF NEUTRON RICH ^{93,94,95}Sr ISOTOPES

4.1 Introduction

Nuclei in the region of the neutron rich strontium isotopes have been of great interest because of the seemingly anomalous strength of the Z=38,40 and N=56 sub-shell closures in this region and because of a "phase transition" with an abrupt change from spherical to strongly deformed shape that occurs at N=60. This is in contrast to the gradual onset of deformation that occurs moving away from typical doubly closed shell nuclei like ^{208}Pb. Several calculations have attempted to explain this phenomenon [25], [26]. However, it is still not totally clear which single particle states are most important in describing the excited states of these strontium nuclei.

It has been proposed that the excited states in ^{93}Sr arise from a νd5/2 hole weakly coupled to a ^{94}Sr core [27], and similarly excited states in ^{95}Sr from νg7/2 particle states coupled to the ^{94}Sr core [28]. However, the spins and parities of many levels in these nuclei have not been explicitly measured, making comparisons to shell model calculations difficult. In particular, there is very little information available on the spins of the levels in ^{93}Sr. Therefore, it is important to measure the spins of excited states in ^{93,95}Sr in order to test the assumption of weak coupling to a ^{94}Sr core.

One interesting feature of ^{94}Sr is the report of excited an 3^- state [29]. The 3^- assignment is based predominantly on the angular correlations performed by [29] for transitions in the beta-decay of ^{94}Rb. However, the angular correlation coefficients

Table IV.1: Comparison of the angular correlation coefficients measured in this work for ^{94}Sr to those previously measured by Jung *et al.*

Transitions	A_2, A_4 (This work)	A_2, A_4 (Jung *et al.* [29])
1308.7-836.7	0.101(8),0.012(13)	0.105(16), 0.028(30)
1089.1-836.7	-0.052(9),0.007(13)	-0.059(16), 0.003(22)
677.4-1089.1	0.270(16),-0.036(24)	0.273(46), -0.034(86)
710.5-1308.7	-0.235(29),-0.062(44)	
1577.4-836.7	-0.083(32),-0.033(47)	-0.086(12), -0.007(22)
458.7-1308.9	-0.189(31),0.110(46)	
502.7-1308.9	0.177(51),-0.128(77)	0.252(91),-0.067(167)
1009.7-1308.9	0.082(17),0.012(25)	
767.7-1308.9	-0.055(29),-0.046(44)	

have been determined much more precisely in the present work. The angular correlations for ^{94}Sr in this work are compared to the previous measurement by Jung *et al.* [29] in table IV.1. The new data indicate that the proposed 3^- level at 1926 keV is in fact 3^+.

In ^{95}Sr, recent work by the Vanderbilt group has led to the proposal of a band built on the νg7/2 orbital. In order to test this, spins and parities of several excited states are assigned in this work. Furthermore, mixing ratios and the g-factor of the proposed bandhead are measured. These measurements give further insight into the single particle structure near the doubly-closed subshell ^{94}Sr.

4.2 The hyperfine field for Sr in Fe

The measured magnitudes of the hyperfine field of Sr in Fe as listed in [18] are 10(3), 3.9(1.8), and 5.4(1.1). To test the applicability of these values, the g-factor of the 2^+ state in ^{98}Sr, which has been previously measured by [30] to be g(2^+)=0.38(7),

was used to calibrate the field. The coefficient A_2=0.051(21) yields B_{HF}(Sr)=13^{+16}_{-6} T, which is most consistent with the value of B_{HF}(Sr)=10(3) given in [18]. Therefore, the value of 10(3) T is adopted for the Sr isotopes in this experiment.

4.3 ^{93}Sr

The level scheme for ^{93}Sr is shown in figure 4.1. The ground state in ^{93}Sr has been measured by [31] to be 5/2. The magnetic moment is given by [32] to be μ=-0.7942(5). This is most consistent with a d5/2 neutron, so the ground state is assigned $J^{\pi}=5/2^{+}$. The spin and parity assignments of the excited states populated in fission have been tentatively made by [27] based on comparison to ^{94}Sr and shell model calculations. They concluded that the excited states are based on the coupling of a νd5/2 hole state to the ^{94}Sr core. This work tests this assertion by using angular correlations to confirm the level spins and multipolarities.

The 794-986 keV angular correlation and the 1183-986 keV angular correlation are measured for ^{93}Sr. The 794-986 keV angular correlation is shown in figure 4.2. The results of both correlations plotted against the theoretical values of A_2 and A_4 for various spin sequences are shown in figure 4.3. The spin assignments made in this work become clear from this figure. The result of the 794-986 keV correlation, shown as a red circle, is only consistent with a 9/2→9/2→5/2 correlation, which is given as the solid black line in figure 4.3. The measured correlation is consistent with a pure quadrupole multipolarity for the 986 keV transition, and a mixed E2/M1 transition for the 794 keV decay, with δ(E2/M1;794)=-0.97(14). Therefore, the 986 keV level is assigned as $9/2^{+}$ and the 1780 keV level is assigned $9/2^{+}$.

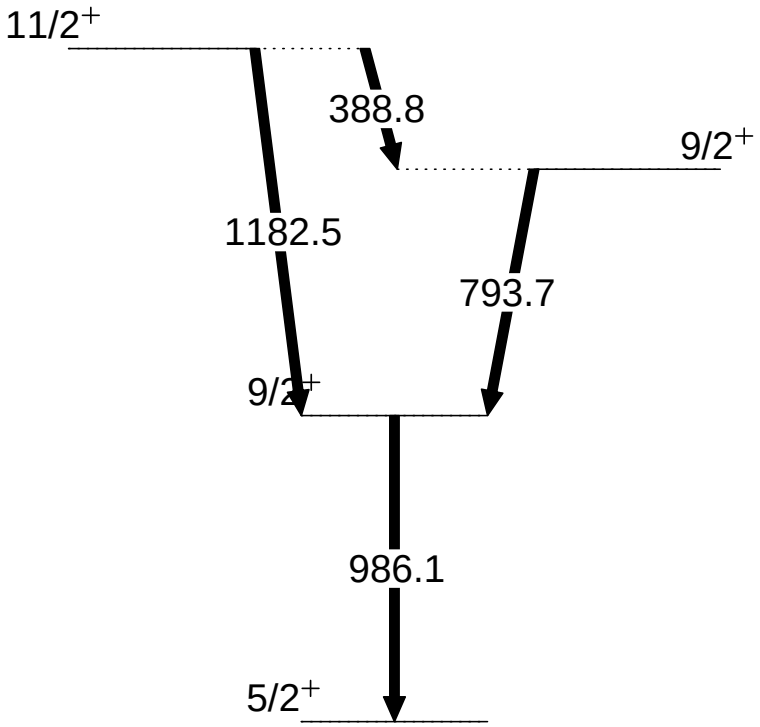

Figure 4.1: Partial level scheme of ^{93}Sr showing the spins and parities assigned in this work.

Figure 4.4 shows the 1183-986 keV angular correlation. The result is shown in figure 4.3 as a black square. Because of the large error bars on A_4, the cascade is consistent with a spin of either 11/2 or 13/2 for the 2169 keV level. However, the measured value is in much better agreement with an 11/2 assignment. Furthermore, if the level is 13/2, the 1183 transition must be quadrupole-octupole mixed (M3/E2 or E3/M2) to be in agreement with the measured correlation. The strong octupole mixing and and the strength of the 1183 keV transition do not suggest a 13/2 assignment for the 2169 keV state. Therefore, this level is assigned as $11/2^+$. With this assignment made, the E2/M1 mixing ratio of the 1183 keV transition is found to be -0.24(5).

Figure 4.5 shows the absolute values for the E2/M1 mixing ratios of the 794 and

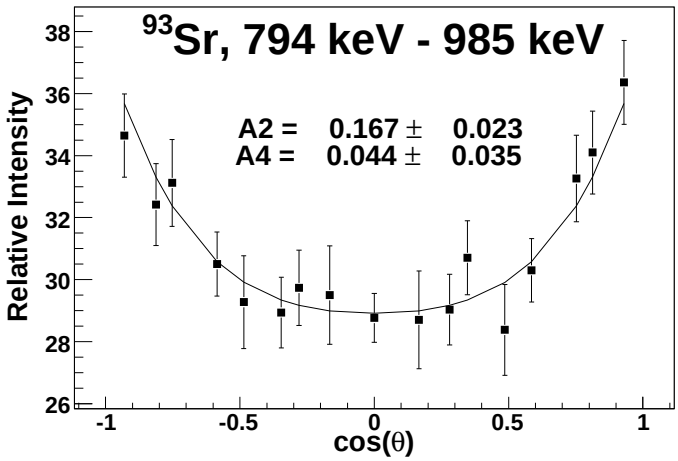

Figure 4.2: The angular correlation for the 794 keV and 896 keV transitions in ^{93}Sr.

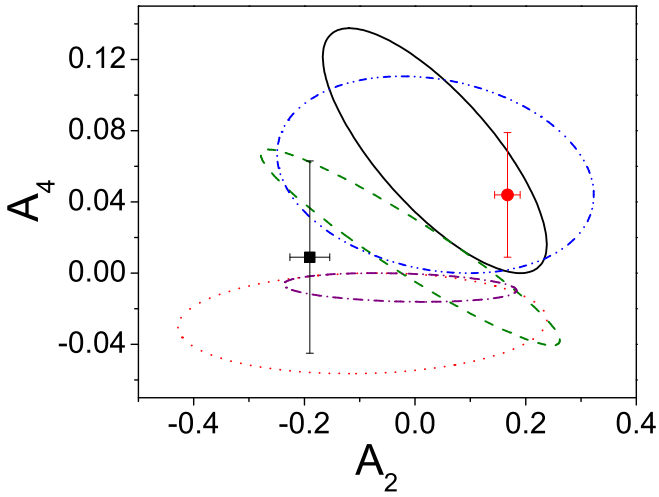

Figure 4.3: Theoretical values of A_2 and A_4 for several spin sequences, along with the experimental data from the 1183-986 keV angular correlation (black square) and the 794-986 keV angular correlation (red circle). The solid black line is for a 9/2→9/2→5/2 cascade. The red dotted line is for an 11/2→9/2→5/2 cascade. The olive dashed line is for a 13/2→9/2→5/2 cascade. The blue dash-dot-dot line is for a 9/2→7/2→5/2 cascade. The purple dash-dot is for a 11/2→7/2→5/2 cascade.

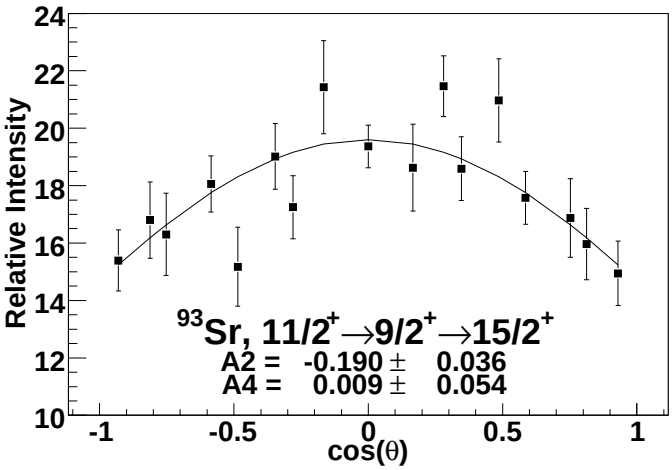

Figure 4.4: The angular correlation for the 1182.5 keV and 986.1 keV transitions in ^{93}Sr.

1183 keV transitions compared to the Weisskopf estimate for single particle transitions and the collective model estimate, as given by equations 2.13 and 2.14, respectively. Also shown in this table are the mixing ratios measured for ^{95}Sr (shown as the round, red points) which are discussed in a later section.

4.4 ^{94}Sr

Angular correlations in ^{94,96}Sr have been previously measured by Jung *et al.* [29] with gamma-decays following the beta-decay of ^{94}Rb. Most of the currently accepted spins and parities of levels in ^{94}Sr come from Jung *et al.*'s work [29] or are inferred from log(*ft*) values from the beta-decay of ^{94}Rb. However, it is advantageous to study angular correlations from fission fragments because several states are populated in fission that are not populated in beta-decay, and it may be possible to assign spins to these unknown levels. Furthermore, Gammasphere has much better angular resolution than previous experiments, with 17 discrete angles for this analysis as

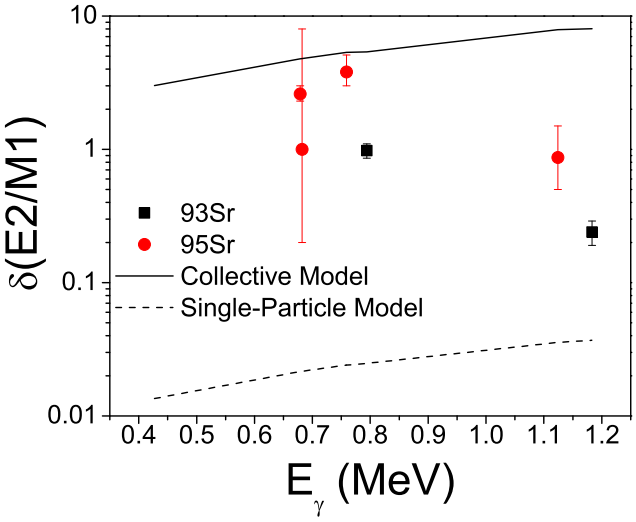

Figure 4.5: Mixing ratios for transitions in ^{93,95}Sr, compared to predictions for the single particle and collective models. The corresponding data are found in table IV.2.

opposed to 6 discrete angles for the analysis by [29]. The partial level scheme of ^{94}Sr with the spins and parities determined in this work is shown in figure 4.6.

1926 keV level: There are several evidences that the 1926 keV level does not have odd parity, as originally suggested by [29]. The odd-parity was proposed because of the dipole nature of the 3→2 transition. However, with the more sensitive measurement of the present work, it is found that the multipolarity of this transition deviates slightly from pure dipole.

The result of the angular correlation of the 1089-837 keV transitions is A_2^{exp}=-0.052(9) and A_4^{exp}=0.007(13), given in table IV.2. From this correlation, the quadrupole-dipole mixing ratio for the 1089 keV transition is δ=0.025(12). Furthermore, as discussed below, the 457.5 keV transition from the 2603 keV level is very highly mixed, implying that the 2603 keV level is 4^+ (not 4^-) and the 457.5 keV transition is

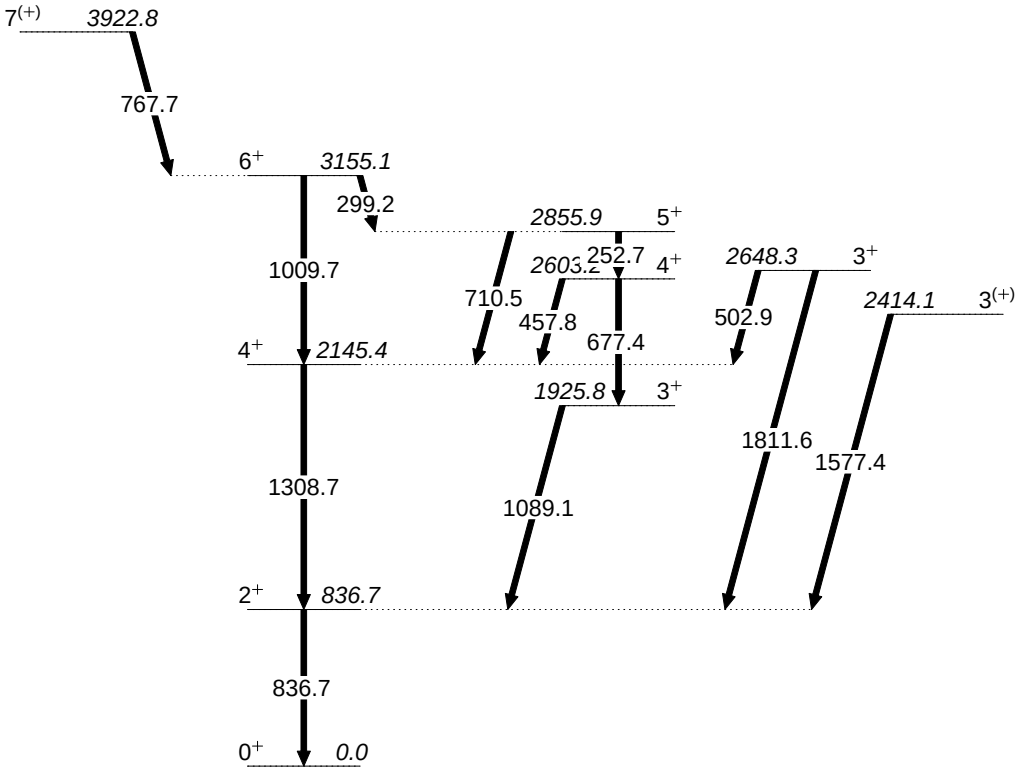

Figure 4.6: The partial level scheme of ^{94}Sr with the measured spins and parities established from measuring the transition multipolarities.

E2/M1. Furthermore, the result of the 677-1089 keV correlation is A_2^{exp}=0.270(16) and A_4^{exp}=-0.036(24), which indicates that the 677.4 keV transition has a mixing ratio of δ(E2/M1;677.4)=-1.7$^{+1.0}_{-0.5}$. This result is clearly not consistent with and assignment of 3^- for the 1926 keV level, in which case the 677.4 keV transition should be nearly pure dipole. Therefore, based on all these considerations, the 1926 keV level is assigned as 3^+, rather than 3^-.

2603 keV level: The result of the angular correlation for the 458-1309 keV transitions is A_2^{exp}=-0.189(31), A_4^{exp}=0.110(46). The ovals for this correlation are shown in figure 4.7. From this figure it is clear that the correlation is only consistent with $4 \rightarrow 4^+ \rightarrow 2^+$. Although there is a slight possibility, within error bars, that the level could have a spin of 6, the fact that it also decays strongly to the 3^+ state at 1926 keV rules out this possibility. The mixing ratio for the 457.5 keV transition from this correlation is δ=2.1$^{+2.8}_{-0.7}$. It is very unlikely that this degree of quadrupole mixing would occur for an M2/E1 transition, so the state is assigned a positive parity of 4^+.

2648 keV level: The angular correlation for the 503-1309 keV cascade is shown in figure 4.8. From this correlation alone, the level most likely has a spin of 3, although a spin of 5 is within 1.5 sigma, as shown in figure 4.7. However, since the level also decays to the 2^+ level at 837 keV, a spin of 5 is not consistent with the decay pattern. For a spin 3 state, the mixing ratio is found to be -4.9$^{+1.4}_{-2.6}$. Because the mixing ratio is very large, it is extremely unlikely that this state has odd parity and the transition is mixed M2/E1. Therefore, the state at 2648 keV is assigned a spin and parity of 3^+.

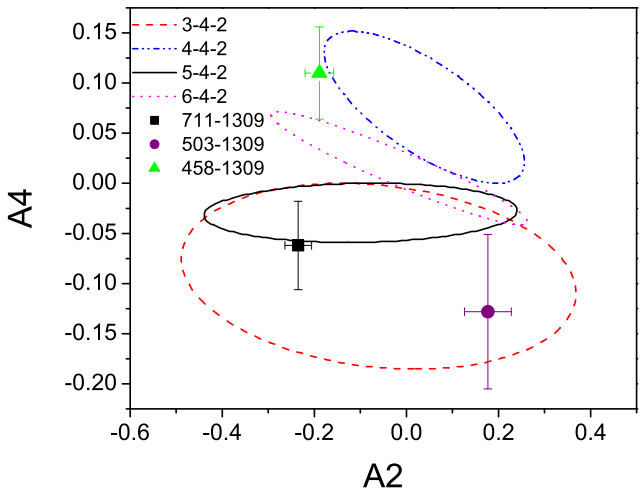

Figure 4.7: The result of the 711-1309 keV, 503-1309 keV, and 458-1309 keV angular correlations in ^{94}Sr, compared to the theoretical values for several different spin sequences. It is clear that only the 5 and 3 spin assignments are consistent with experiment for the 2856 and 2648 keV levels, respectively.

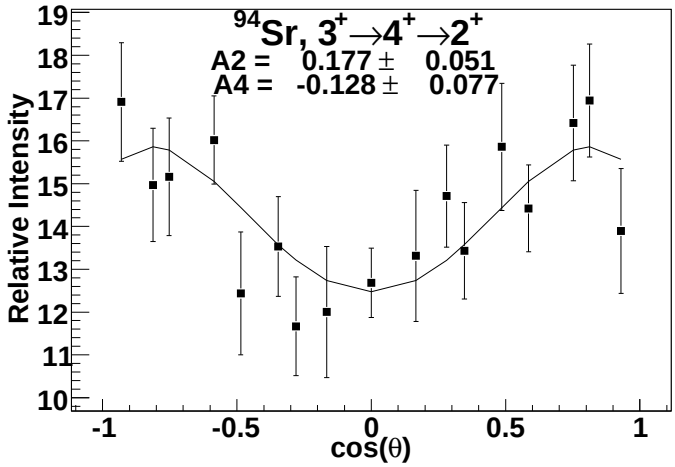

Figure 4.8: The angular correlation of the 503 keV and 1309 keV transitions in ^{94}Sr. This correlation is consistent with either a $3^+ \rightarrow 4^+ \rightarrow 2^+$ cascade.

2856 keV level: The angular correlation for the 711-1309 keV cascade is shown in figure 4.9. With the 1309 keV transition already established as an un-attenuated $4^+ \rightarrow 2^+$ transition, this correlation can be used to determine the spin of the 2856 keV level. The data are consistent with a $5^+ \rightarrow 4^+ \rightarrow 2^+$ cascade. The spin and parity of this level were not determined by [29], perhaps because this level is not highly populated in beta decay. The National Nuclear Data Center proposes this as a 4^+ level because of the log(ft)=7.1 in β- decay from the $3(^-)$ level of ^{94}Rb. However, it is very clear from figure 4.7 that this assignment is completely inconsistent with the observed angular correlation. A spin assignment of 5^+ for this level is still consistent with the measured lof(ft) value however, as this is now a first forbidden decay from the 3^- ground state in ^{94}Rb.

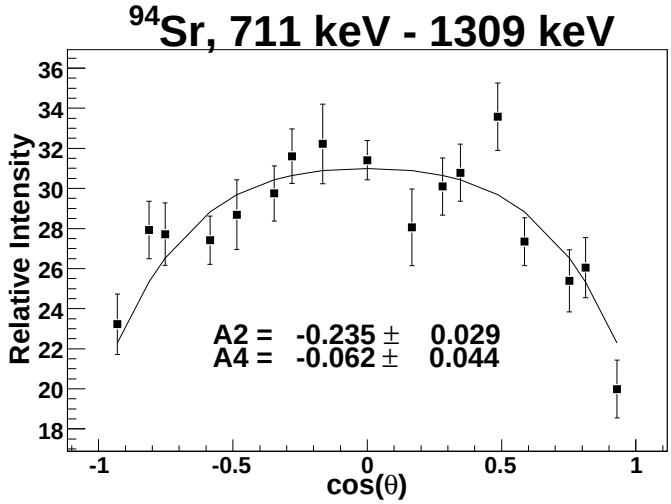

Figure 4.9: The 711-1309 keV angular correlation in ^{94}Sr with no additional gates

3155 keV level: The 3155 keV level was tentatively assigned as 6^+ by [33]. The result of the correlation for the 1010-1309 keV transitions, given in table IV.2,

is A_2^{exp}=0.082(17), A_4^{exp}=0.012(25). This angular correlation is consistent with the assignment made by [33], and a J^π of 6^+ is assigned to the 3155 keV level.

3923 keV level: The 3923 keV level, which was not observed by [29], was assigned a J^π of 8^+ by [33]. This assignment was based on the fact that this level seems to be yrast. However, the angular correlation for the 767.7-1308.7 keV cascade shows conclusively that the 3155 keV state is not 8^+. If the level were 8^+, A_2^{theory}=0.102 and A_4^{theory}=0.009 for the 768-1309 keV correlation. The experimental values are A_2^{exp}=-0.055(29) and A_4^{exp}=-0.046(44), as given in table IV.2 and figure 4.10. These experimental values are most consistent with a spin of 7 for the 3923 keV level, although a spin of 5 cannot be excluded because the error bars are rather large. However, the absence of a transition to the 5^+ level at 2856 keV seems to rule out this possibility. Therefore, a spin of 7 is assigned to this level. The parity is tentatively assigned as positive, because the transition is strongly quadrupole-dipole mixed, as shown in table IV.2. However, a pure dipole transition is consistent within just over one sigma of this measurement, with A_2^{theory}=-0.071 and A_4^{theory}=0.0, so the parity assignment remains tentative.

4.5 ^{95}Sr

4.5.1 Spin assignments and mixing ratios

The level scheme of ^{95}Sr with the spins and parities assigned in this work are shown in figure 4.11. The ground state spin in ^{95}Sr was measured by [31] to be 1/2, and the

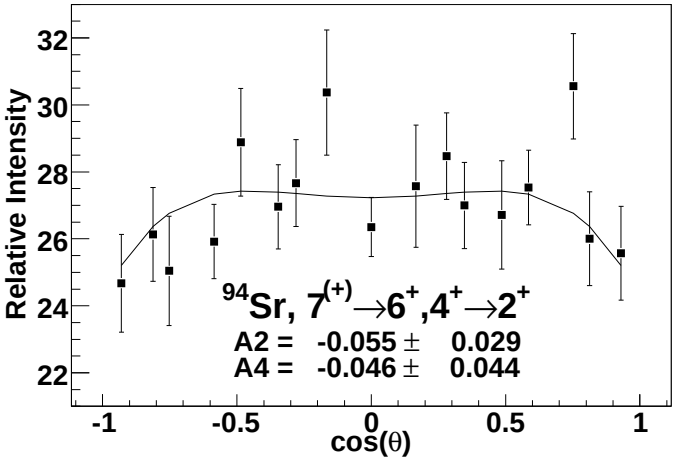

Figure 4.10: The angular correlation for the 768-1309 keV transitions in ^{94}Sr. This correlation is inconsistent with the proposed J^{π} of 8^{+} for the 3923 keV level. The best fit is for a spin of 7.

magnetic moment was measured by [34] to be -0.537(2). These values suggest that the ground state is an s1/2 proton state and has positive parity. According to the NNDC [35], the 352.0 keV transition is an M1 transition to the $1/2^{+}$ ground state, constraining the level to be either $3/2^{+}$ or $1/2^{+}$. However, for any correlation involving a 1/2→1/2 transition, A_2 and A_4 are identically zero. Therefore, the measurement of a non-zero value for A_2 and A_4 for the 204.0-352.0 keV angular correlation (see table IV.2) fixes the spin of the 352.0 keV level at $3/2^{+}$.

The multipolarity of the 204.0 keV transition to the $3/2^{+}$ level has been determined by Kratz *et al.* [36] to be E2 from its α(K) value. This constrains the parity of the 556.0 keV level to be positive and its spin to be 1/2, 3/2, 5/2, or 7/2. A spin of 3/2 can be ruled out based on the fact that the 204.0-352.0 keV angular correlation is non-zero, because the angular correlation coefficients for a 3/2→3/2→1/2 cascade are identically zero. Therefore, the spin of the 556.0 keV level is restricted to 1/2,

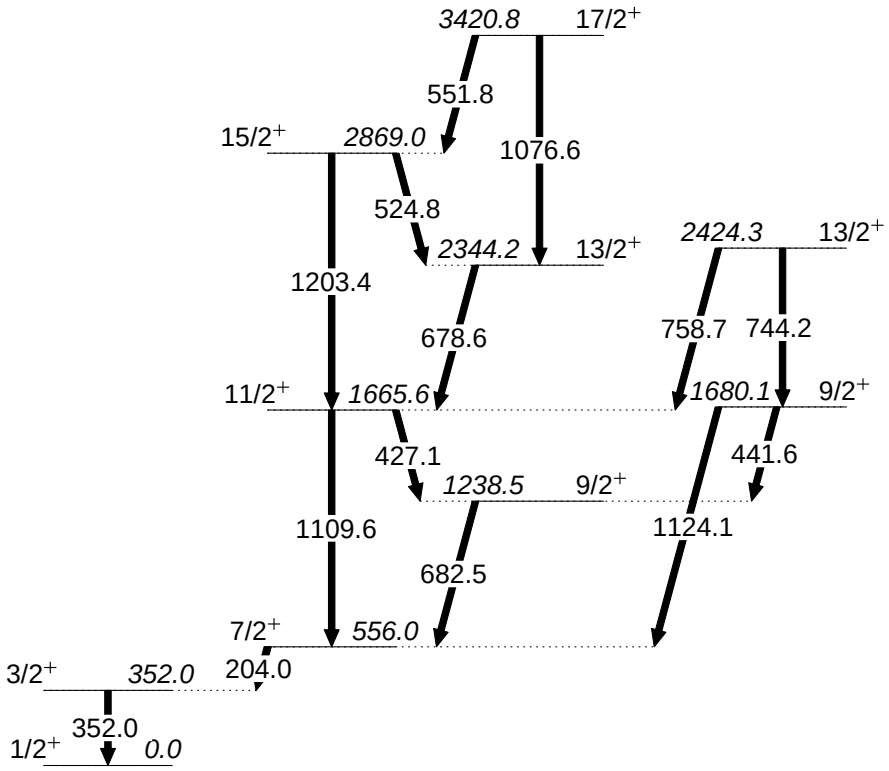

Figure 4.11: The partial level scheme of ^{95}Sr with the measured spins and parities established by measuring the transition multipolarities.

5/2, or 7/2.

From the decay pattern going up the band built on the 556.0 keV level, with a series of crossover transitions characteristic of a ΔI=1 rotational band, it is concluded that the spins increase by one going up the levels of this band. Therefore, the angular correlation between the 427.1-682.4 keV transitions is either 11/2→9/2→7/2, 9/2→7/2→5/2, or 5/2→3/2→1/2. The experimental result of the angular correlation can be used to rule out a spin of 1/2, as shown in figure 4.12. This figure shows the A_2 parameter as a function of $\tan^{-1}(\delta)$ for the three possible spin sequences, along with the A_2^{exp} for the 427.1-682.4 keV angular correlation. The A_4 values are not pictured because A_4=0 for all values of δ for these correlations. This figure demonstrates that

a spin of 1/2 is not consistent for the 556.0 keV level.

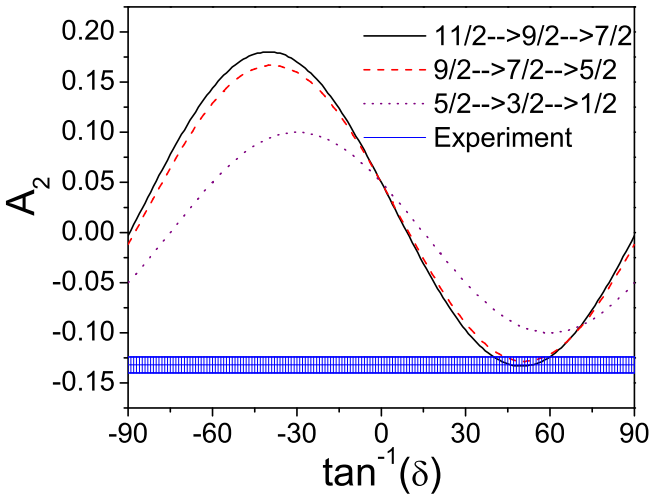

Figure 4.12: Angular correlation for the 427.1-682.4 keV cascade in ^{95}Sr.

To determine if the 556.0 keV level has a spin of 7/2 or 5/2, it is necessary to measure the mixing ratios of the ΔI=1 transitions above this level. As a starting point, it is assumed that the 1076.6 keV crossover transition is E2, as suggested by [28]. The 1076.6-678.6 keV angular correlation (figure 4.13) can then be used to determine the mixing ratio of the 678.8 keV transition. The experimental result of this angular correlation yields δ(E2/M1;679)=$2.6^{+0.4}_{-0.3}$. Comparing this value with the results of the 679-427 keV and 427-682 keV angular correlations (figure 4.14), the mixing ratios of the 679, 427, and 682 keV transitions can be determined. The results of this procedure are given in table IV.2, and the spin assignments for several of the levels are discussed in further detail below. It should be noted that for these

ΔI=1 transitions, the determination of the mixing ratios does not depend on the the absolute value of the spin.

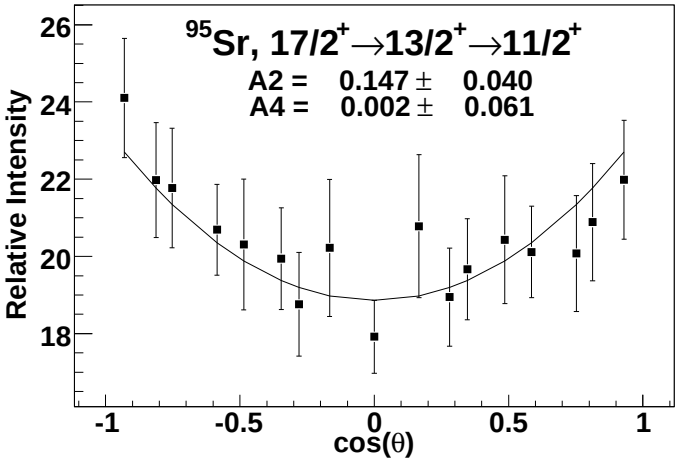

Figure 4.13: The angular correlation for the 1076.6 keV and 678.6 keV transitions in ^{95}Sr.

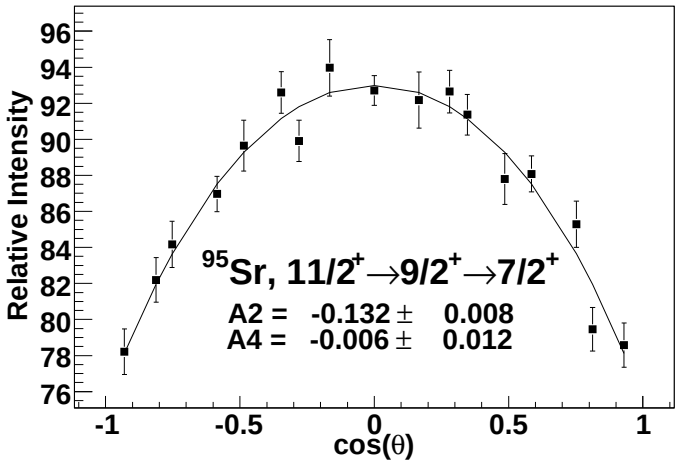

Figure 4.14: The angular correlation for the 427.2 keV and 682.5 keV transitions in ^{95}Sr.

With the mixing ratio of the 682.4 keV transition found to be δ(E2/M1;682.4)=$1.0^{+7.0}_{-0.8}$, the theoretical unattenuated angular correlation coefficients for the 682.4-204.0 keV angular correlation can be determined. The experimental values are A_2=0.095(11) and A_4=0.012(17). For a 9/2→7/2→3/2 cascade, A_2^{theory}=0.242 and A_4^{theory}=-0.031, in which case the cascade is highly attenuated as expected for a state with a 31.4 ns lifetime. For a 7/2→5/2→3/2 cascade, A_2^{theory}=0.089, A_4^{theory}=0.041. In this case, the measured correlation is nearly un-attenuated. Given the 31.4 ns lifetime of the state, it is unlikely that the correlation through this state is not attenuated. In fact, the g-factor would have to be very small (<<0.01) for this to be true. Therefore, the spin and parity of the 556.0 keV level are adopted as $7/2^+$, in agreement with the assignment proposed by [28]. The further spin-parity assignments and mixing ratio measurements are discussed in detail below.

1238.5 keV level: Beta decay measurements [37] found an 886 keV transition to the 352 keV level and used this as evidence that the 1238.5 keV level has spin≤7/2, but this transition is not seen in the present fission data, as discussed by [28]. However, the 1238.5 keV state does decay strongly to the $7/2^+$ state at 556.0 keV. Furthermore, the A_2 and A_4 coefficients are consistent with either an E2-E2 correlation or an E2/M1-E2 correlation. If the 682.4-204.0 keV correlation were E2-E2, the transitions could safely be assumed to be un-mixed, for which the A_2^{theory}=0.102 and A_4^{theory}=0.0091. Furthermore, if the state were of negative parity, then the 682.4 keV transition would be pure dipole, for which A_2^{theory}=-0.071 and A_4^{theory}=0.0, which is clearly in disagreement with the measured angular correlation. Therefore, the 1238.5 keV level is assigned $J^\pi=9/2^+$ and the 682.4 keV transition is mixed E2/M1 multi-

polarity, with δ(E2/M1;682)=$1.0^{+7.0}_{-0.8}$.

1680 keV level: The 1124-204 keV angular correlation yields A_2=0.119(28) and A_4=0.037(43). Hwang *et al.* proposed this level as either $9/2^+$ or $11/2^+$. If the level were $11/2^+$, the angular correlation would be consistent with a completely unattenuated, stretched E2 cascade. However, as mentioned above, the relatively long lifetime of the 556 keV level suggests that cascades through this level must be somewhat attenuated. Therefore, an assignment of $11/2^+$ for the 1680 keV level is not consistent with the observed correlation. If a level spin of $9/2^+$ is adopted, then the mixing ratio of the 682.4 keV transition is δ(E2/M1;682)=$1.0^{+7.0}_{-0.8}$.

Higher excited states: The spins and parities of the higher excited states in the ΔI=1 band built on the 556.0 keV level are assigned based on the 758.7-427.1 keV, 678.6-427.1 keV, 1203.4-427.1 keV, and 1076.6-678.6 keV angular correlations, all given in table IV.2. The spins and parities are chosen to be consistent with the result of all these correlations. In particular, the spin of the 2424.3 keV state, which is outside the band, is constrained to be $13/2^+$ from the 758.7-427.1 keV correlation. The resulting mixing ratios of all the transitions are also given in table IV.2.

4.5.2 The g-factor of the $7/2^+$ level

With the mixing ratio for the 682.4 keV transition fixed at δ(E2/M1;682)=1.0 and the 204 keV transition determined to be pure E2, the theoretical correlation coefficients for a $9/2^+ \rightarrow 7/2^+ \rightarrow 3/2^+$ cascade are A_2^{theory}=0.240, A_4^{theory}=-0.032, as discussed above. The experimental result for this correlation, shown in figure 4.15, is A_2^{exp}=0.095(11), A_4^{exp}=0.012(17), yielding G_2=0.396(46). Taking the hyperfine

field as 10(3)T [18] and the level lifetime as 31.3(7) ns, the g-factor of the state is $|g(7/2^+)|$=0.08(3).

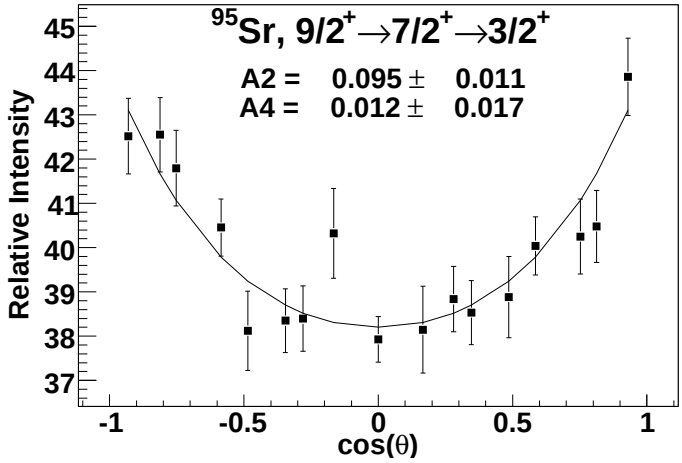

Figure 4.15: The angular correlation for the 682.4-204.0 keV cascade in ^{95}Sr. The unattenuated coefficients for this correlation are A_2=0.240 and A_4-0.032

4.6 Discussion

The bands in ^{93}Sr have been proposed to be based on νd5/2 hole-state weakly coupled to a ^{94}Sr core [27]. The spin assignments made in this work clearly do not agree with this interpretation. For further comparison, the mixing ratio of the $11/2^+ \rightarrow 9/2^+$, 1182.5 keV transition is compared to calculations from the particle-axial rotor model with Q_0=1.07, g_R=$0.5\frac{Z}{A}$, and g_k calculated from the matrix elements tabulated in [10] for beta$_2$=0.1. The result is $\delta_{calc}(1182.5)$=1.7, in clear disagreement with the measured value of $\delta_{exp}(1182.5)$=-0.97(14).

The proposed existence of a 3^- state in ^{94}Sr indicates the presence of an octupole

Table IV.2: Angular correlations measured for ^{93,94,95,98}Sr isotopes. The columns δ_1 and δ_2 refer to the mixing ratios of the first and second transition in the cascade, respectively. [a]This value is adjusted to the attenuation found from the 682-204 keV angular correlation to extract δ(E2/M1;1124.0).

Nucleus	Transitions (keV)	Cascade	A_2^{exp}, A_4^{exp}	δ_1	δ_2	A_2^{theory}, A_4^{theory}
^{93}Sr	793.7-986.1	9/2(1,2)9/2(2)5/2	0.167(23),0.044(35)	$-0.18^{+0.06}_{-0.05}$	0	0.172,0.066
^{93}Sr	1182.5-986.1	11/2(1,2)9/2(2)5/2	-0.190(36),0.009(54)	$-0.97^{+0.14}_{-0.14}$	0	-0.190,-0.002
^{94}Sr	1308.7-836.7	4(2)2(2)0	0.101(8),0.012(13)	0	0	0.102,0.091
^{94}Sr	1089.1-836.7	3(1,2)2(2)0	-0.052(9),0.007(13)	0.025(12)	0	-0.052,0.0
^{94}Sr	677.4-1089.1	4(1,2)3(1,2)2	0.270(16),-0.036(24)	$-1.7^{+1.0}_{-0.5}$	0.025(12)	0.270,0.0
^{94}Sr	710.5-1308.7	5(1,2)4(2)2	-0.235(29),-0.062(44)	$-6.5^{+1.4}_{-2.4}$	0	-0.235,-0.057
^{94}Sr	1577.4-836.7	3(1,2)2(2)0	-0.083(32),-0.033(47)	-0.015(41)	0	-0.083,0.0
^{94}Sr	458.7-1308.9	4(1,2)4(2)2	-0.189(31),0.110(46)	$2.1^{+2.9}_{-0.7}$	0	-0.177,0.123
^{94}Sr	502.7-1308.9	3(1,2)4(2)2	0.177(51),-0.128(77)	$-4.9^{+1.4}_{-2.6}$	0	0.179,-0.178
^{94}Sr	1009.7-1308.9	6(2)4(2)2	0.082(17),0.012(25)	0	0	0.102,0.089
^{94}Sr	767.7-1308.9	7(1,2)6,4(2)2	-0.055(29),-0.046(44)	$0.026(46),13.5^{+21.9}_{-5.2}$	0	-0.055,-0.051
^{95}Sr	204.0-352.0	7/2(2)3/2(1,2)1/2	-0.021(7), 0.001(11)	0	–	–
^{95}Sr	682.4-204.0	9/2(1,2)7/2(2)3/2	0.095(11), 0.012(17)	$1.0^{+7.0}_{-0.8}$	0	0.240,-0.032
^{95}Sr	1124.0-204.0	9/2(1,2)7/2(2)3/2	0.119(28), 0.037(43)	$0.87^{+0.63}_{-0.37}$	0	0.243, -0.027[a]
^{95}Sr	427.1-682.4	11/2(1,2)9/2(1,2)7/2	-0.132(8), -0.006(12)	$0.00^{+0.09}_{-0.07}$	$1.0^{+7.0}_{-0.8}$	-0.132,0.0
^{95}Sr	758.7-427.1	13/2(1,2)11.2(1,2)9/2	0.185(25), 0.006(38)	$-3.8^{+0.8}_{-1.3}$,$-0.32^{+0.07}_{-0.08}$	$0.00^{+0.09}_{-0.07}$	0.185,0.0
^{95}Sr	678.6-427.1	13/2(1,2)11.2(1,2)9/2	-0.082(16), -0.013(24)	$2.6^{+0.4}_{-0.3}$	$0.00^{+0.09}_{-0.07}$	-0.082,0.0
^{95}Sr	1203.4-427.1	15/2(2)11/2(1,2)9/2	-0.058(23), -0.088(35)	0	$0.00^{+0.09}_{-0.07}$	-0.071,0.0
^{95}Sr	1076.6-678.6	17/2(2)13/2(1,2)11/2	0.147(40), 0.015(62)	0	$2.6^{+0.4}_{-0.3}$	0.141,-0.021
^{98}Sr	289.0 144.3	4(2)2(2)0	0.051(21), 0.034(32)	0	0	0.102,0.091

vibrational state. However, the evidence presented above demonstrates that the state is actually 3^+. The change in parity suggests that the structure of this state must be re-examined.

The band built on the 556.1 keV state in ^{95}Sr has been proposed as a 7/2[404] neutron coupled to the ^{94}Sr core. The spin assignments in this work support this assignment. The mixing ratio measured for the 682.4 keV transition is compared to a particle-axial rotor calculation by using the same parameters as ^{93}Sr, except the matrix element is now taken for an M1 transition in a 7/2[404] band. The resulting prediction of $\delta_{calc}(682.4)=2.0$ is in agreement with the measured value of $\delta(682.4)=1.0^{+7.0}_{-0.8}$. This calculation provides further evidence that this band is in fact built on the 7/2[404] Nilsson single-particle state.

CHAPTER V

PROPERTIES OF NEUTRON RICH, A≥100 NUCLEI.

5.1 Introduction

Neutron rich nuclei with A≥100 produced in spontaneous fission such as $^{102-108}$Mo, $^{106-112}$Ru, and $^{112-116}$Pd have protons occupying the πg9/2 orbital and neutrons filling the νh11/2 orbital. A shape transition from prolate to oblate has been predicted to occur as nucleons fill these shells. A calculation by Skalski, Mizutori, and Nazarewicz [26] indicated that this transition from prolate to oblate should occur around 68-70 for Mo isotopes, N=66 for Ru isotopes, and N=70 for Pd isotopes. The exact nature and location of this transition depends on the interplay between deformation and single particle effects. Complicating this picture is the proposed triaxial shape of some of the nuclei in this region.

Fission fragment spectroscopy has been the primary method employed for the experimental study of these nuclei. However, until now detailed angular correlations of non-yrast states have not been possible for many nuclei. Therefore, the magnetic properties of the nuclei in this region, such as E2/M1 mixing ratios and g-factors, are investigated in this work. Specifically, determination of mixing ratios from γ-band to ground-band transitions in these nuclei enriches the understanding of the triaxial and γ degrees of freedom in this region, and the mixing ratios of ΔI=1 transitions in odd-A nuclei can help distinguish between single particle states. Furthermore, the measurement of g-factors of excited states can give insight into the interplay between

the single-particle and collective properties that drive the shape transitions in this region.

As previously discussed, angular correlations from the year 2000 experiment involving states with relatively long lifetimes will be attenuated. In cases where the lifetime of the state is known, the g-factor can be determined from the attenuation. If the lifetime is short, the correlations will be unattenuated and can be used to determine level spins or transition multipolarities. For several cases in this work, angular correlations through a certain state are corrected for the known attenuation of correlations through that state. For example, in ^{106}Mo, the attenuation of correlations through the 2^+ state is measured from the $4^+ \rightarrow 2^+ \rightarrow 0^+$ cascade, and this attenuation is used to correct the $2^+_\gamma \rightarrow 2^+ \rightarrow 0^+$ and $3^+_\gamma \rightarrow 2^+ \rightarrow 0^+$ angular correlation coefficients in order to measure the mixing ratios of the $2^+_\gamma \rightarrow 2^+$ and $3^+_\gamma \rightarrow 2^+$ transitions.

5.2 $^{100-102}$Zr

The zirconium isotopes with A$\geq$100 are of interest because they represent the transition from the subshell closure at N=58 to the filling of the νh11/2 subshell and strong- to super-deformed ground states [3]. This is evidenced by the abrupt drop in 2^+ level energies, from 1750 to 1223 to 213 keV at ^{96}Zr, ^{98}Zr, ^{100}Zr, respectively. Another interesting aspect of the ^{100,102}Zr nuclei is the existence of excited low lying 0^+ states, with 0^+ states being the second and third excited states in ^{100}Zr, ^{102}Zr, respectively. This has been interpreted as evidence of shape coexistence in ^{100}Zr [38], [39], with the ground state being strongly prolate deformed and the first excited state spherical. The transition rates from states in the band built on the 0^+_2 state have

been used as a test of the configuration mixing between these two shapes [38]. The measurement of mixing ratios of transitions between analog states in these bands can provide a further test of the configuration mixing in ^{100}Zr.

The results of all the angular correlations measured in $^{100-102}$Zr are given in table V.1. The hyperfine field used for the zirconium isotopes is 25.60(1) T, taken from [18] for a room temperature foil. The level schemes of $^{100-102}$Zr are shown in figures 5.1, 5.2, and 5.3.

The g-factor of the 2^+ state in ^{100}Zr is measured from the 352.0-212.6 keV angular correlation. The half-life of the 2^+ state is 0.59(3) ns [35]. This gives a g-factor of $g(2^+)=0.30(8)$, which is in agreement with the value of $g(2^+)=0.30(3)$ measured by [40] and the value of $g(2^+)=0.22(5)$ measured by [41]. This agreement indicates that the hyperfine field adopted for Zr is correct.

The mixing ratio of the 849.9 keV transition from the 4_2^+ state in the spherical band to the 4_1^+ state in the deformed ground band is determined from the 849.9-352.0 keV angular correlation, given in table V.1 and shown in figure 5.4. From this correlation, δ(E2/M1;849.9)$=1.4^{+0.4}_{-0.2}$. To verify that the 849.9-352.0 keV angular correlation is not attenuated, the 497.0-352.0 keV angular correlation was measured. The result of $A_2=0.095(8)$, is consistent with an unattenuated correlation, for which $A_2=0.102$.

For ^{101}Zr, the mixing ratio of the 98.5 keV transition from the first excited state, as well as the attenuation of angular correlations through this state, are determined from the 309.9-97.8 (figure 5.5) and 222.9-97.8 keV angular correlations. In cases where the mixing ratio and attenuation are determined simultaneously from two correlations

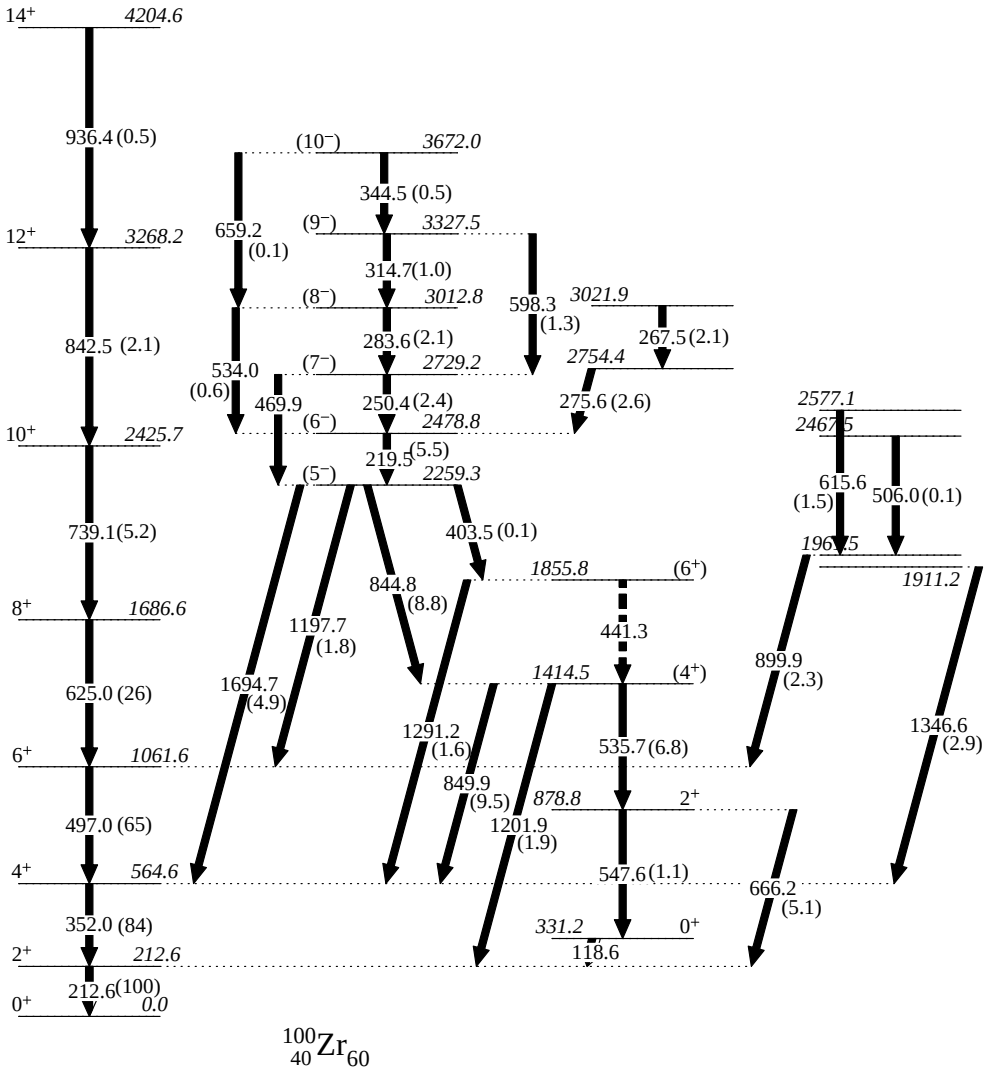

Figure 5.1: The level scheme of ^{100}Zr considered in this work.

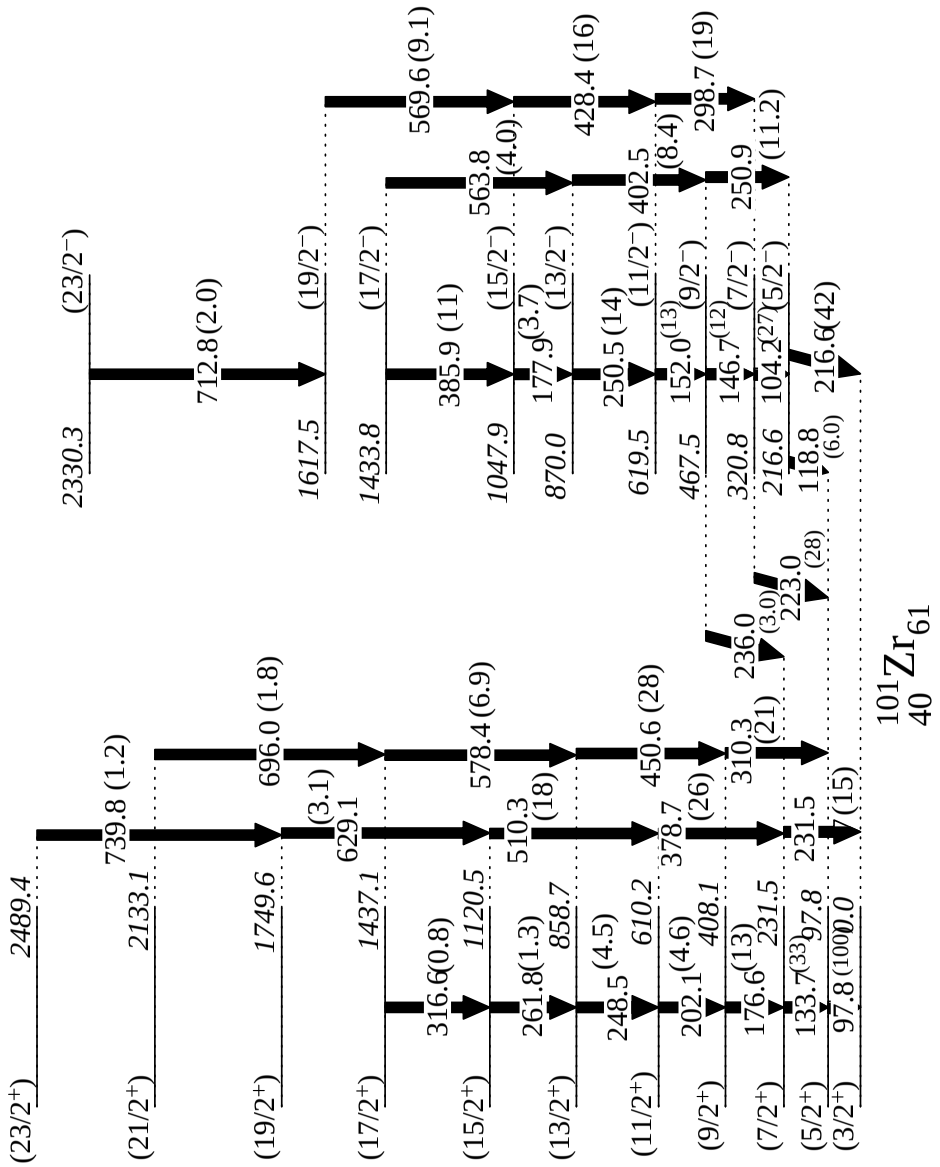

Figure 5.2: The level scheme of ^{101}Zr considered in this work.

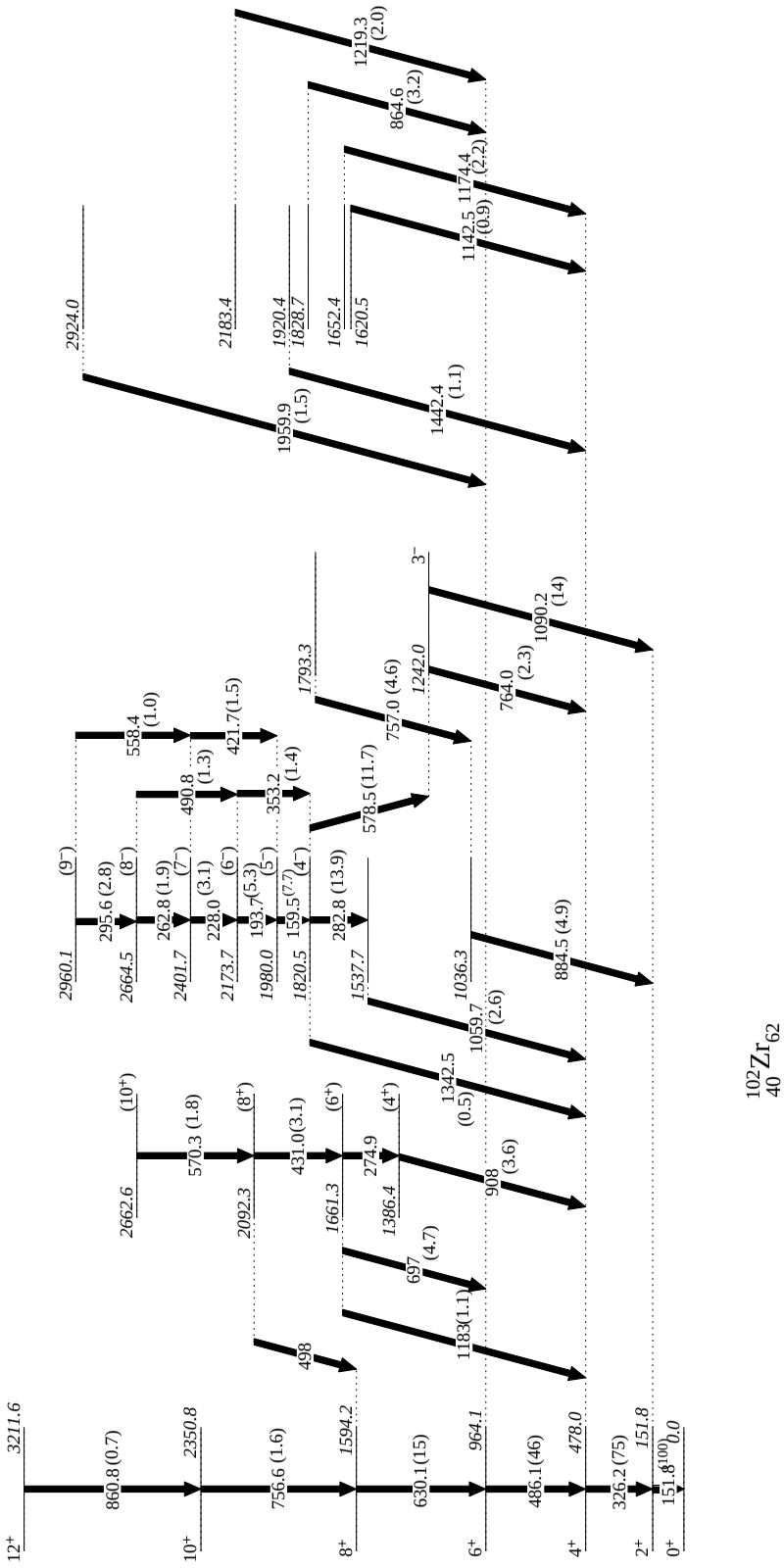

Figure 5.3: The level scheme of ^{102}Zr considered in this work.

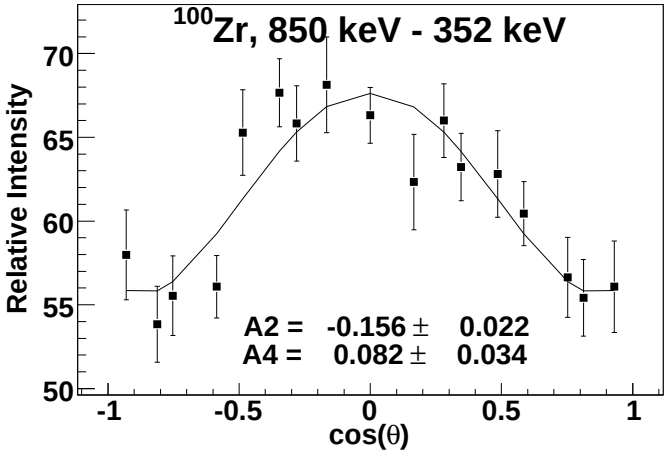

Figure 5.4: The $4^+_\gamma \rightarrow 4^+ \rightarrow 2^+$ angular correlation in ^{100}Zr, used to find the mixing ratio of the 849.9 keV transition.

with one transition in common, δ and the attenuation are found by minimizing the parameter ξ according to the equation

$$\xi = \frac{(A_2^a(\phi,\delta) - A_{2_{exp}}^a)^2 + (A_2^b(\phi,\delta) - A_{2_{exp}}^b)^2}{(\delta A_2^a)^2 + (\delta A_2^b)^2} \tag{5.1}$$

where δA$_2$ is the uncertainty from the angular correlation. The ϕ dependency of A$_2$ is taken into account by

$$A_2(\phi,\delta) = \frac{A_2(\delta)}{G_2(\phi)} \tag{5.2}$$

By using this procedure, it was determined that angular correlations through the first excited $7/2^+$ state are unattenuated. This is not surprising, given that Orlandi *et al.* [9] measured the g-factor of this state to be g=0.047(26). The lifetime of the state is only 0.6(2) ns, and the expected attenuation factor is then G$_2$=0.99, which is

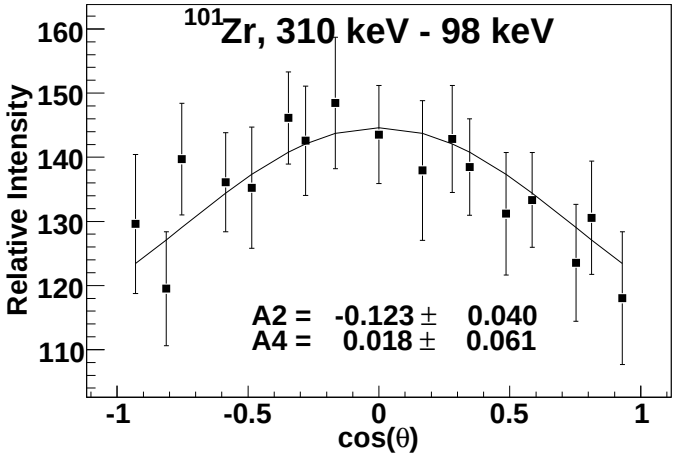

Figure 5.5: The 310-98 keV angular correlation in ^{101}Zr.

consistent with the measurement in this work.

The mixing ratio of the 97.8 keV transition is determined to be δ(E2/M1;97.8)=-$0.25^{+.16}_{-.26}$. This is consistent with the measurement by [9], who found δ(E2/M1;97.8)=-0.112(44). This agreement with previous results demonstrates the validity of this method of simultaneous determination of the attenuation and mixing ratio by using independent correlations.

For ^{102}Zr, the g-factor of the first 2^+ state was measured by using the 326.2-151.8 keV angular correlation. The half-life of the 2^+ state was taken from the NNDC [35] to be 1.91(25) ns. This gives a g-factor of g(2^+)=0.23(6). This is in excellent agreement with the value measured by [40] of 0.22(5).

The 1090.2-151.8 keV angular correlation measured for ^{102}Zr is used to assign the spin of the 1242.0 keV level. The result of this correlation is shown in table V.1. The correlation is consistent with an assignment of 1^- or 3^- for the 1242.0 keV level. Since 1^- states are usually not populated in the fission of ^{252}Cf, a spin of 3^- is adopted for

Table V.1: Angular correlations measured in this work for zirconium isotopes.

Correlation	Energies (keV)	A_2^{exp}, A_4^{exp}	Additional Gates
		^{100}Zr	
$4^+ \rightarrow 2^+ \rightarrow 0^+$	352.0-212.6	0.085(6), 0.010(10)	497,625,159,295,386
$6^+ \rightarrow 4^+ \rightarrow 2^+$	497.0-352.0	0.095(8), 0.013(13)	None
$4_2^+ \rightarrow 4_1^+ \rightarrow 2^+$	849.9-352.0	-0.156(22), 0.083(34)	None
		^{101}Zr	
$9/2^+ \rightarrow 5/2^+ \rightarrow 3/2^+$	309.9-97.8	-0.123(40), 0.019(61)	None
$7/2^- \rightarrow 5/2^+ \rightarrow 3/2^+$	222.9-97.8	0.105(32), 0.036(49)	None
		^{102}Zr	
$4^+ \rightarrow 2^+ \rightarrow 0^+$	326.2-151.8	0.056(7), 0.010(11)	486,630,159,295,382,118,284,258,410
$3^+ \rightarrow 2^+ \rightarrow 0^+$	1090.2-151.8	-0.075(14), -0.014(21)	None

this level.

5.3 $^{102-108}$Mo

The heavy molybdenum nuclei are expected from theory to be triaxial [42], [26], [43], and the observation of γ vibrational bands in ^{104,106,108}Mo provides experimental evidence for their triaxiality. Cranked Strutinsky calculations indicate that the transition from prolate to oblate should occur around N=68-70 in molybdenum nuclei, as do FRDM calculations [44]. To further determine the nature of these nuclei, the mixing ratios from the gamma-vibrational bands have been measured for $2_\gamma^+ \rightarrow 2_g^+$, $3_\gamma^+ \rightarrow 2_g^+$, and $4_\gamma^+ \rightarrow 4_g^+$. These measurements, when compared with similar measurements from the ruthenium and palladium isotopes, give a unique test of the changing shape and gamma softness over this region.

Several correlations were measured for ^{102}Mo, with the level scheme shown in figure 5.6. The $4^+ \rightarrow 2^+ \rightarrow 0^+$ angular correlation, shown in table V.2, demonstrates that the

2^+ state is unattenuated. The mixing ratios for the $4^+_\gamma \rightarrow 4^+$ and $3^+_\gamma \rightarrow 2^+$ transitions were determined from the 654.6-446.5 keV and 953.2-295.5 keV angular correlations, respectively, and are given in table V.2. The 1632.6-847.4 keV correlation from the 2481 keV level was used to determine the mixing ratio of the 1632.6 keV transition, which was found to be δ(E2/M1;1632.6)=0.27(4). Taking this into account with the 1632.6-551.5 keV angular correlation, the mixing ratio of the 551.5 keV transition is found to be δ(E2/M1;1632.6)=4.3(1.4), which is also consistent with the result from the 551.5-295.5 keV angular correlation. The results of these angular correlations are given in table V.2.

The level scheme for ^{103}Mo is shown in figure 5.7. The ground band in ^{103}Mo has been assigned as based on the 3/2[411] state, and an excited band has been identified as a 5/2[532] band [45]. Later work verified these assignments through g-factor and mixing ratio measurements [9]. In the present work, these assignments are checked by using the high statistics data from the 2000 experiment. Three angular correlations have been measured, one within the proposed 3/2[411] band, and two with the 251.2 keV crossover transition from the 5/2[532] band. These correlations are shown in table V.2. The g-factor of the 102.8 keV, $5/2^+$ state has been measured by [9] to be g=0.057(13). Given the half life of the state is 435(14) ps [35] and the hyperfine field is 27.4 T [18], angular correlations through this state are not expected to be attenuated. From the 251.2-102.8 keV angular correlation (figure 5.8), δ(E2/M1;102.8)=-0.19(5), which is in reasonable agreement with the value of -0.284(88) found by [9].

The attenuation of the $7/2^-$ state is found from the $11/2^- \rightarrow 7/2^- \rightarrow 5/2^+$, 144.3-251.2 keV angular correlation, which is pure Q-D. The g-factor is found to be g($7/2^-$)=-

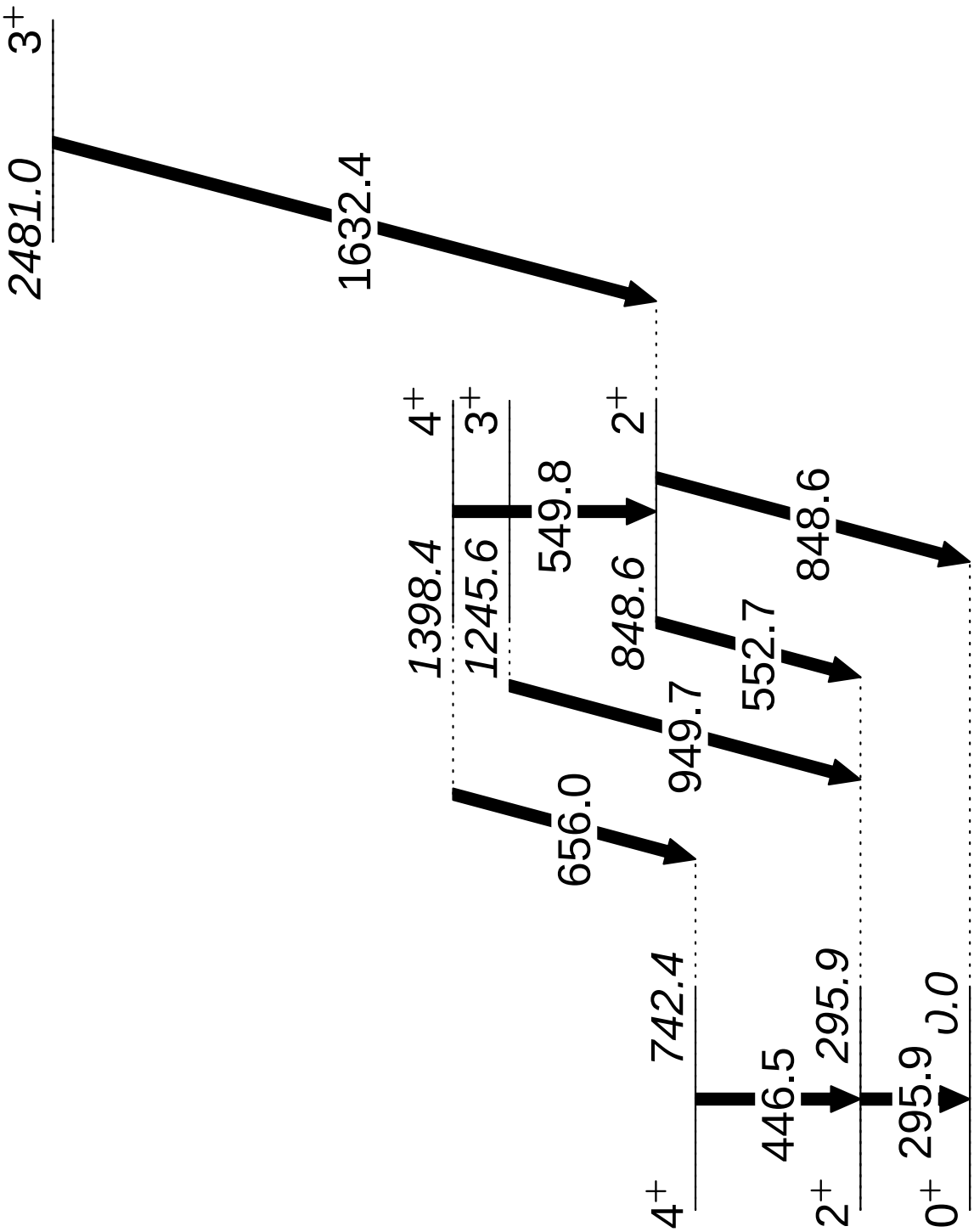

Figure 5.6: The level scheme of ^{102}Mo considered in this work.

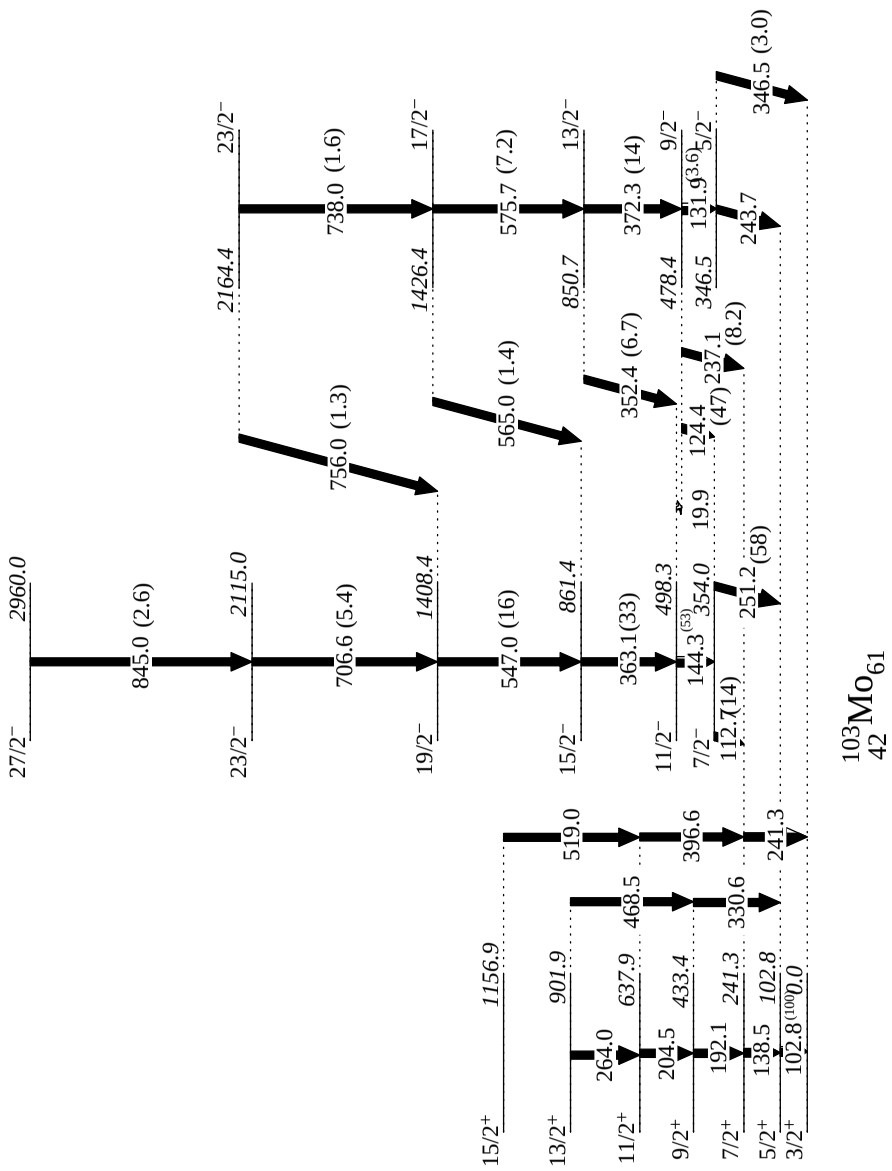

Figure 5.7: The level scheme of ^{103}Mo considered in this work.

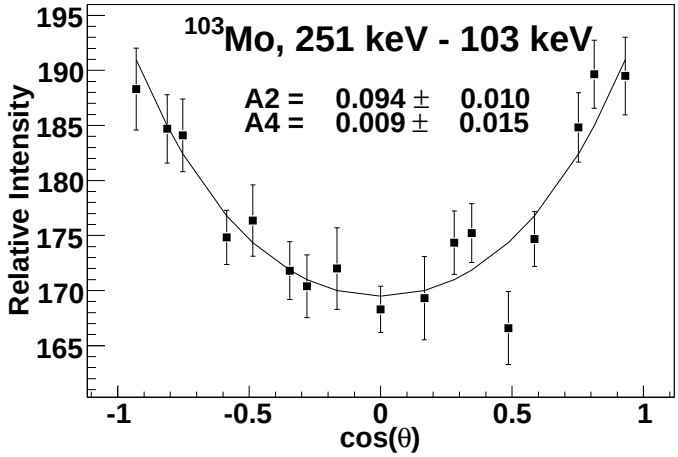

Figure 5.8: The 251-103 keV angular correlation in ^{103}Mo.

0.21(8), which is in general agreement with the previously measured value of g=-0.094(31) [9]. Note that [9] found this g-factor to be negative, and since the present method cannot be used to determine the sign, the negative value is adopted for g($7/2^-$).

The mixing ratio of the 124.7 keV transition in the proposed 5/2[532] band is found by using the 372.3-124.7 keV angular correlation, which is assumed to be unattenuated because of the relatively high energy (237.3 keV), and thus short lifetime, E1 decay of the $9/2^-$ state to the $7/2^+$ state in the ground band. The mixing ratio is determined to be δ(E2/M1;124.7)=-0.37(7). This mixing ratio is also consistent with the coefficients measured for the 124.7-251.2 keV angular correlation.

The level scheme of ^{104}Mo considered in this work is shown in figure 5.9. The g-factor of the 2^+ state has been measured by using the $4^+ \rightarrow 2^+ \rightarrow 0^+$ angular correlation with a state lifetime of 1.40(12) ns [35] and a hyperfine field of 25.60(1) T [18]. The mixing ratios of the $2^+_\gamma \rightarrow 2^+$, $3^+_\gamma \rightarrow 2^+$, and $4^+_\gamma \rightarrow 4^+$ transitions have been measured in

the present work by using the 620.0-192.0 keV, 835.6-192.0 keV, and 654.1-368.5 keV angular correlations, respectively, and are given in table V.2.

Two rotational bands have been identified in ^{105}Mo, with the ground band built on the 5/2[532] and an excited band built on the 3/2[411] configuration. The level scheme with these bands is shown in figure 5.10. Note that this is the opposite arrangement as in ^{103}Mo, indicating the evolution of the single particle levels with the changing shape. Correlations in this work are used to check the assignment of these levels through analysis of the mixing ratios and g-factors of levels in the ground band. The correlations measured for ^{105}Mo in this work are shown in figure V.2.

The g-factor of the $7/2^-$ state at 95.3 keV has been measured as -0.064(8), [9], and correlations through this state will not be attenuated. The mixing ratio of the 95.3 keV transition is found from the 283.2-95.3 keV angular correlation to be δ(E2/M1;95.3)=-0.20(6), in agreement with the value of δ(E2/M1;95.3)=-0.238(39) measured by [9]. The mixing ratio of the 138.3 keV transition is determined from the 390.6-138.3 keV angular correlation to be δ(E2/M1;138.3)=-0.25(4), in agreement with the value of -0.225(26) measured by [9].

The level scheme of ^{106}Mo is shown in figure 5.11. The g-factor was measured from the 350.6-171.5 keV angular correlation, with a 2^+ lifetime of 1.80(4) ns [35]. The mixing ratios of the $2^+_\gamma \rightarrow 2^+$, $3^+_\gamma \rightarrow 2^+$, and $4^+_\gamma \rightarrow 4^+$ transitions have been measured in the present work by using the 538.9-171.5 keV (figure 5.12), 713.4-171.5 keV, and 545.5-350.6 keV angular correlations, respectively.

For ^{107}Mo, the angular correlations measured in this work are consistent with the spin and parity assignments (shown in figure 5.13) of Urban *et al.* [46] rather

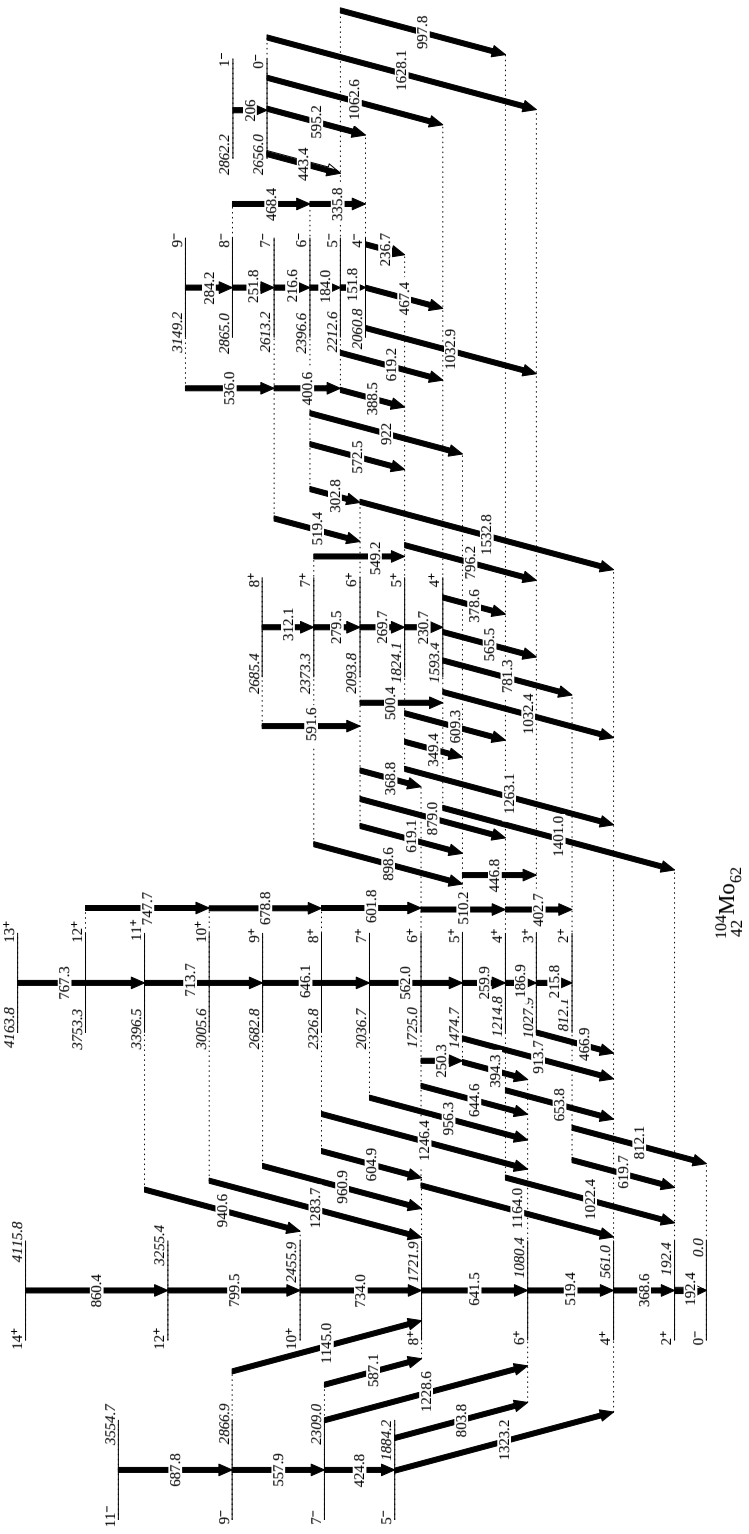

Figure 5.9: The level scheme of ^{104}Mo considered in this work.

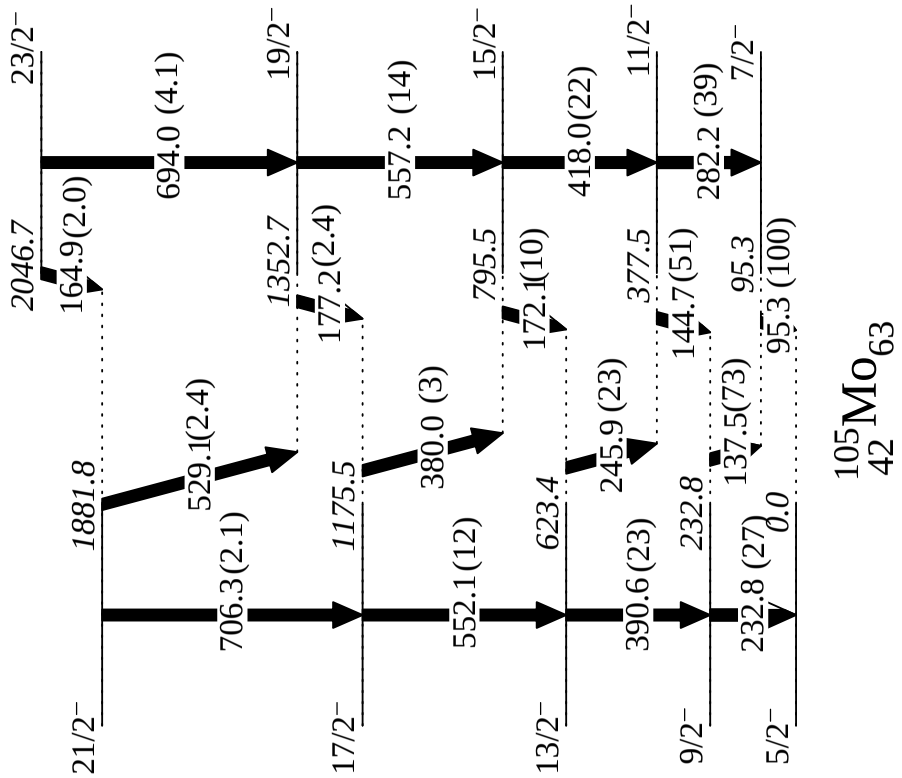

Figure 5.10: The level scheme of ^{105}Mo considered in this work.

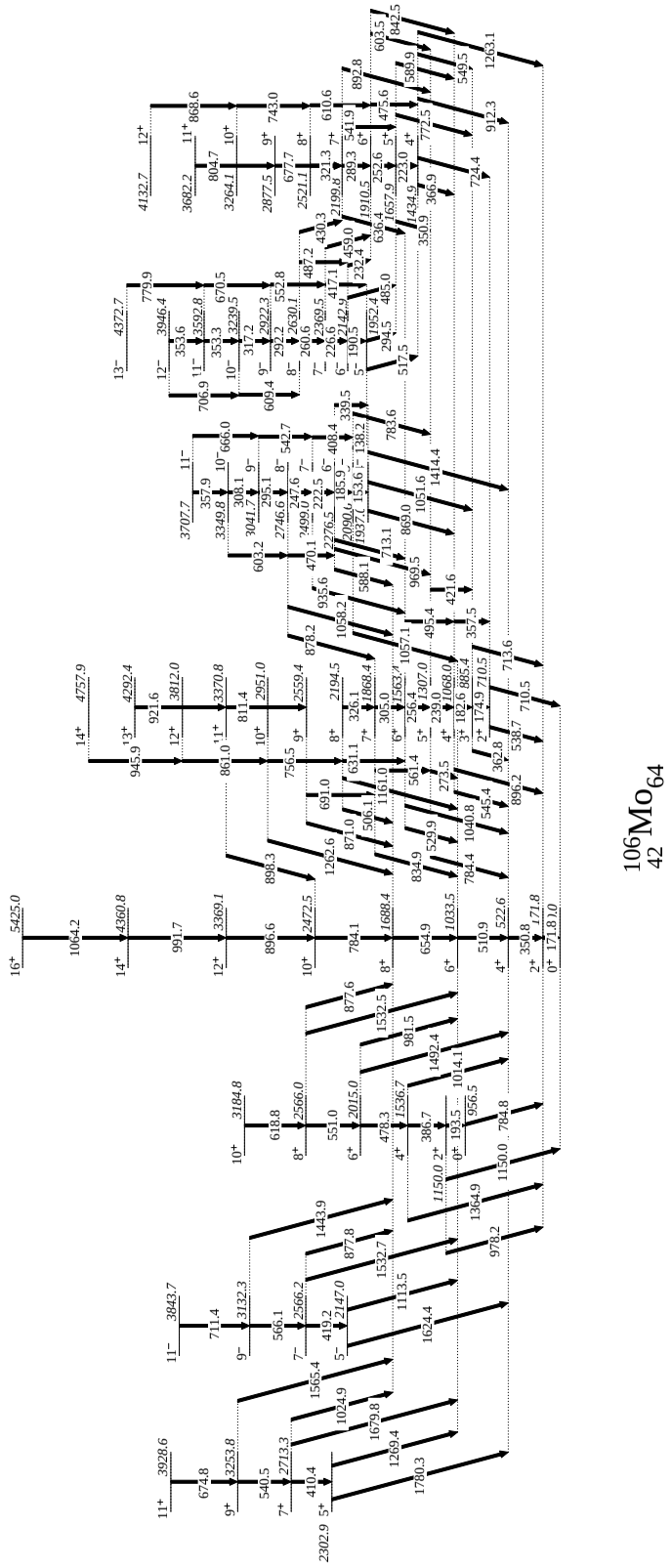

Figure 5.11: The level scheme of ^{106}Mo considered in this work.

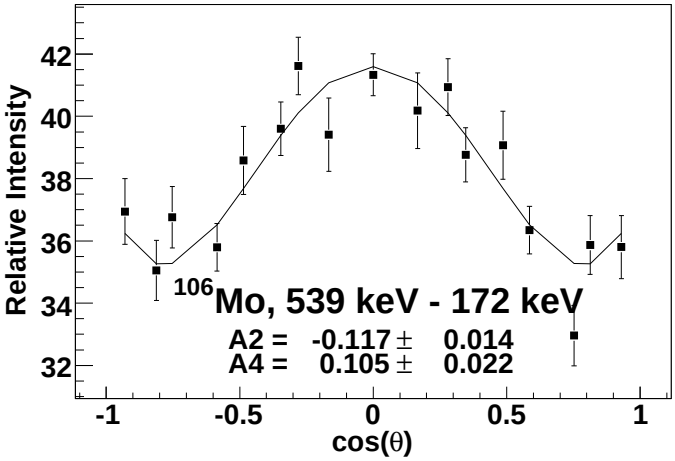

Figure 5.12: The 539-172 keV angular correlation in ^{106}Mo.

than the assignments of Hwang *et al.* [47], who did not have angular correlation information. The $11/2^+ \rightarrow 7/2^+ \rightarrow 5/2^+$ (415 keV-152 keV) and the $9/2^- \rightarrow 7/2^+ \rightarrow 5/2^+$ (306-415 keV) angular correlations were used to simultaneously determine the attenuation and mixing ratio using the method discussed above. It is found that the correlations are un-attenuated, and the mixing ratio of the 152.2 keV transition is δ(152.2;E2/M1)=-0.36$^{+9}_{-12}$. The $9/2^- \rightarrow 7/2^- \rightarrow 5/2^+$ (110-348 keV) angular correlation was measured to determine the mixing ratio of the 110.2 keV transition. The angular correlation was assumed unattenuated because of the relatively high energy of the 348.3 keV transition. The result of the angular correlation, shown in table V.2, gives δ(110.2;E2/M1)=-0.18(8).

The level scheme of ^{108}Mo is shown in figure 5.14. The g-factor of the 2^+ state was measured from the 370.9-192.7 keV angular correlation, with a 2^+ lifetime of 0.72(43) ns [35]. Note that the large uncertainty in the lifetime of the 2^+ state contributes to the large error in the g-factor quoted in table V.6. The mixing ratios $2^+_\gamma \rightarrow 2^+$,

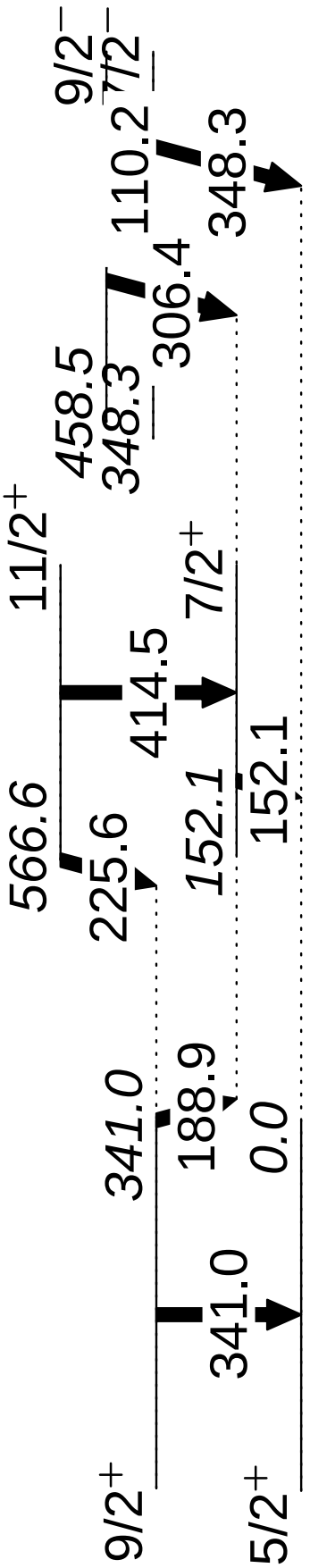

Figure 5.13: The level scheme of ^{107}Mo considered in this work.

$3^+_\gamma \rightarrow 2^+$, and $4^+_\gamma \rightarrow 4^+$ transitions have been measured with the 393.2-192.7 keV, 590.1-192.7 keV, and 414.6-370.9 keV angular correlations, respectively.

5.4 $^{108-112}$Ru

The g-factors of the first 2^+ states in ^{108,110,112}Ru have been measured for comparison with previous measurements. The mixing ratios of $2^+_\gamma \rightarrow 2^+$, $3^+_\gamma \rightarrow 2^+$, and $4^+_\gamma \rightarrow 4^+$ transitions have been measured for ^{108,110}Ru, and the mixing ratio of the $2^+_\gamma \rightarrow 2^+$ and $3^+_\gamma \rightarrow 2^+$ transitions have been measured for ^{112}Ru. The g-factor and mixing ratio measurements are discussed in section 5.6. The hyperfine field adopted for ruthenium isotopes is taken from [18] for a room temperature iron foil to be 48.4(10) T. All correlations are summarized in V.3. The mixing ratios and g-factors are discussed in the "Discussion" section. The level schemes of ^{108,110,112}Ru (figures 6.2, 6.6, and6.9) are given in the following chapter discussing the chiral nature of these nuclei.

The level scheme for ^{109}Ru is shown in figure 5.15. The mixing ratios of the $9/2^+ \rightarrow 7/2^+$ and $7/2^+ \rightarrow 5/2^+$ transitions have been measured. The result of the 472.8-185.1 keV angular correlation is δ(E2/M1;185.1)=-0.25(6). The result of the 541-223 keV angular correlation is δ(E2/M1;222.7)=-0.35(10). The result of the 223-185 keV (figure 5.16) angular correlation is also consistent with this result.

In ^{111}Ru, the angular correlations for the 166.6-150.2 keV, 103.8-150.2 keV, and 431.3-150.2 keV cascades were measured, with the results shown in V.3. The level scheme of ^{111}Ru considered in this work is shown in figure 5.17. These correlations are all consistent with δ(E2/M1;150.2)=-0.32(2). The 357.8-75.7 keV angular correlation

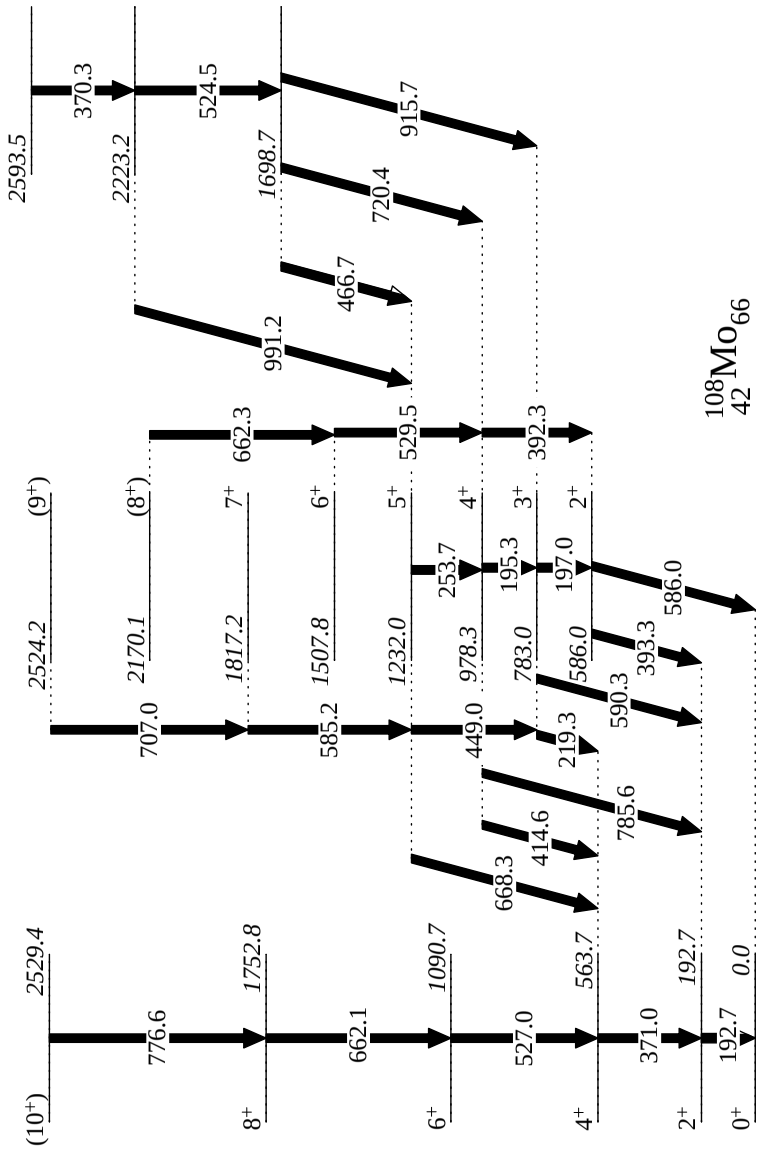

Figure 5.14: The level scheme of ^{108}Mo considered in this work.

Table V.2: Angular correlations measured in this work for molybdenum isotopes.

Correlation	Energies (keV)	A_2^{exp}, A_4^{exp}	Additional Gates (keV)
		^{102}Mo	
$4^+ \rightarrow 2^+ \rightarrow 0^+$	446.5-295.9	0.107(14), 0.010(21)	None
$2^+_\gamma \rightarrow 2^+ \rightarrow 0^+$	551.5-295.9	-0.153(11), 0.289(16)	None
$3^+_\gamma \rightarrow 2^+ \rightarrow 0^+$	953.2-295.9	0.240(38), -0.057(58)	None
$4^+_\gamma \rightarrow 4^+ \rightarrow 2^+$	654.6-446.5	-0.134(27), 0.113(41)	None
$3^+_2 \rightarrow 2^+_2 \rightarrow 0^+$	1632.6-847.4	0.117(23), -0.033(34)	None
$3^+_2 \rightarrow 2^+_2 \rightarrow 2^+$	1632.6-551.6	0.036(8), -0.013(12)	None
		^{103}Mo	
$7/2^- \rightarrow 5/2^+ \rightarrow 3/2^+$	251.2-102.8	0.094(10), 0.009(15)	144,363,547,707,125,327,199,113,181
$9/2^+ \rightarrow 5/2^+ \rightarrow 3/2^+$	330.7-102.8	-0.058(12), -0.001(19)	468,581,205,519,199,331,431,509,181,113
$11/2^- \rightarrow 7/2^- \rightarrow 5/2^+$	144.3-251.2	-0.054(13), 0.007(20)	103,353,363,547,707,113,199 331,181,431
$9/2^- \rightarrow 7/2^- \rightarrow 5/2^+$	124.7-251.2	0.251(40), -0.073(62)	None
		^{104}Mo	
$4^+ \rightarrow 2^+ \rightarrow 0^+$	368.5-192.0	0.082(5), 0.017(7)	519,642
$6^+ \rightarrow 4^+ \rightarrow 2^+$	519.4-368.5	0.096(6), 0.007(10)	None
$2^+_\gamma \rightarrow 2^+ \rightarrow 0^+$	620.0-192.0	-0.136(11),0.207(17)	771,478,241,403,510
$3^+_\gamma \rightarrow 2^+ \rightarrow 0^+$	835.8-192.0	-0.135(9), -0.051(19)	None
$4^+_\gamma \rightarrow 4^+ \rightarrow 2^+$	654.0-368.5	-0.136(14), 0.152(21)	192,510,199,331
		^{105}Mo	
$11/2^- \rightarrow 7/2^- \rightarrow 5/2^-$	283.2-95.3	-0.148(20), -0.003(31)	None
$13/2^- \rightarrow 9/2^- \rightarrow 7/2^-$	390.6-138.3	-0.171(14), -0.021(22)	None
$9/2^- \rightarrow 7/2^- \rightarrow 5/2^-$	138.3-95.3	0.325(14), -0.006(22)	None
$11/2^- \rightarrow 9/2^- \rightarrow 7/2^-$	145.2-138.3	0.230(26), -0.017(41)	None
$11/2^- \rightarrow 9/2^- \rightarrow 7/2^-$	245.7-145.2	0.299(26), -0.036(40)	None
$15/2^- \rightarrow 11/2^- \rightarrow 9/2^-$	418.0-145.2	-0.118(12), 0.000(18)	None
$11/2^- \rightarrow 9/2^- \rightarrow 5/2^-$	145.2-232.8	-0.160(28), 0.001(43)	None
$15/2^- \rightarrow 11/2^- \rightarrow 7/2^-$	418.0-283.2	0.082(11), 0.000(17)	None
		^{106}Mo	
$4^+ \rightarrow 2^+ \rightarrow 0^+$	350.6-171.5	0.053(5), 0.005(8)	118343,360,475,199,331,655,784
$6^+ \rightarrow 4^+ \rightarrow 2^+$	511.0-350.6	0.096(9), 0.012(13)	None
$2^+_\gamma \rightarrow 2^+ \rightarrow 0^+$	538.9-171.5	-0.117(14), 0.105(22)	118,343,360,475,199,331,724,518
$3^+_\gamma \rightarrow 2^+ \rightarrow 0^+$	713.4-171.5	-0.064(7), -0.035(11)	None
$4^+_\gamma \rightarrow 4^+ \rightarrow 2^+$	545.5-350.6	-0.157(14), 0.124(22)	172,118,199,359,496
		^{107}Mo	
$9/2^- \rightarrow 7/2^+ \rightarrow 5/2^+$	306.5-152.2	-0.194(23), 0.033(36)	None
$11/2^+ \rightarrow 7/2^+ \rightarrow 5/2^+$	414.6-152.2	0.148(20), -0.003(33)	None
$9/2^- \rightarrow 7/2^- \rightarrow 5/2^+$	110.3-348.3	0.138(25), 0.062(39)	None
		^{108}Mo	
$4^+ \rightarrow 2^+ \rightarrow 0^+$	370.9-192.7	0.089(10), 0.006(16)	527,662,415
$6^+ \rightarrow 4^+ \rightarrow 2^+$	527-370.9	0.069(17), 0.009(25)	None
$2^+_\gamma \rightarrow 2^+ \rightarrow 0^+$	393.2-192.7	-0.021(11), 0.016 (24)	199,331,431
$3^+_\gamma \rightarrow 2^+ \rightarrow 0^+$	590.1-192.7	-0.106 (57), 0.048 (100)	449,359
$4^+_\gamma \rightarrow 4^+ \rightarrow 2^+$	414.6-370.9	-0.167 (34), 0.024 (61)	193,359,530

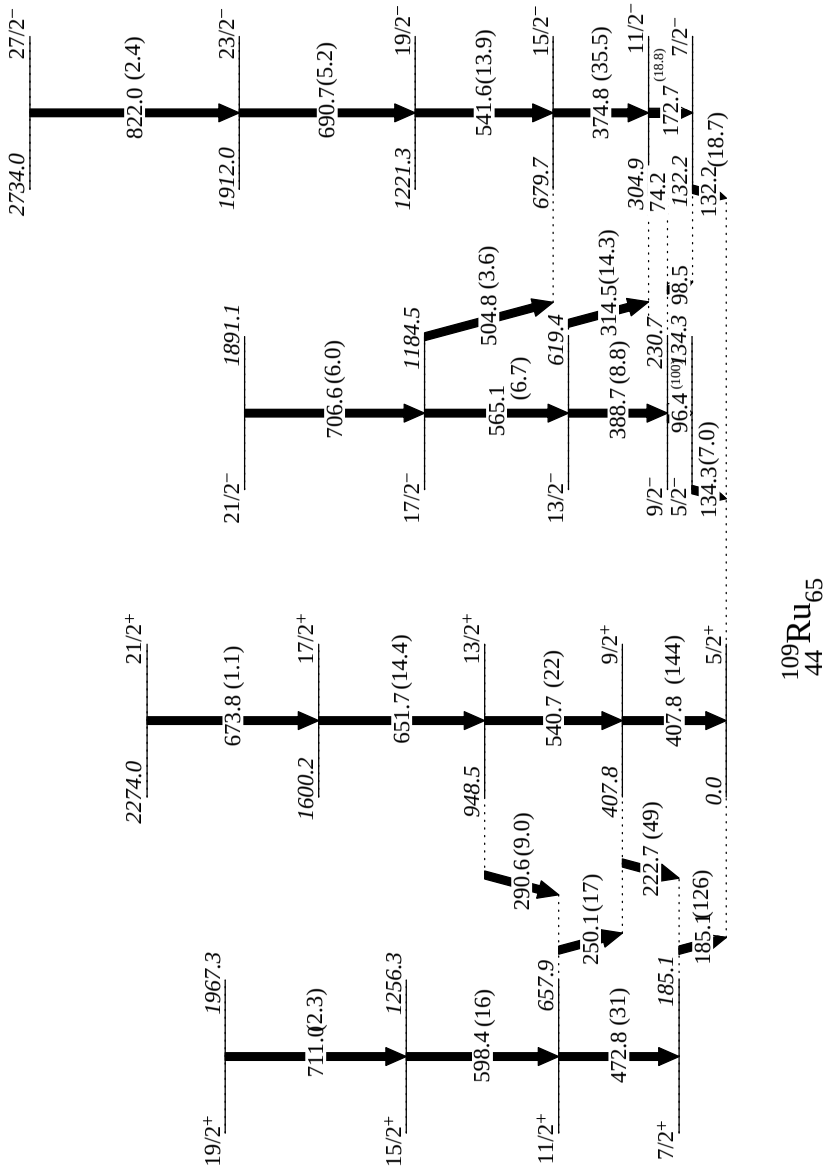

Figure 5.15: The level scheme of ^{109}Ru considered in this work.

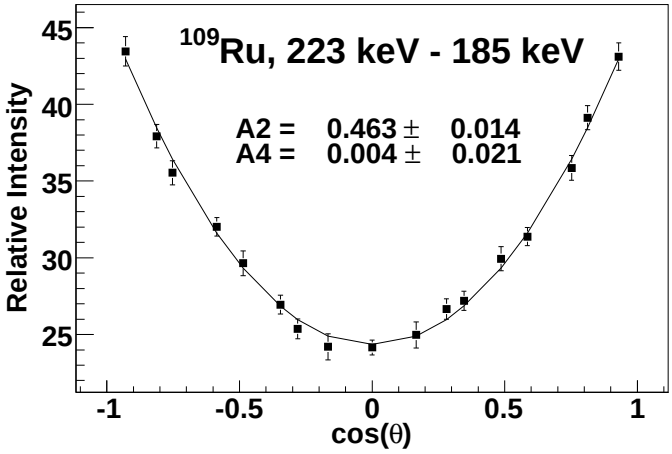

Figure 5.16: The 223-185 keV angular correlation in ^{109}Ru.

was also measured, from which δ(E2/M1;75.7)=-0.05(5).

5.5 ^{112,114,116}Pd

The lifetimes of 2^+ states in the Pd isotopes are short, so the angular correlations involving these states are not attenuated. The $4^+ \rightarrow 2^+ \rightarrow 0^+$ cascades in ^{112,114,116}Pd have been measured to verify that there is no attenuation in the angular correlations through the 2^+ states. The mixing ratios of gamma-band to ground band transitions are measured here and discussed in the next section. As an example of the unattenuated correlations in the palladium isotopes, the $2^+_\gamma \rightarrow 2^+ \rightarrow 0^+$ angular correlation for ^{114}Pd is shown in figure 5.18. The level schemes for ^{112,114,116}Pd are shown in figures 5.19, 5.20, and 5.21, respectively.

The mixing ratios of the $2^+_\gamma \rightarrow 2^+$, $3^+_\gamma \rightarrow 2^+$, and $4^+_\gamma \rightarrow 4^+$ transitions have been measured for ^{112,114}Pd, and of the $2^+_\gamma \rightarrow 2^+$ and $3^+_\gamma \rightarrow 2^+$ transitions for ^{116}Pd. These are the first measurements of mixing ratios of transitions in these isotopes and reveal

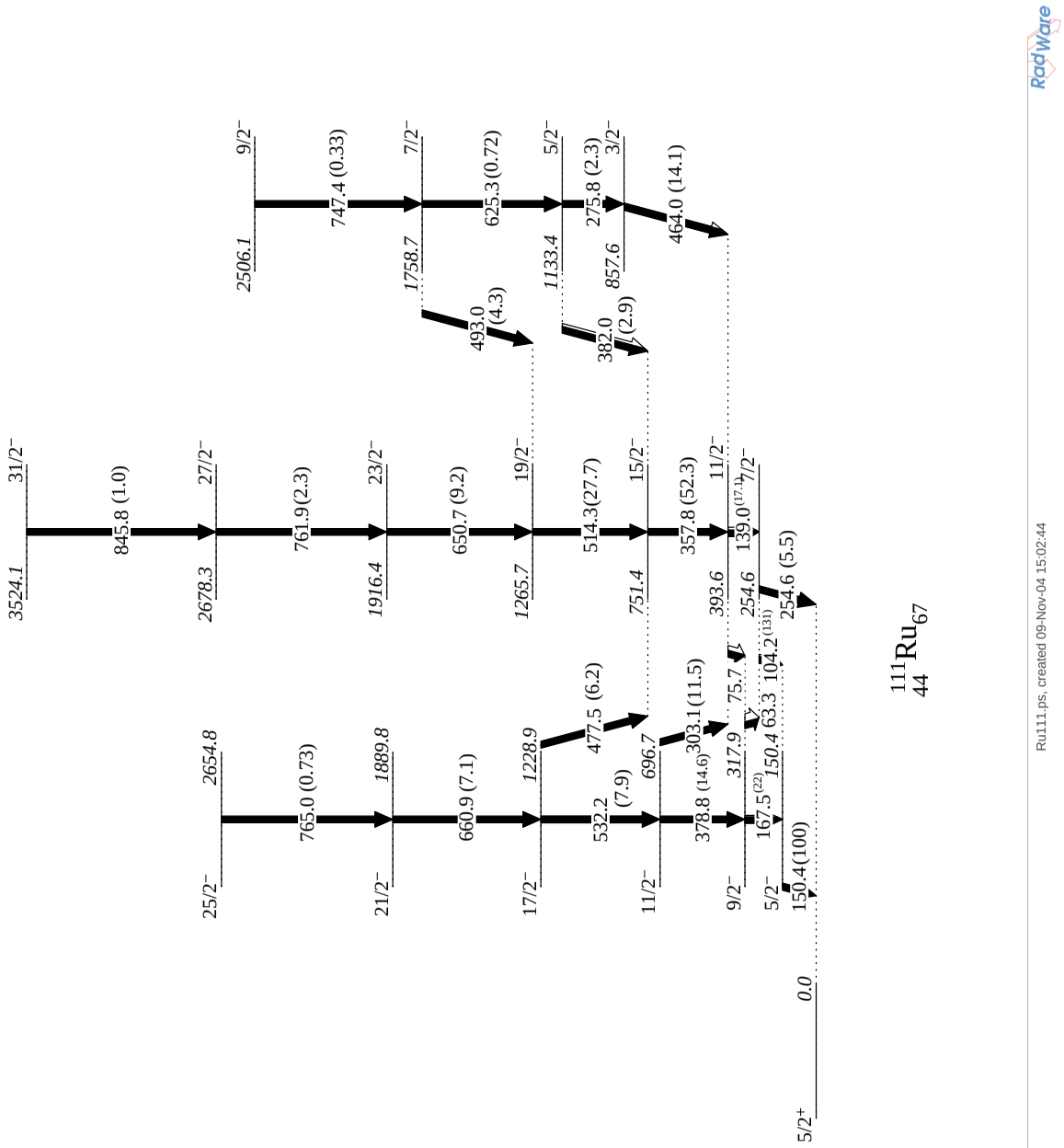

Figure 5.17: The level scheme of ^{111}Ru considered in this work.

Table V.3: Angular correlations measured for transitions in the ruthenium isotopes

Correlation	Energies (keV)	A_2^{exp}, A_4^{exp}	Additional Gates
		^{108}Ru	
$4^+ \rightarrow 2^+ \rightarrow 0^+$	422.5-242.1	0.071(6), -0.001(9)	None
$6^+ \rightarrow 4^+ \rightarrow 2^+$	574.6-422.5	0.090(11), 0.014(17)	None
$2^+_\gamma \rightarrow 2^+ \rightarrow 0^+$	465.8-242.1	0.083(15), 0.222(22)	267,475,1118,579
$3^+_\gamma \rightarrow 2^+ \rightarrow 0^+$	732.5-242.1	-0.193(8), 0.001(12)	None
$4^+_\gamma \rightarrow 4^+ \rightarrow 2^+$	517.9-422.5	-0.169(26), 0.055(40)	243,579
		^{109}Ru	
$13/2^+ \rightarrow 9/2^+ \rightarrow 7/2^+$	541-223	-0.200(26), -0.028(40)	185,652,377,458,484,589,571,
$9/2^+ \rightarrow 7/2^+ \rightarrow 5/2^+$	223-185	0.463(14), 0.004(20)	250,541,598,290,652,377,548,484,571,589
$11/2^+ \rightarrow 7/2^+ \rightarrow 5/2^+$	473-185	-0.164(18), 0.007(28)	290,598,652,377,458,572,589,484
		^{110}Ru	
$4^+ \rightarrow 2^+ \rightarrow 0^+$	422.2-240.7	0.081(7), 0.006(10)	705,815
$6^+ \rightarrow 4^+ \rightarrow 2^+$	575.9-422.2	0.090(11), 0.014(17)	None
$2^+_\gamma \rightarrow 2^+ \rightarrow 0^+$	372.0-240.7	0.067(11), 0.197(17)	247,472,515,600
$3^+_\gamma \rightarrow 2^+ \rightarrow 0^+$	618.7-240.7	-0.184(11), -0.075(17)	None
$4^+_\gamma \rightarrow 4^+ \rightarrow 2^+$	421.5-422.2	-0.183(17), 0.133(26)	241,600
		^{111}Ru	
$7/2^- \rightarrow 7/2^+ \rightarrow 5/2^+$	104-150	-0.367(12), 0.000(18)	None
$9/2^- \rightarrow 7/2^+ \rightarrow 5/2^+$	167-150	0.151(16), 0.028(24)	358,514,651,379
$11/2^+ \rightarrow 7/2^+ \rightarrow 5/2^+$	431-150	-0.205(37), -.055(57)	None
		^{112}Ru	
$4^+ \rightarrow 2^+ \rightarrow 0^+$	408.4-236.6	0.084(7), -0.005(10)	545,651,589,1220,1313,400,723,484
$6^+ \rightarrow 4^+ \rightarrow 2^+$	544.9-408.4	0.098(10), 0.024(15)	None
$2^+_\gamma \rightarrow 2^+ \rightarrow 0^+$	287.0-236.6	-0.041(14), 0.192(21)	224,457,589,488,693,1220,1313,400
$3^+_\gamma \rightarrow 2^+ \rightarrow 0^+$	510.8-236.6	-0.134(18), -0.067(28)	488,606,589,1313,1220
$5^+_\gamma \rightarrow 3^+_\gamma \rightarrow 2^+$	487.9-510.8	0.036(16), 0.014(24)	237,605,589,484,1220,400

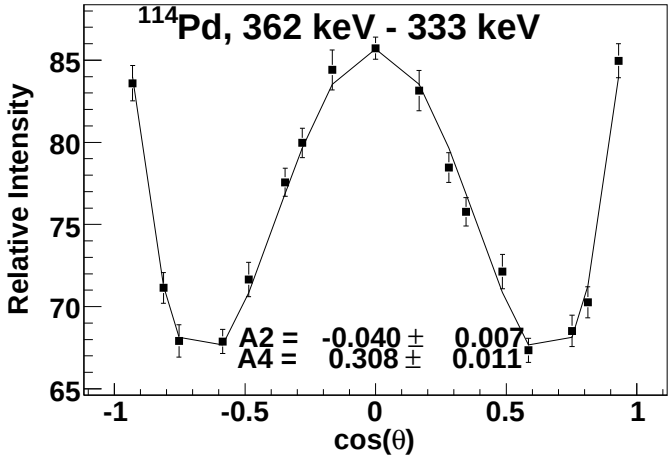

Figure 5.18: The $2^+_\gamma \rightarrow 2^+ \rightarrow 0^+$ angular correlation in ^{114}Pd.

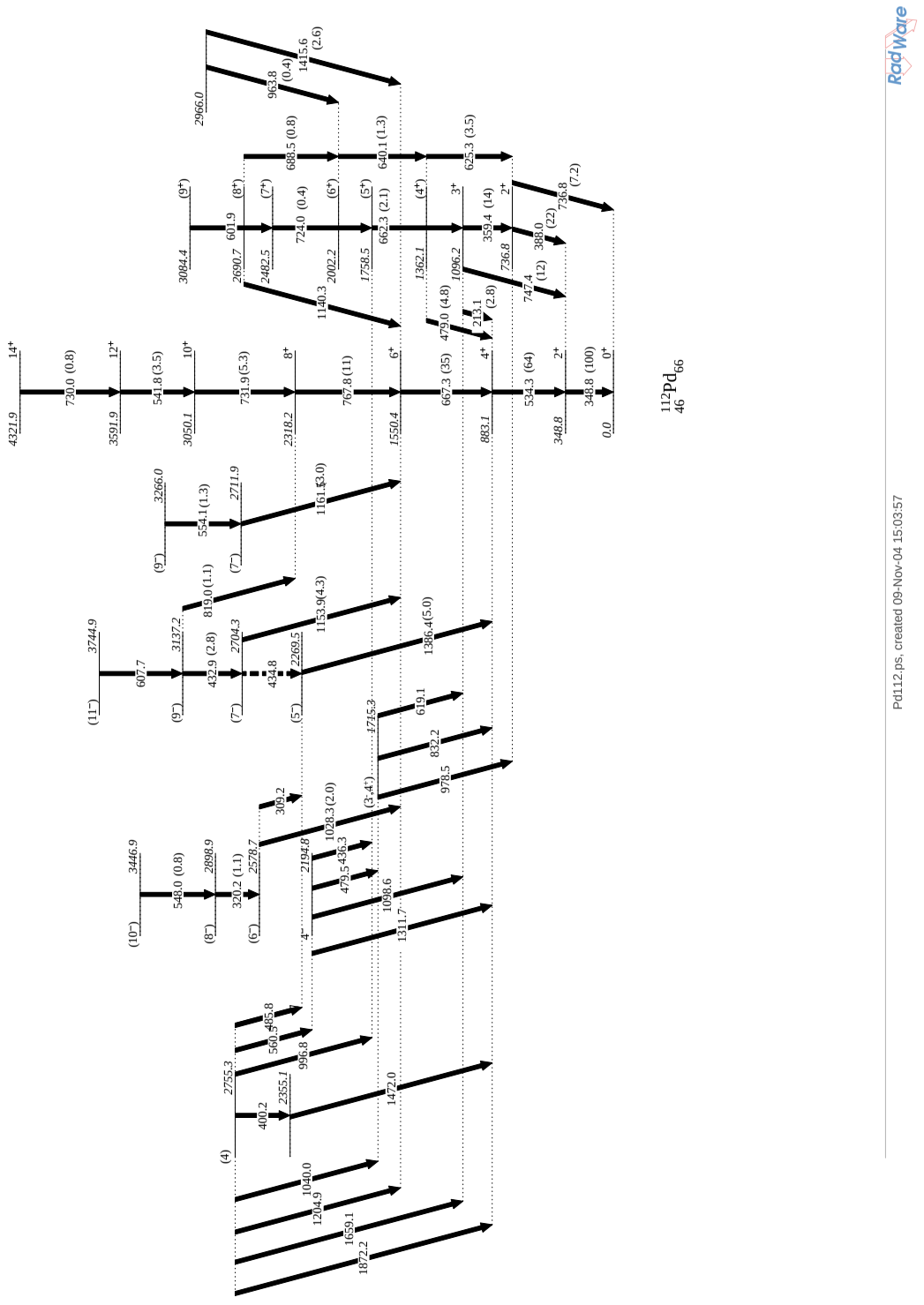

Figure 5.19: The level scheme of ^{112}Pd considered in this work.

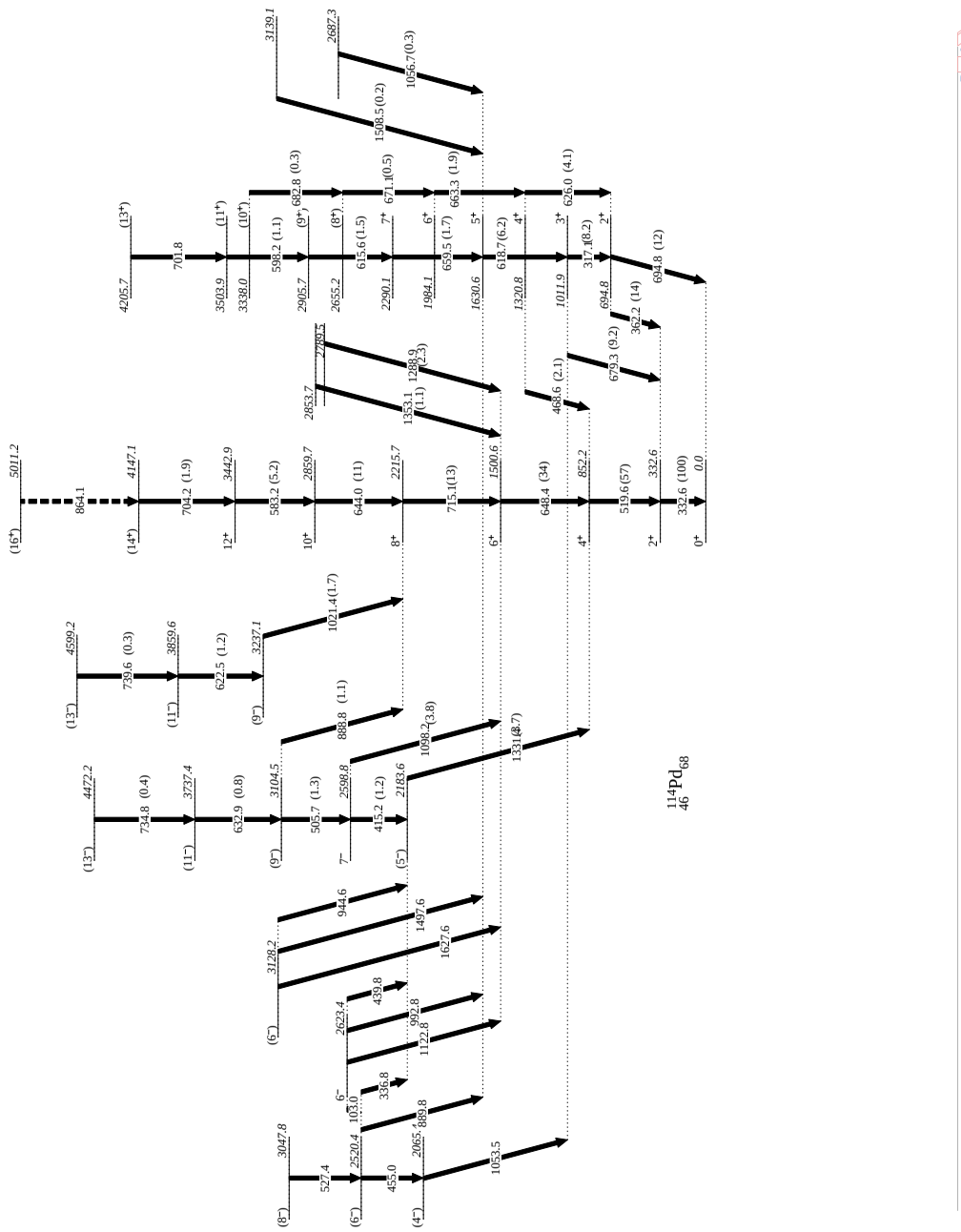

Figure 5.20: The level scheme of ^{114}Pd considered in this work.

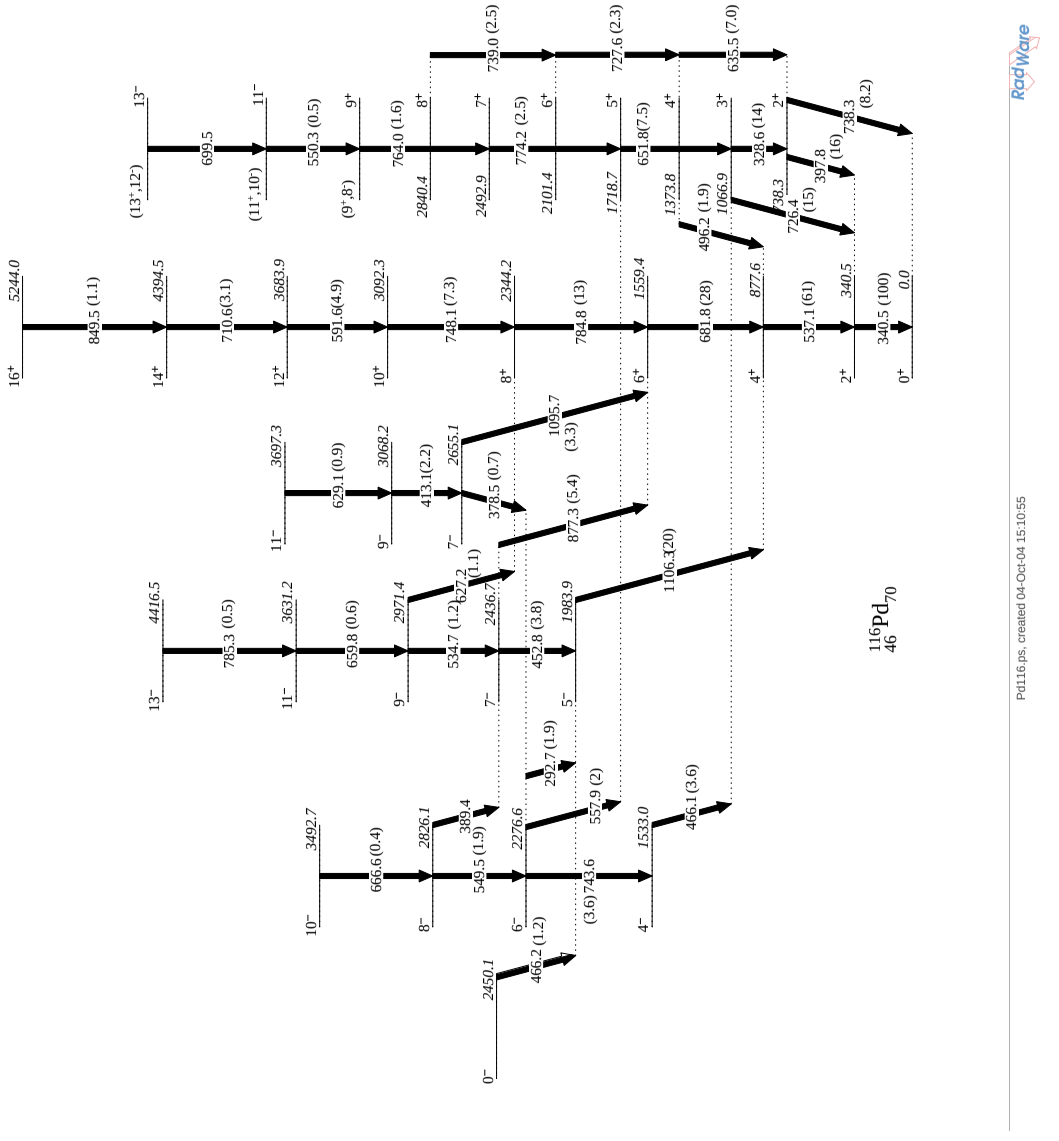

Figure 5.21: The level scheme of ^{116}Pd considered in this work.

an unexpected change in phase moving up the gamma-band, which will be discussed below. The angular correlations measured for the Pd isotopes are shown in table V.4.

Table V.4: Angular correlations in the palladium isotopes measured in this work.

Correlation	Energies (keV)	A_2^{exp}, A_4^{exp}	Additional Gates
		^{112}Pd	
$4^+ \rightarrow 2^+ \rightarrow 0^+$	534.3-348.8	0.098(7), 0.013(10)	667,768,732,1279,297,607,424
$2^+_\gamma \rightarrow 2^+ \rightarrow 0^+$	388.0-348.8	0.021(6), 0.298(9)	359,625
$3^+_\gamma \rightarrow 2^+ \rightarrow 0^+$	747.4-348.8	-0.472(15), -0.114(23)	None
$4^+_\gamma \rightarrow 4^+ \rightarrow 2^+$	479.0-534.3	-0.088(52), 0.162(77)	349,640
		^{114}Pd	
$4^+ \rightarrow 2^+ \rightarrow 0^+$	519.6-332.6	0.101(5), 0.013(8)	648,715,644,1279,297
$2^+_\gamma \rightarrow 2^+ \rightarrow 0^+$	362.2-332.6	-0.040(7), 0.308(11)	317,626,619,1279,297
$3^+_\gamma \rightarrow 2^+ \rightarrow 0^+$	679.3-332.6	-0.376(11), -0.075(18)	619,660,616,297,1279
$4^+_\gamma \rightarrow 4^+ \rightarrow 2^+$	468.6-519.6	-0.179(65), 0.022(98)	333,664
		^{116}Pd	
$4^+ \rightarrow 2^+ \rightarrow 0^+$	537.1-340.5	0.096(7), 0.025(11)	682,785,748,1106,1279,297,1151
$2^+_\gamma \rightarrow 2^+ \rightarrow 0^+$	397.8-340.5	-0.075(18), 0.297(27)	329,636,652,1279,297,1151
$3^+_\gamma \rightarrow 2^+ \rightarrow 0^+$	726.4-340.5	-0.261(20), -0.075(30)	None

5.6 Discussion

5.6.1 Single particle states in odd-N nuclei

The mixing ratios and g-factors measured for the odd-N nuclei are compared here in terms of the axial particle-rotor model, which is discussed in chapter II. In order to interpret the mixing ratios of the ΔI=1 transitions within rotational bands, calculations were made for various single particle states and compared to experiment. The results are shown in table V.5. These calculations were made with Q_0 values from [26] and $g_R=\frac{1}{2}Z/A$. The matrix elements taken from [10] are for β=0.3. The value of β=0.3 was chosen based on the experimentally known quadrupole moments, given in table V.5

The neutron orbitals that are expected to be important in this region are the d5/2, g7/2, h11/2, and d3/2 orbitals. As seen in table V.5, the 3/2[411] single-particle state is seen in ^{101}Zr and ^{103}Mo, while the 5/2[532] state is seen in ^{103,105}Mo. For ^{107}Mo and ^{109,111}Ru, the 5/2[402] and 7/2[523] orbitals are observed. These results indicate that the h11/2 and g7/2 orbitals are the most important for the nuclei in this region.

5.6.2 Mixing ratios of γ-band to ground band transitions

The g-factors measured for 2^+ states are shown in table V.6, where they are compared to previous measurements. There is generally good agreement with previously measured values, with the two exceptions of ^{106}Mo and ^{108}Ru, both of which were

Table V.5: Experimental mixing ratios for ΔI=1 transitions within rotational bands of odd-A nuclei measured in this work. The experimental values are compared to the predictions of the particle-axial rotor model for various single particle states. The Q_0 values are taken from [26].

Nucleus	Transition (keV)	Orbital	Q_0	δ_{calc}	δ_{exp}
^{101}Zr	97.8	3/2[411]	3.01	-0.14	$-0.25^{+.16}_{-.26}$
^{101}Zr	97.8	3/2[422]	3.01	0.46	$-0.25^{+.16}_{-.26}$
^{101}Zr	97.8	3/2[402]	3.01	0.24	$-0.25^{+.16}_{-.26}$
^{103}Mo	102.8	3/2[411]	3.26	-0.16	-0.19(5)
^{103}Mo	102.8	3/2[422]	3.26	0.54	-0.19(5)
^{103}Mo	102.8	3/2[402]	3.26	0.27	-0.19(5)
^{103}Mo	124.7	5/2[532]	3.26	-0.16	-0.37(7)
^{105}Mo	95.3	5/2[532]	3.29	-0.13	-0.20(6)
^{105}Mo	138.3	5/2[532]	3.29	-0.18	-0.25(4)
^{107}Mo	152.2	5/2[413]	3.68	0.95	-0.36^{+9}_{-12}
^{107}Mo	152.2	5/2[402]	3.68	-0.24	-0.36^{+9}_{-12}
^{107}Mo	110.2	7/2[523]	3.68	-0.18	-0.18(8)
^{109}Ru	185.1	5/2[413]	3.34	1.09	-0.25(6)
^{109}Ru	185.1	5/2[402]	3.34	-0.26	-0.25(6)
^{109}Ru	222.7	5/2[413]	3.34	1.00	-0.35(10)
^{109}Ru	222.7	5/2[402]	3.34	-0.24	-0.35(10)
^{111}Ru	150.2	5/2[413]	3.36	0.87	-0.32(2)
^{111}Ru	150.2	5/2[402]	3.36	-0.22	-0.32(2)
^{111}Ru	75.7	7/2[523]	3.36	-0.09	-0.05(5)

measured by Smith *et al.* [40] with a similar IPAC technique. For ^{106}Mo and ^{108}Ru, Smith *et al.* used the average of the $4^+ \rightarrow 2^+ \rightarrow 0^+$ and $6^+ \rightarrow 4^+, 2^+ \rightarrow 0^+$ angular correlations to determine the g-factors of the 2^+ states, whereas in this work only the $4^+ \rightarrow 2^+ \rightarrow 0^+$ angular correlations are considered. This might explain the difference between these two measurements.

Table V.6: The g-factors of 2^+ states measured in this work compared to previously measured values.

Nucleus	$\tau(2^+)$ (ns)	B_{HF} (T)	g	Previously measured
^{100}Zr	0.85(4)	27.4(4)	0.33(7)	0.30(3) [40], 0.26(6) [30], 0.22(5) [41]
^{102}Zr	2.6(5)	27.4(4)	0.26(7)	0.22(5) [40]
^{104}Mo	1.40(12)	25.60(1)	0.22(4)	0.27(2) [40], 0.25(2) [48]
^{106}Mo	1.80(4)	25.60(1)	0.40(5)	0.21(2) [40]
^{108}Mo	0.72(43)	25.60(1)	0.32(25)	0.5(3) [40]
^{108}Ru	0.52(4)	48.4(10)	0.45(8)	0.23(8) [40]
^{110}Ru	0.43(3)	48.4(10)	0.39(10)	0.44(7) [40]
^{112}Ru	0.46(4)	48.4(10)	0.33(9)	0.45(5) [40]

Table V.7 shows the E2/M1 mixing ratios for transitions from the gamma band to the ground band for $^{102-108}$Mo, $^{108-112}$Ru, and $^{112-116}$Pd. In the cases where an infinity is given, this means that the transition is not distinguishable from pure quadrupole within one sigma errors. These are the first measurements for mixing ratios of gamma-band to ground band transitions in the neutron rich, A$\geq$100 isotopes and present a unique opportunity for the study of the structure of these nuclei.

An examination of table V.7 reveals the change in sign of the mixing ratios of the transitions for the $2^+ \rightarrow 2^+$ transitions above ^{110}Ru. As pointed out by K.S. Krane [49], the absolute sign of the mixing ratio is a matter of convention, but the relative sign

Table V.7: The mixing ratios of γ-band to ground band crossing transitions. Note that the given A_2 and A_4 values have been corrected by the attenuations found from the $4^+ \rightarrow 2^+ \rightarrow 0^+$ and $6^+ \rightarrow 4^+ \rightarrow 2^+$ correlations. [a]The $\delta(3^+ \rightarrow 2^+)$ was constrained by the result of the $5^+_\gamma \rightarrow 3^+_\gamma \rightarrow 2^+$ cascade for ^{112}Ru.

Nucleus	A_2	A_4	δ	A_2^{theory},A_4^{theory}
		$2^+_\gamma \rightarrow 2^+$		
^{102}Mo	-0.153(11)	0.289 (16)	$8.8^{+3.6}_{-2.1}$	-0.155, 0.322
^{104}Mo	-0.170 (14)	0.343 (28)	$7.2^{+1.4}_{-1.1}$	-0.169, 0.320
^{106}Mo	-0.225 (27)	0.309 (65)	$4.2^{+1.2}_{-0.8}$	-0.225, 0.309
^{108}Mo	-0.024 (13)	0.023 (34)	0.36(2)	-0.023, 0.038
^{108}Ru	-0.119 (21)	0.453 (45)	$17.3^{+\infty}_{-10.3}$	-0.118, 0.325
^{110}Ru	-0.085 (14)	0.328 (28)	$85.3^{+\infty}_{-53.2}$	-0.085, 0.326
^{112}Ru	-0.050(17)	0.305 (33)	$-27.9^{+10.8}_{-48.5}$	-0.050, 0.326
^{112}Pd	0.021 (6)	0.298 (9)	$-7.7^{+1.0}_{-1.1}$	0.022, 0.321
^{114}Pd	-0.040 (7)	0.308 (11)	$-20.3^{+4.5}_{-8.0}$	-0.040, 0.326
^{116}Pd	-0.075 (18)	0.297 (27)	$\gtrsim \pm 57$	-0.077, 0.327
		$3^+_\gamma \rightarrow 2^+$		
^{102}Mo	0.240 (38)	-0.057 (58)	$0.64^{+0.88}_{-0.17}$, 1.2(4)	0.245, -0.024 *or* 0.239, -0.047
^{104}Mo	-0.169 (11)	-0.085 (23)	$22.4^{+10.2}_{-5.3}$	-0.169, -0.081
^{106}Mo	-0.123 (13)	-0.103 (32)	$9.7^{+1.8}_{-1.3}$	-0.123, -0.081
^{108}Mo	-0.122 (66)	0.068 (115)	$-0.06(8), 10^{273}_{-5}$	-0.122,0.0 *or* -0.121, -0.081
^{108}Ru	-0.276 (11)	0.002 (24)	-0.27(2)	-0.276, -0.005
^{110}Ru	-0.233 (14)	-0.095 (28)	$-26.8^{+8.8}_{-25.5}$	-0.233, -0.082
^{112}Ru[a]	-0.163 (22)	-0.106 (44)	$19.2^{+22.1}_{-6.7}$	-0.163, -0.081
^{112}Pd	-0.472 (15)	-0.114 (23)	-2.3(4)	-0.469, -0.069
^{114}Pd	-0.376 (11)	-0.075 (18)	-4.2(3)	-0.376, -0.077
^{116}Pd	-0.261 (20)	-0.075 (30)	$-13.5^{+3.6}_{-7.5}$	-0.261, -0.081
		$4^+_\gamma \rightarrow 4^+$		
^{102}Mo	-0.134 (27)	0.113 (41)	$1.2^{+0.4}_{-0.2}$	-0.140, 0.091
^{104}Mo	-0.136 (14)	0.152 (21)	$1.4^{+\infty}_{-0.3}$	-0.152, 0.099
^{106}Mo	-0.157 (14)	0.124 (22)	$1.6^{+.4}_{-.2}$	-0.163, 0.107
^{108}Mo	-0.167 (34)	0.024 (61)	$1.4^{+1.2}_{-0.3}$	-0.151, 0.098
^{108}Ru	-0.192 (30)	0.076 (56)	$1.9^{+2.1}_{-0.5}$	-0.174, 0.119
^{110}Ru	-0.208 (19)	0.185 (30)	$3.0^{+4.3}_{-1.3}$	-0.177, 0.137
^{112}Pd	-0.088 (52)	0.162 (77)	$1.0^{+0.7}_{-0.3}$	-0.107, 0.074
^{114}Pd	-0.179 (65)	0.022 (98)	$1.4^{+5.2}_{-0.1}$	-0.154, 0.100

of the mixing ratios for gamma-band to ground band transitions should be constant moving up the gamma-band. Because the mixing ratio is proportional to the electric quadrupole operator, it is evident that the mixing ratio is related to the shape of the nucleus. Therefore, there is an indication that the change in *sign* of the mixing ratio corresponds to the change in *shape* of the nucleus that is expected to occur around ^{110,112}Ru.

The $\frac{\delta}{E}$ values measured in this work are plotted for the $2^+_\gamma \rightarrow 2^+$ transitions in figure 5.22 and for the $4^+_\gamma \rightarrow 4^+$ in figure 5.23. The experimental results in these plots are compared to the prediction of Greiner's model [6] for rotational (equation 2.15) and vibrational (equation 2.16) nuclei. Figure 5.22 shows that the molybdenum nuclei all have positive $2^+_\gamma \rightarrow 2^+$ transitions, while the ruthenium and palladium isotopes have shifted to negative values. The mixing ratios for ^{108,110}Ru are not shown in this plot because they are indistinguishable from pure quadrupole. As discussed above, this sharp change in the mixing ratios of nuclei moving away from the closed subshell at ^{98}Zr could be indicative of the shape transition discussed above.

Figure 5.23 indicates that, unlike the $2^+_\gamma \rightarrow 2^+$ transitions, the $4^+_\gamma \rightarrow 4^+$ transitions all have very similar and positive mixing ratios. This figure also seems to indicate that the nuclei become more rotational moving toward the midshell region. The differences in mixing ratios compared to the $2^+_\gamma \rightarrow 2^+$ transitions suggest that at higher spin and excitation energy, the ground state shape differences become less important. This could also be evidence that the lower states in the γ-band are somewhat mixed, while the higher states are more pure. The mixing ratios of the $3^+_\gamma \rightarrow 2^+$ transitions do not demonstrate a definitive trend. This may be because of the interplay between band

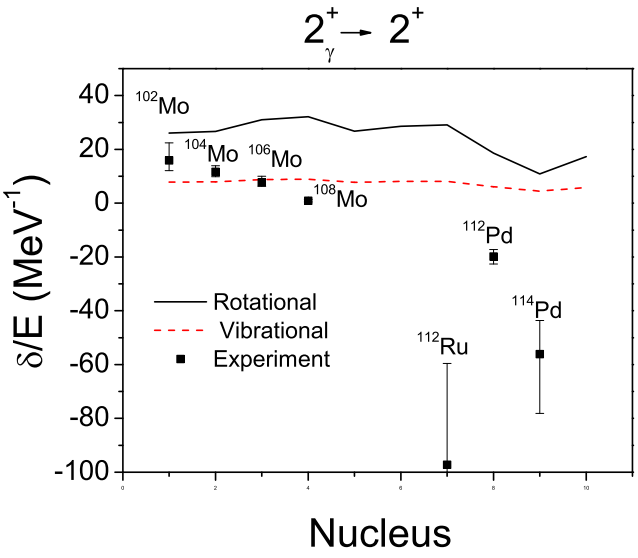

Figure 5.22: The mixing ratios of $2^+_\gamma \rightarrow 2^+$ transitions in A$\simeq$100 nuclei measured in this work compared to Greiners' theory [6] for rotational and vibrational nuclei. The sharp change from positive to negative values is seen at ^{112}Ru.

mixing and shape change moving up the γ-band.

Calculations by Skalski *et al.* [26] indicated that the transition from prolate to oblate should occur around ^{110,112}Ru, and the $2^+_\gamma \rightarrow 2^+$ mixing ratios measured in this work support this conclusion. However, they [26] also predicted that the palladium isotopes would be prolate up to N=70, but the mixing ratios suggest that this transition has already taken place at N=66.

5.7 Conclusions

The properties of nuclei in the A$\geq$100 region of neutron rich nuclei between the subshell closing at Z=40, N=58 and the doubly closed shell at Z=50, N=82 are determined by the filling of the πg9/2 and νh11/2 orbitals. The filling of these

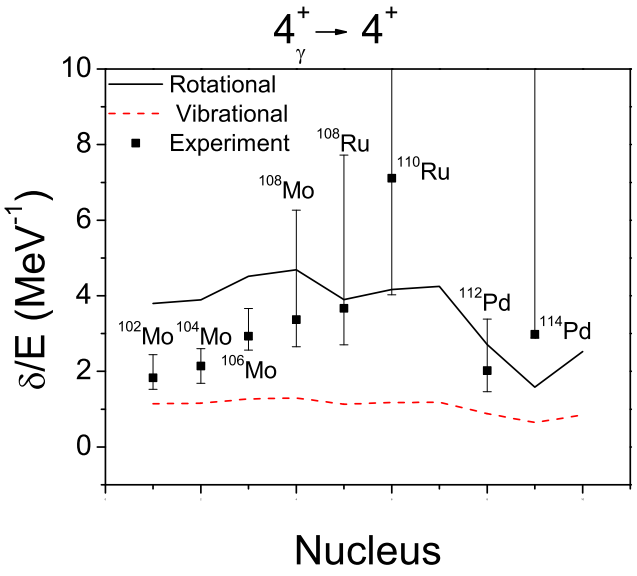

Figure 5.23: The mixing ratios of $4^+_\gamma \rightarrow 4^+$ transitions in A$\simeq$100 nuclei measured in this work compared to Greiners' theory [6] for rotational and vibrational nuclei. The change in phase is not seen for these transitions. There does seem to be a trend from vibrational to rotational going away from ^{98}Zr.

orbitals drives a shape change from prolate to oblate around ^{110}Ru, as evidenced by the change in phase of the $2^+_\gamma \rightarrow 2^+$ mixing ratios near this nucleus. Contrary to some previous predictions, the mixing ratios indicate that the ^{112,114,116}Pd nuclei have already shifted from prolate to oblate. The measurements of mixing ratios for gamma-band to ground-band transitions in this work are the first for these nuclei.

The determination of g-factors and mixing ratios in odd-N Zr, Mo, and Ru isotopes in this region is used to distinguish between single particle states via the axial particle-rotor model. From this, it is seen that the 3/2[411], 5/2[532], 5/2[402], and 7/2[523] neutron orbitals become more important with increasing proton and neutron number. This indicates that, although the νhll/2 orbital is important for nuclei in this region, the νg7/2 also plays a role in determining the structure of these nuclei.

CHAPTER VI

SPIN ASSIGNMENTS AND TRANSITION MULTIPOLARITIES IN CHIRAL BANDS IN ^{108,110,112}Ru

6.1 Introduction

Unlike molecules, nuclei were long thought to be achiral. However, Frauendorf and Meng [50] pointed out in 1997 that triaxial nuclei with significant components of angular momentum along the three principle axes could meet the conditions of nuclear chirality. The conditions they proposed are a particle in a high-j orbital along one axis, a hole in a high-j orbital aligned along another axis, and the rotational angular momentum along the third axis such that the total angular momentum is not aligned along any of the principal axes. This configuration is pictured in figure 6.1. The experimental signature for nuclear chirality is two sets of nearly degenerate odd-parity bands corresponding to the two-reflected orientations of the total angular momentum. This experimental signature of a pair of nearly degenerate in energy, ΔI=1 bands, has been found around ^{136}Nd [51] and ^{104,105,106}Rh [52], [53], [54]. Possible perturbed chiral bands related to γ-softness have also been proposed in ^{106}Ag [55].

If chirality is a global nuclear property, then it might be seen in odd-even or even-even nuclei. Chirality in an even-even nucleus was first proposed for ^{106}Mo by Zhu *et al.* [56], [43]. The chiral bands were interpreted as soft chiral vibrations with a complex structure where the configuration of quasi-neutrons nearly fills the

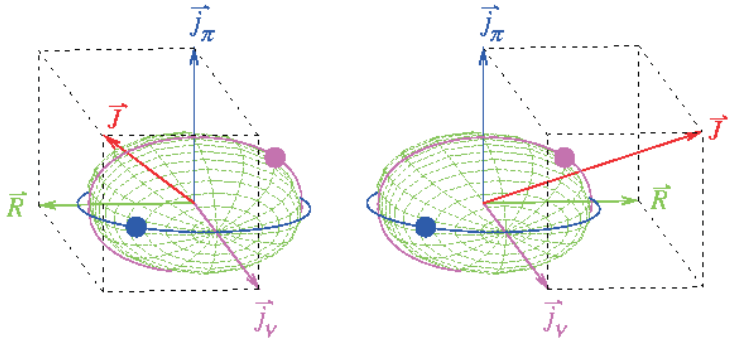

Figure 6.1: The possible alignments of the angular momentum vector in a chiral nucleus. The two alignments result in a pair of nearly degenerate odd-parity bands.

$g_{7/2}$ orbital (hole) and the $h_{11/2}$ orbital is just beginning to fill (particle). Recent theoretical calculations of all nuclei [57] found that nuclei around ^{108}Ru should have a deformed triaxial shape. The ^{108,110,112}Ru nuclei were searched by Luo *et al.* [58] for the chiral signature bands, and a set of nearly degenerate bands was found in each nucleus.

In order to determine if these bands are actually chiral bands, it is important to determine their spins and parities. If the bands are chiral, they will have odd-parity, so that the decays out of these bands to the gamma-band or ground-band will be pure or nearly pure dipole transitions. Therefore, angular correlations between crossover transitions from the proposed chiral bands and E2 transitions in the gamma-band or ground-band should be dipole-quadrupole. Angular correlations between dipole and quadrupole transitions give a unique signature, depending on the spin. Therefore, determining the dipole or quadrupole nature of the transitions depopulating the proposed bands is an important test of their chirality.

The energy difference between levels of the same spin in chiral bands, ΔE, is

another important test of chirality. In the ideal case, ΔE=0. Although this is not practically true for any proposed chiral nuclei, large values of ΔE might indicate that a pair of similar bands are not actually chiral bands. Besides ΔE, the signature splitting of the two chiral bands should be small. The signature splitting for a band is given by the equation

$$S(I) = \frac{[E(I) - E(I-1)]}{[E(I) - E(I-2)]} \times \frac{2I-1}{I} - 1 \tag{6.1}$$

As can be seen from this equation, the signature splitting depends on the spins of the levels, so it is important to determine the spins of the band-heads and other levels in the proposed chiral bands in order to see if the bands satisfy the requirement of signature splitting.

A similar value which has been used for comparison of chiral bands is

$$V(I) = \frac{E(I) - E(I-1)}{2I} \tag{6.2}$$

This value is given by Vaman *et al.* [52] as S(I), but to avoid confusion with the signature splitting, it will be referred to as V(I) in this work. Chiral bands should have a value of V(I) that is the same for the two doublet bands and constant with spin. By determining the spin and parity of the newly proposed levels in ^{108,110,112}Ru, the above tests for chirality can be made to see if the proposed bands are indeed chiral.

6.2 ^{108}Ru

The level scheme for ^{108}Ru is shown in figure 6.2. The proposed chiral doublets are bands 4-7. It is important to establish the spins of the proposed band-heads at 2424.5 and 2110.7 keV, and also determine if the 1445.5 and 1184.5 keV transitions are dipole, to indicate negative parity for the bands. Because these bands are not very strongly populated in fission, statistics for the angular correlations of interest are relatively low. However, four correlations were performed from levels in bands 5, 6, and 7. The results are listed in table VI.1.

Figure 6.3 shows the angular correlation between the 1445.5 keV transition depopulating band 7 and the $4^+ \rightarrow 2^+$ transition in the ground band. The result of this angular correlation, A_2=-0.080(10) and A_4=-0.001(16), indicates that it is a dipole-quadrupole transition, for which A_2^{theory}=-0.071 and A_4^{theory}=0. However, the spin can only be constrained to 3 or 5 from the angular correlation alone. To distinguish between these two, the 162.3-1445.5 keV angular correlation was measured, with the result shown in figure 6.4. The large absolute value of A_2 measured for this correlation is only consistent with a $5 \rightarrow 4 \rightarrow 4$ or a $6 \rightarrow 5 \rightarrow 4$. Therefore, from these results, the 2110.7 keV level is assigned as 5^- and the 2273.0 keV level is assigned 6^-.

With these level spins established, it is also possible to determine the mixing ratio of the 162.3 keV, $6^- \rightarrow 5^-$ transition. From the 162.3-1445.5 keV angular correlation, δ=-2.2(3) or δ=$-0.51^{+0.06}_{-0.08}$. In the paper by Frauendorf and Meng [50], equations for both the B(E2) and B(M1) were proposed. These strengths are dependent on the shape of the nucleus as well as the specific orbitals occupied by the particles and holes

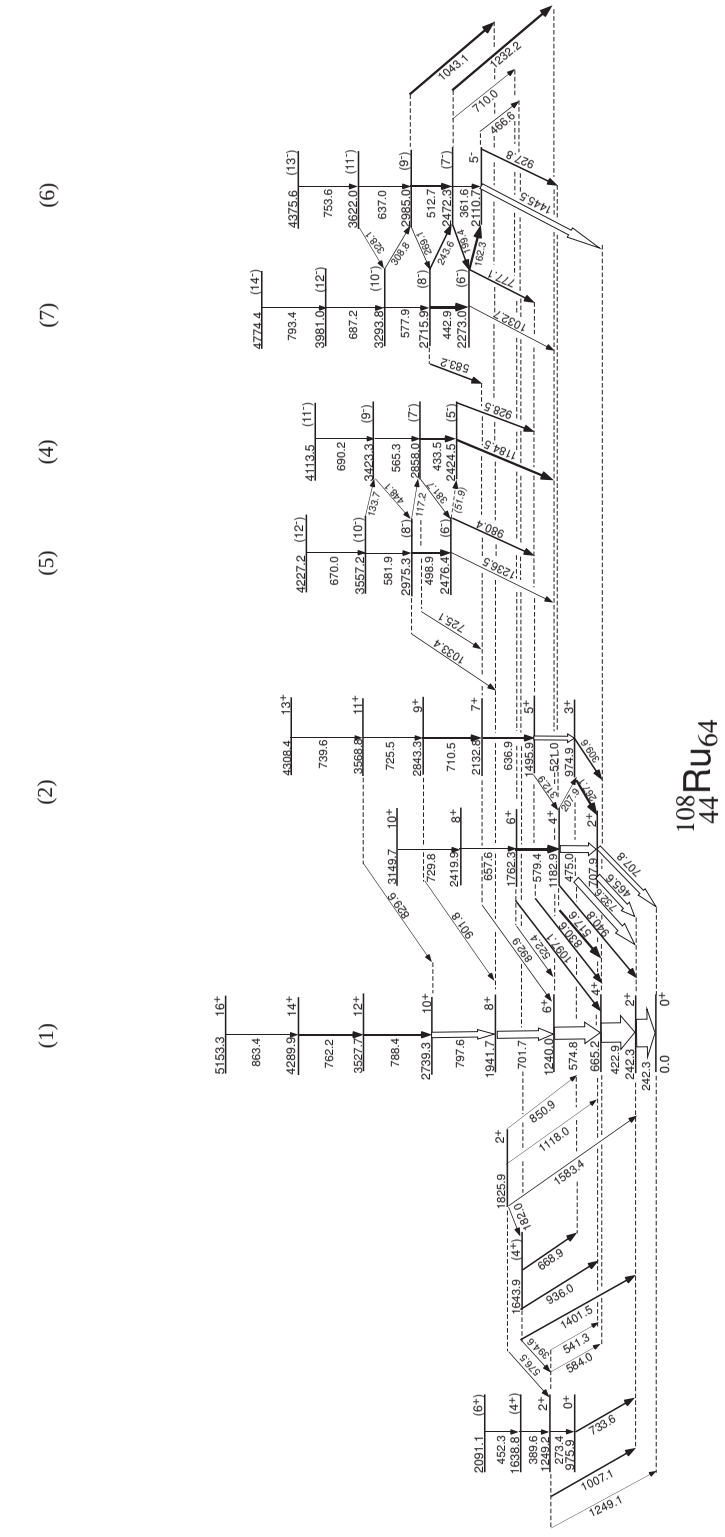

Figure 6.2: The level scheme for ^{108}Ru. The possible chiral bands are labeled 4-7.

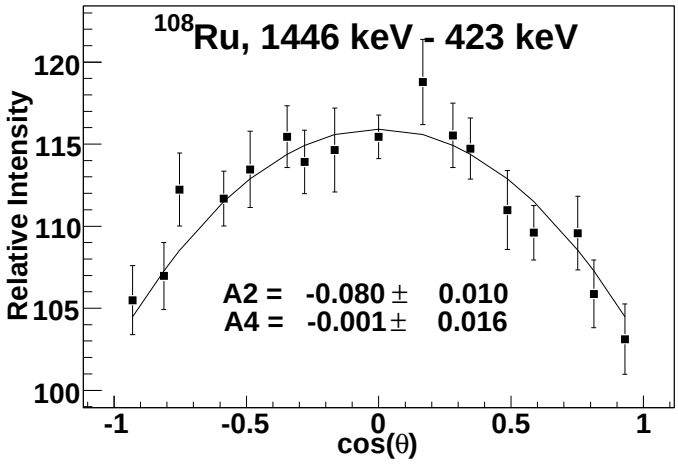

Figure 6.3: The angular correlation between the 1445.5 and 422.9 keV gamma-rays in ^{108}Ru. This angular correlation indicates that the 1445.5 keV transition is pure or nearly pure dipole.

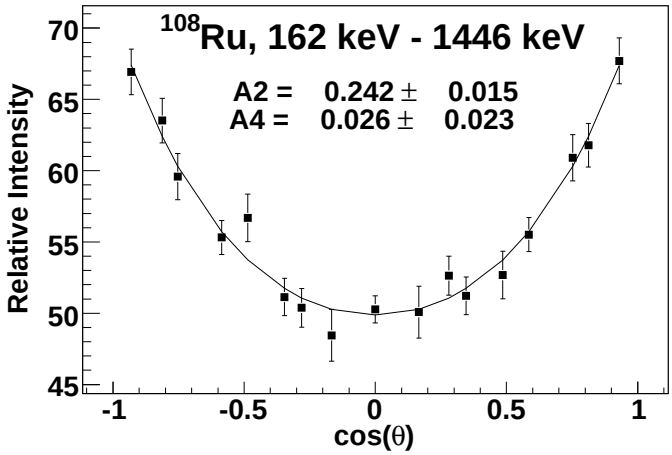

Figure 6.4: The angular correlation between the 162.3 and 1445.5 keV gamma-rays in ^{108}Ru. This angular correlation gives a distinctive signature of the spin sequence.

that give the nucleus its triaxiality. Therefore, this fairly precise measurement of the mixing ratio could provide an important test of these proposed transition strengths.

For the assignment of the 2424.5 keV level, the 1184.5-574.8 keV angular correlation was measured. The result of this correlation is shown in figure 6.5, which demonstrates definitively that the 2424.5 keV level is not 5^-, in which case the expected coefficients would be A_2=-0.071 and A_4=0. The result *is* in agreement with a spin of 4 or 6 for the 2424.5 keV level, with the 1184.5 keV transition being dipole, but the correlation is most consistent with an assignment of 6^-, for the 2424.5 keV level. Moreover, a 4^- assignment is not consistent with the absence of a decay to the 4^+ level in the ground band. An assignment of 6^- for the 2424.5 keV level is also consistent with the systematics of the ^{110,112}Ru isotopes.

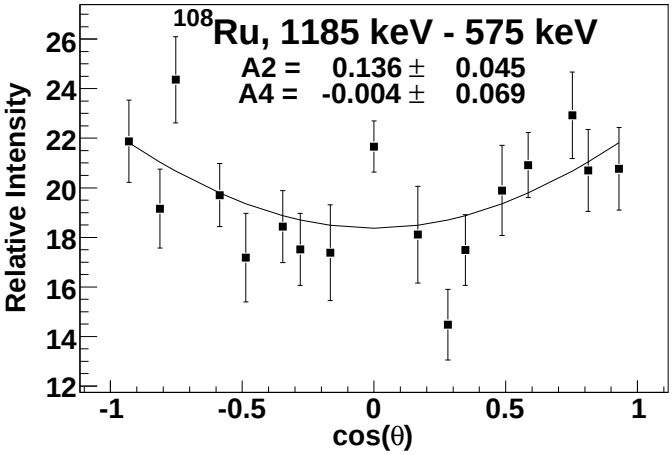

Figure 6.5: The angular correlation of the 1184.5 and 574.8 keV transitions in ^{108}Ru.

6.3 ^{110}Ru

The proposed level scheme for ^{110}Ru is shown in figure 6.6. Several correlations are measured for these bands, with the results given in table VI.1. Spins are assigned in all four bands, strengthening the interpretation of these bands as chiral doublets.

The 2426.5 keV level decays to the 5^+ state in the gamma band, constraining its spin to 4, 5, or 6 for dipole radiation. From the 867.5-515.5 keV angular correlation, the 2242.9 keV level either has a spin of 6 or 4, as shown in figure 6.7, with the 867.5 keV transition being dipole. The result of the 394.5-867.5 keV correlation (A_2=-0.079(14), A_4=0.023(20)) is consistent with an 8→6→5 correlation, for which A_2^{theory}=-0.071, A_4^{theory}=0.0, but not a 6→4→5 correlation, for which A_2^{theory}=-0.036, A_4^{theory}=0.0. Therefore, the 2242.9 keV levels is assigned 6^- and the 2637.4 keV level is assigned 8^-. This implies that 2426.5 keV level is 7^-, and the correlation between the 1187.2 keV and 575.7 keV transitions, shown in figure 6.8, is consistent with this assignment.

For bands 6 and 7, angular correlations of transitions from the 2328.0 and 2516.7 keV levels were measured. The results are given in table VI.1. The 952.5-515.5 keV angular correlation is consistent with a spin assignment of either 4 or 6 for the 2328.0 keV level with the 952.5 keV transition being dipole. Similarly, the 1277.5-575.7 keV angular correlation is consistent with a spin assignment of either 5 or 7 for the 2516.7 keV level, with the 1277.5 keV transition being dipole.. If the lower spins are chosen, this would indicate the 2016.2 keV level is 2^-, but based on its decay to both the 3^+ and 4^+ states of the gamma band, an assignment of 2^- is not plausible. An

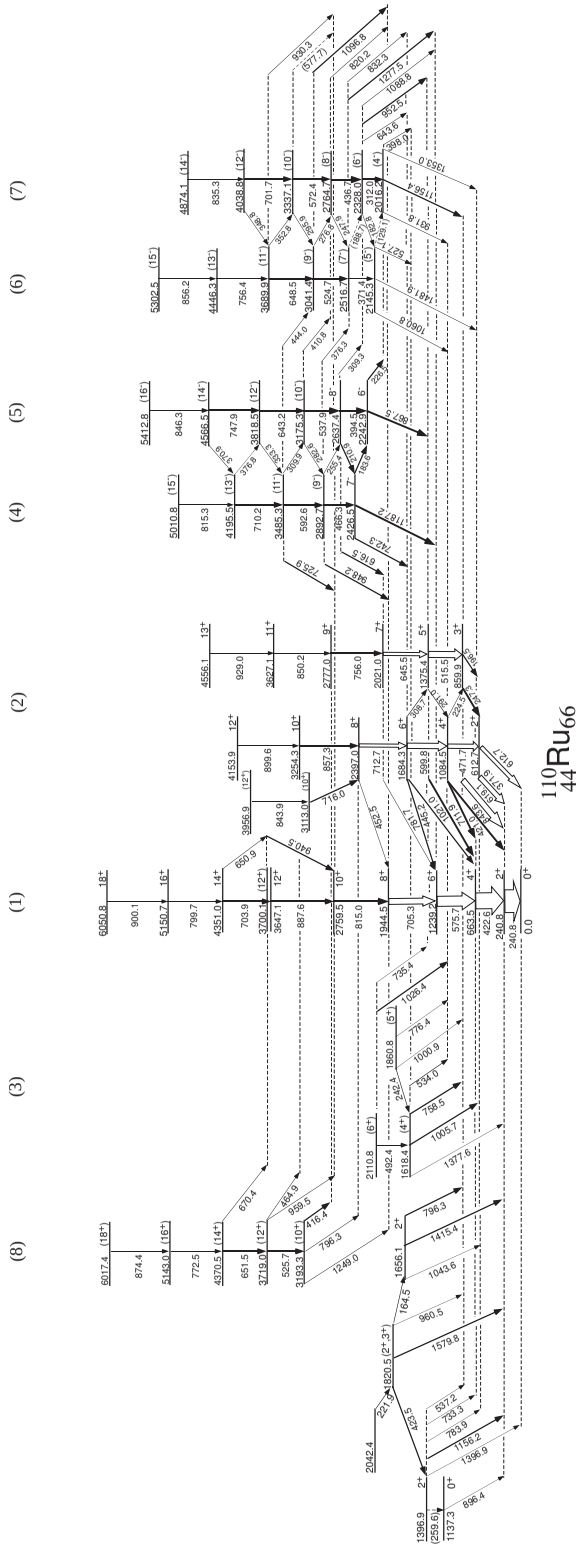

Figure 6.6: The level scheme for ^{110}Ru. The possible chiral bands are labeled 4-7.

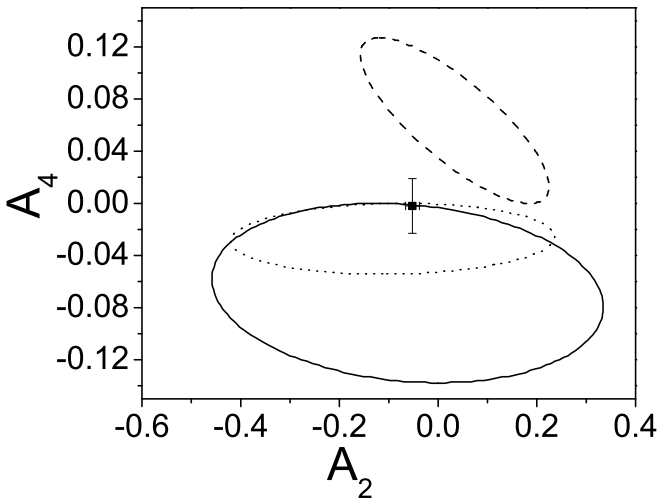

Figure 6.7: The result of the angular correlation of the 867.5 keV and 515.5 keV transitions in ^{110}Ru. The solid black oval is the theoretical range for a 4→5→3 correlations. The dotted line is for a 6→5→3 correlation, and the dashed line is for a 5→5→3 correlation.

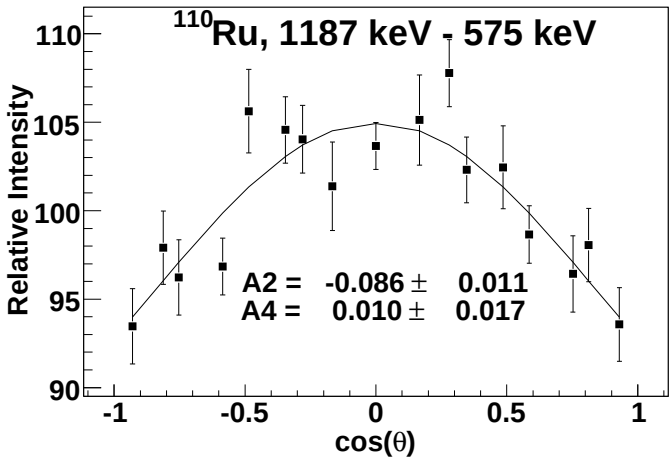

Figure 6.8: The angular correlation of the 1187.2 keV and 575.7 keV transitions in ^{110}Ru.

assignment of 4^- for the 2016.2 keV level, however, is in agreement with these decays. Therefore, the 2328.0 keV level is assigned a spin and parity of 6^-, and the 2516.7 keV level is assigned 7^-.

6.4 ^{112}Ru

The level scheme for ^{112}Ru is shown in figure 6.9. There are three angular correlations measured for ^{112}Ru, listed in table VI.1, and spins are assigned in bands 4, 6, and 7. The 2574.3 keV level in band 4 decays strongly to the 6^+ state in the ground band. Therefore, its spin is constrained to be 5, 6, or 7 for dipole radiation. The experimentally measured values of A_2=-0.067(56), A_4=-0.047(91) are most consistent with a spin of 5 or 7 for the 2574.3 keV level, with the 1384.6 keV transition being dipole. Based on the fact that the 2234.2 keV level in band 5, which is presumably one unit of spin lower than the 2574.3 keV level, decays to both the 6^+ state in the ground band and the 5^+ state in the gamma band, the 2574.3 keV level is assigned a spin and parity of 7^-.

For the 2230 keV level, based on its decay to the 5^+ state in the gamma band and 6^+ state in the ground band, the state should have a spin of 5 or 6 for dipole radiation. The experimentally measured correlation between the 1299.6 and 544.7 keV transitions is only consistent with a pure or nearly dipole transition from a state with a spin of 6; if the state had spin of 5 then A_2 would be negative. Therefore, the 2230.2 keV level is given a spin and parity of 6^-.

The spin and parity assignment for the 2489.2 keV level is most consistent with either 7 or 5, based on the 1299.6-544.7 keV angular correlation, shown in figure 6.10.

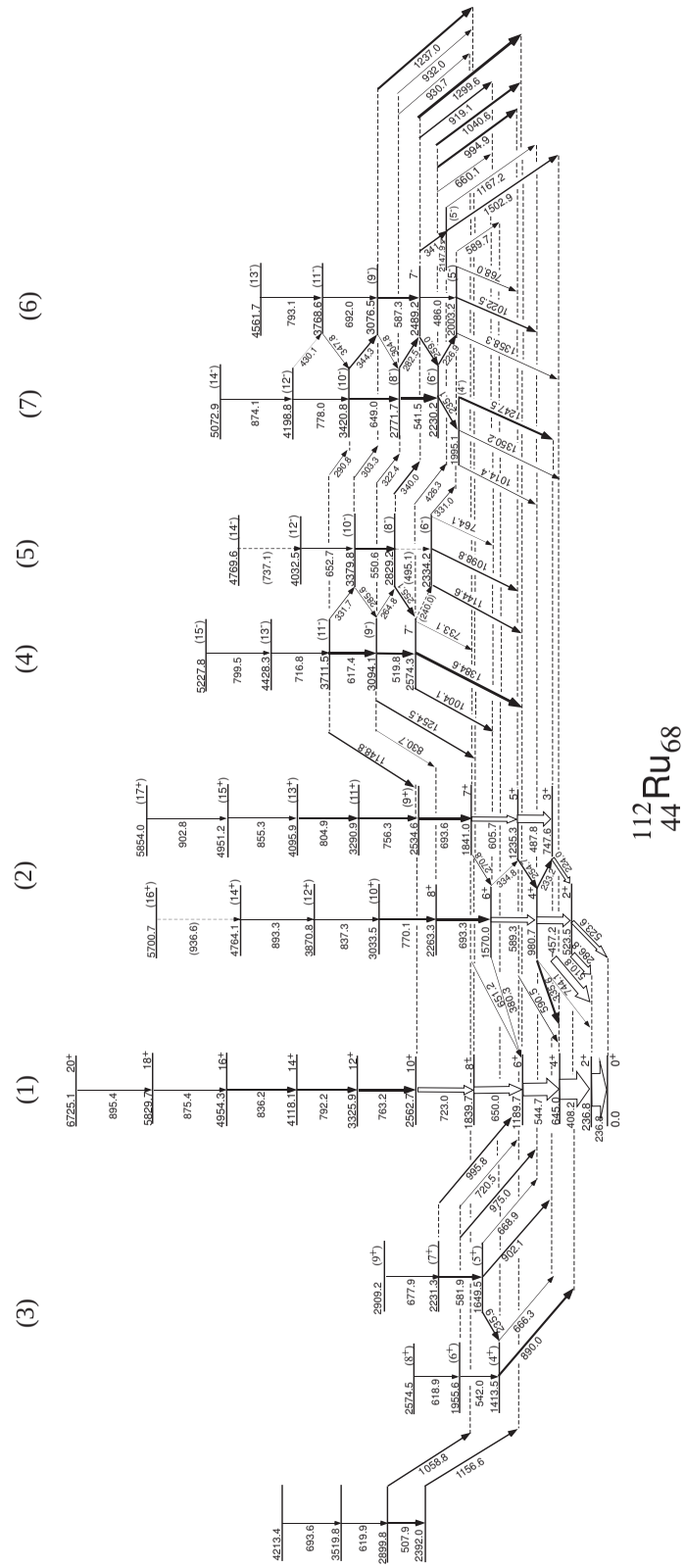

Figure 6.9: The level scheme for ^{112}Ru. The possible chiral bands are labeled 4-7.

With the 2230.2 keV level already assigned as 6^-, the 2489.2 keV level is assigned as 7^-. It should be noted that the rather large uncertainties of the angular correlation makes it impossible to rule out a mixed transition, but the results presented here are most consistent with the spin sequences given in table VI.1.

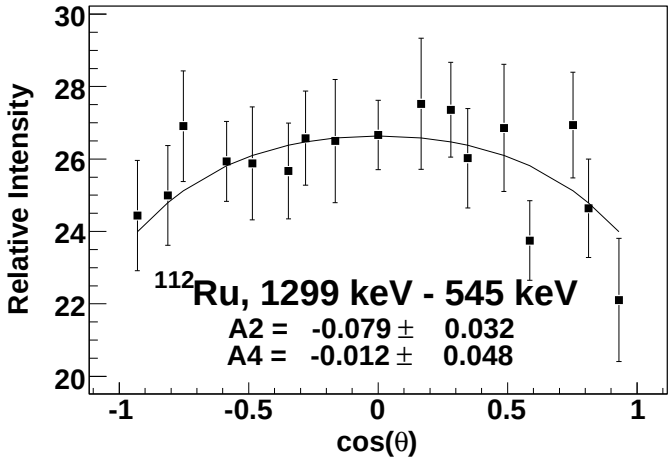

Figure 6.10: The angular correlation of the 1299.6 keV and 544.7 keV gamma rays in ^{112}Ru.

6.5 Discussion

The assignment of spins in the sets of chiral bands allows for the comparison of the ΔE values between bands. As mentioned in the introduction, this value is zero in the ideal case of chiral doublets. Figure 6.11 shows ΔE *vs* spin for the spins found in this work in ^{108,110,112}Ru. Figure 6.11 also shows proposed chiral nuclei ^{136}Nd and ^{104}Rh for comparison. The nuclei in this work, ^{108,110,112}Ru, all have ΔE values near zero as expected. The quite unique sawtooth shape of the ΔE *vs* I curve for ^{108}Ru is

Table VI.1: A_2 and A_4 parameters for measured cascades compared to theory values for pure dipole and pure quadrupole transitions.

Nucleus	Transitions	Cascade	A_2^{exp}, A_4^{exp}
^{108}Ru	1445.5 - 422.5	5(1,2)4(2)2	-0.073(13), -0.012(19)
^{108}Ru	162.3 - 1445.5	6(1,2)5(1)4	0.242(15), 0.026(23)
^{108}Ru	1184.5 - 574.8	4(1,2)6(1)4	0.136(45), -0.004(69)
^{108}Ru	1232.2 - 574.8	7(1,2)6(1)4	-0.064(25), -0.021(38)
^{110}Ru	867.5 - 515.5	6(1,2)5(2)3	-0.052(14), -0.002(21)
^{110}Ru	1187.2 - 575.5	7(1,2)6(2)4	-0.079(14), 0.023(20)
^{110}Ru	1277.8 - 575.5	7(1,2)6(2)4	-0.078(29), 0.009(44)
^{110}Ru	394.5 - 867.5	8(2)6(1,2)5	-0.079(14), 0.023(20)
^{110}Ru	1277.5 - 575.7	7(1,2)6(2)4	-0.073(31), 0.021(47)
^{110}Ru	952.5 - 515.5	6(1,2)5(2)3	-0.152(56), -0.046(83)
^{110}Ru	948.2 - 705.3	9(1,2)8(2)6	-0.066(19), -0.028(28)
^{110}Ru	466.3 - 1187.2	9(2)7(1,2)6	-0.047(27), 0.073(40)
^{112}Ru	1384.6 - 544.7	7(1,2)6(2)4	-0.067(56), -0.047(91)
^{112}Ru	1299.6 - 544.7	7(1,2)6(2)4	-0.079(32), -0.012(48)
^{112}Ru	1040.6 - 544.7	6(1,2)6(2)4	0.186(56), 0.112(86)

in contrast to the similarity of the shapes of the curves for ^{110,112}Ru, which show a fairly smooth down-sloping behavior. This has been interpreted [58] as an evolution in chirality from γ-soft ^{108}Ru to rigid triaxial ^{110,112}Ru. A similar staggering in the odd-parity non-yrast bands in ^{106}Ag is interpreted as a perturbation of the chiral band structure because of the shape change in the two bands caused by the γ-softness of the ^{106}Ag nucleus [55].

Figures 6.12 and 6.13 show the V(I) curves for band 4-5 and band 6-7, respectively. A signature of chirality is for V(I) to be constant with I and the same for the degenerate bands. It is clear from these figures that the curves for the all the bands are reasonably constant around V(I)=15, except for band 4-5 in ^{108}Ru, which shows large staggering in V(I). This is further evidence for the unique nature of ^{108}Ru

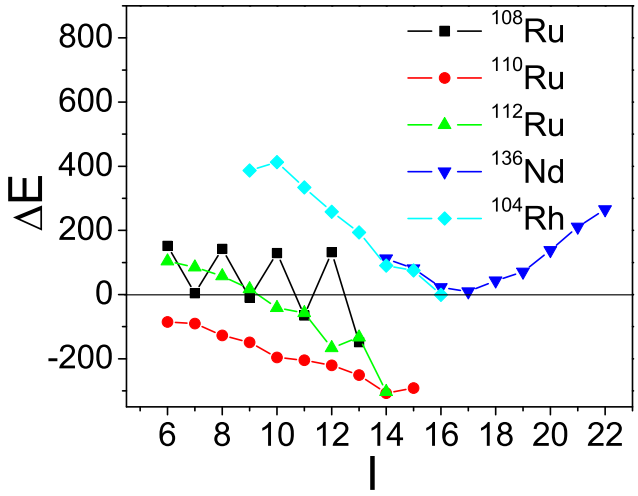

Figure 6.11: ΔE vs J for the proposed chiral bands in ^{108,110,112}Ru, as well as for possible chiral nuclei ^{136}Nd and ^{104}Rh. In the ideal case, ΔE=0 for chiral doublet bands.

compared to ^{110,112}Ru.

Vaman *et al.* [52] list three "fingerprints" of a chiral nucleus. The first is the existence of near degenerate (ΔE=0) doublet bands with ΔI=1. The second fingerprint is that V(I) is independent of spin. It is clear from the evidence presented above that the proposed chiral bands in ^{110,112}Ru meet these criteria. While the bands in ^{108}Ru do not fit the expectation of a rigid chiral rotor, the fact that ^{108}Ru is known to be γ-soft suggests that the bands may be a result of perturbed chiral-vibrations [58] related to the shape differences in the two bands. The last fingerprint concerns the M1 and E2 branching ratios, which are not discussed in this work but are discussed in the work by Luo *et al.* [58]. From these considerations, it can be concluded that the bands in ^{110,112}Ru are chiral rotational bands. Theoretical calculations [58] support the chiral interpretation.

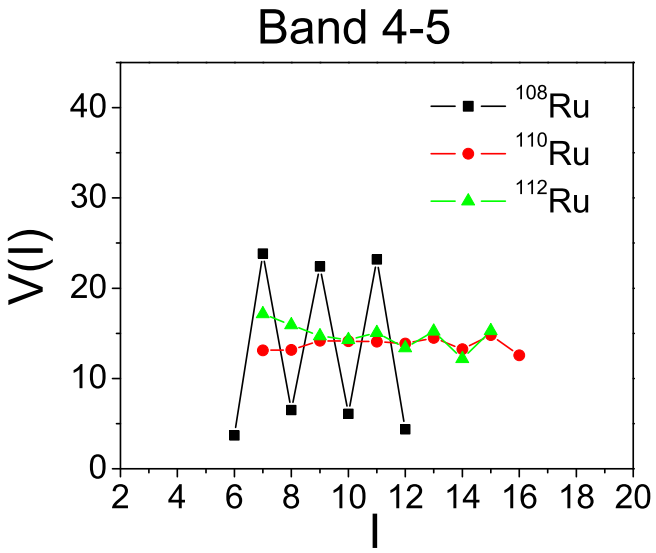

Figure 6.12: V(I) for band 4-5 in ^{108,110,112}Ru.

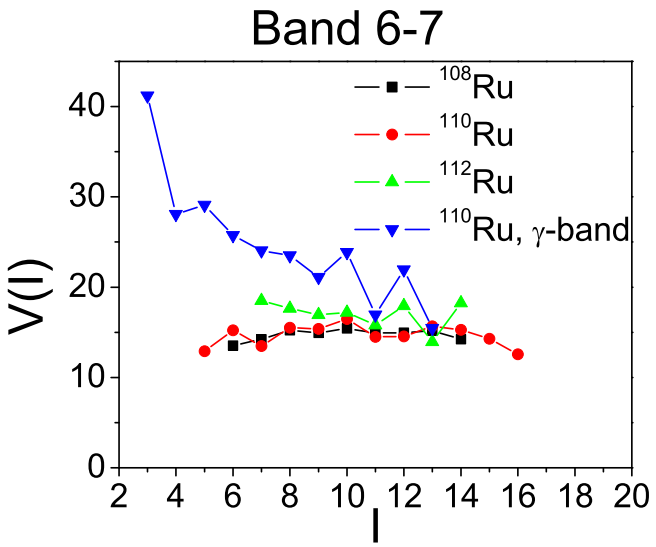

Figure 6.13: V(I) for band 6-7 in ^{108,110,112}Ru. Also shown for comparison is the γ band in ^{110}Ru.

CHAPTER VII

THE g-FACTOR OF THE 4^+ STATE IN ^{134}Te.

7.1 Introduction

The magnetic moments of nuclei with a few nucleons outside doubly-closed shells can give direct insight into the single particle structure of the orbitals outside the shells. The g-factor is also sensitive to the two body interactions of the valence particles and their interactions with the core. Therefore, the measurement of g-factors of excited states in nuclei just outside doubly magic ^{132}Sn provides an important key in understanding the shell structure of nuclei in this region.

The previously unknown g-factor of the 4^+ state in ^{134}Te is measured in this work and compared with the results of a shell-model calculation with a two-body effective interaction derived from the CD-Bonn nucleon-nucleon potential [7]. No additional gates were used for the angular correlations discussed in this chapter because the fission spectrum is relatively clean for high energy transitions, as shown in the two-dimensional spectrum in figure 7.1.

7.2 Result

The g-factor of the 4^+ state in ^{134}Te is measured here for the first time. The level scheme is given in 7.2. The $6^+ \rightarrow 4^+$, $2^+ \rightarrow 0^+$ angular correlation is shown in figure 7.3 and the un-attenuated $4^+ \rightarrow 2^+ \rightarrow 0^+$ cascade is shown in figure 7.4. From the attenuated cascade, $G_2 = \frac{A_2^{exp}}{A_2^{theory}} = \frac{0.029(5)}{0.102} = 0.28(5)$. The hyperfine field was taken

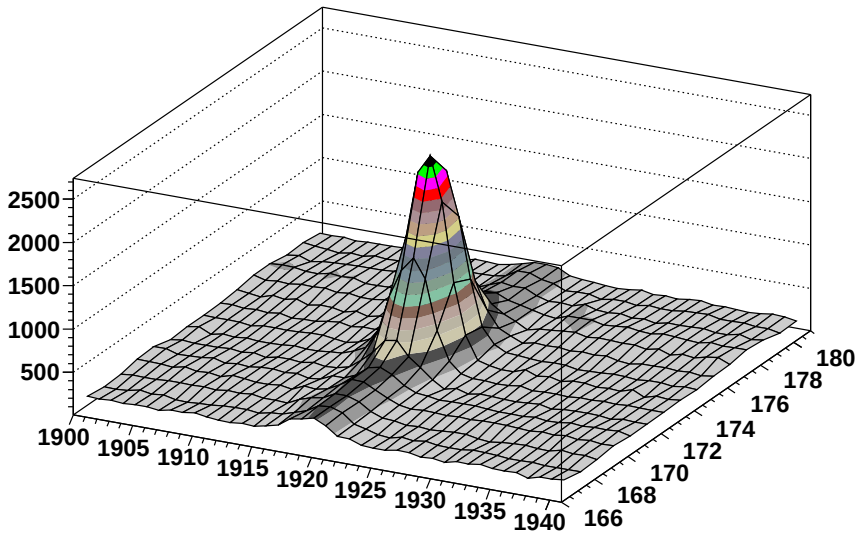

Figure 7.1: Coincidence peak between the 115 keV and 1279 keV transitions in ^{134}Te. The x and y axes are channel numbers ($\frac{2}{3}$keV/channel). The vertical axis is the number of counts. This is the peak for θ=90^o.

from [18] for a room temperature foil to be B_{HF}(Te)=65.9(6). The lifetime of the state is τ_{4^+}=1.96(16) ns [59]. These parameters yield a g-factor of $0.44^{+0.34}_{-0.12}$ for the 4^+ state. These error bars also take into account the uncertainties in the hyperfine field and lifetime.

The large asymmetric errors arise from the fact that the error in equation 3.6 increases dramatically as G_2 approaches the lower limit of G_2=0.2. This is demonstrated in figure 7.5, which shows a plot of equation 3.6 with k=2. The experimental value of G_2=0.28(5) for ^{134}Te is shown in the left figure as dashed horizontal lines. A hypothetical measurement with the same error bars, but for G_2=0.70(5), is shown on the right. The dotted vertical lines then show the resulting range of ϕ values that come from solving equation 3.6. This range is directly proportional to the re-

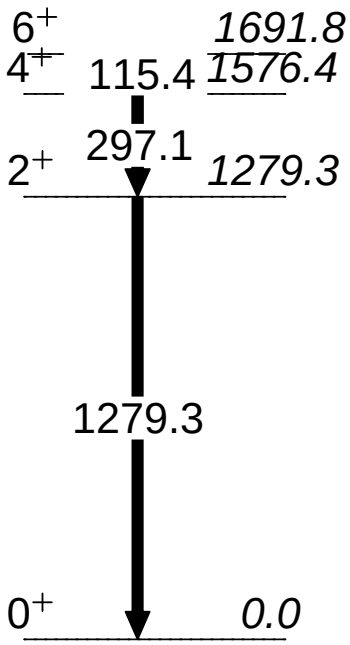

Figure 7.2: The level scheme of ^{134}Te considered in this work.

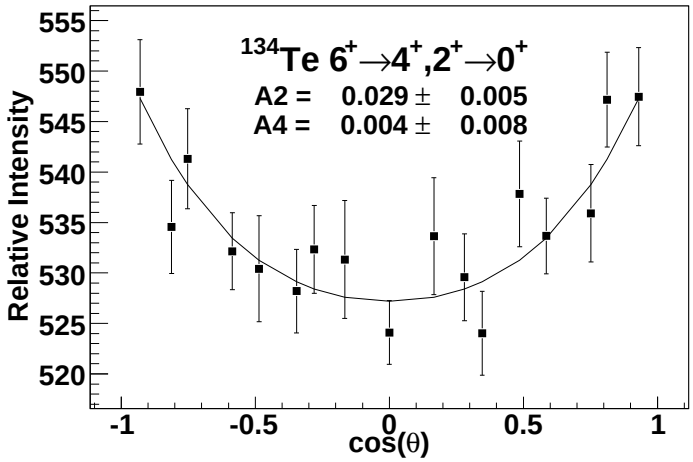

Figure 7.3: The angular correlation of the $6^+ \rightarrow 4^+$, $2^+ \rightarrow 0^+$ cascade in ^{134}Te. This angular correlation gives an attenuation coefficient of G_2=0.28(5).

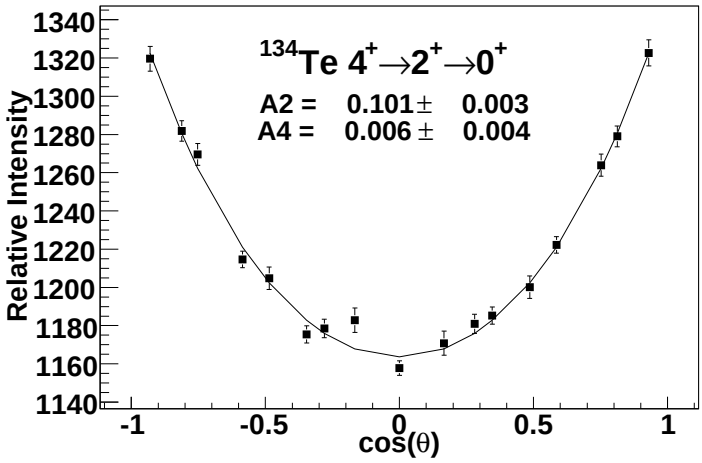

Figure 7.4: The unattenuated correlation for the $4^+ \rightarrow 2^+ \rightarrow 0^+$ cascade in ^{134}Te. The theoretical values for the angular correlation coefficients are A_2=0.102 and A_4=0.009.

sultant error in the g-factor, and it is clear that as the correlation moves closer to the lower limit of G_2=0.2, the resultant error in ϕ increases dramatically. Therefore, although the quality of the experimental measurement is quite good, the fundamental limitations of this technique give a large error in the resultant g-factor.

7.3 Discussion

In this section, the measured g-factor for ^{134}Te is compared to the values obtained from a shell-model calculation performed by A. Gargano in [60]. The calculation has been performed assuming ^{132}Sn as a closed core and letting the two valence protons of ^{134}Te occupy the five levels $0g_{7/2}$, $1d_{5/2}$, $1d_{3/2}$, $2s_{1/2}$, and $0h_{11/2}$ of the 50-82 shell. The corresponding single-particle energies have been taken from the experimental spectrum of ^{133}Sb [59], the only exception being that of the $2s_{1/2}$ level, which is still missing. Its value has been taken from [61], where it was determined through a study

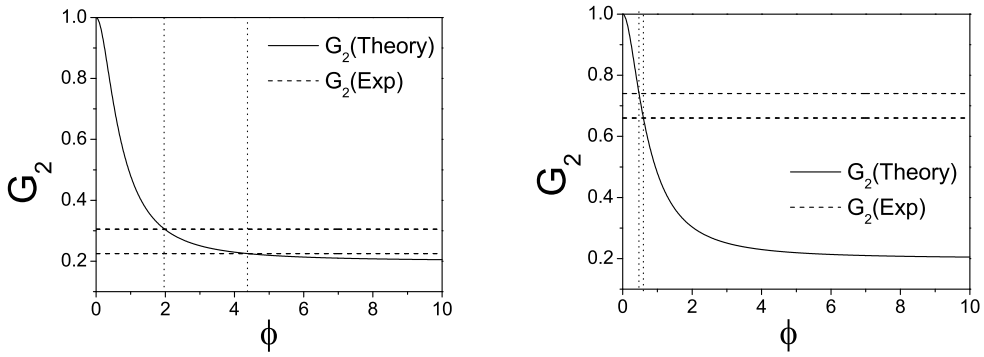

Figure 7.5: These plots demonstrate how the error in $G_2(\phi)$ increases dramatically with ϕ and are discussed in the text. This is a fundamental limitation of the method for attenuations approaching G_2=0.2.

of the $N = 82$ isotones.

As regards the two-body matrix elements of the effective interaction, they have been derived from the CD-Bonn nucleon-nucleon potential [7], and the Coulomb force has been explicitly taken into account. This derivation is performed within the folded-diagram theory. A brief description, including a list of relevant references, can be found in [62], where the single-particle energies are also reported.

The calculations have been carried out with the OXBASH shell-model code [63]. Starting from the obtained wave functions, the g-factors are calculated by using an effective $M1$ operator which takes into account core-polarization effects.

The calculation in this work is similar to a recent calculation by Brown *et al.* [8], who calculated the g-factors of 2^+, and in some cases 4^+ and 6^+, states of N=82 isotones. Their calculation uses an older version of the CD-Bonn potential [64] with a similar model space. For the calculation of g-factors, Brown *et al.* used different effective operators than the present calculation. Namely, the calculation in this work

includes only first-order diagrams in V_{low-k}, while Brown *et al.* also include higher order core polarization and mesonic exchange current corrections.

In table VII.1 the experimental and calculated g-factors for the 4^+ and 6^+ states of ^{134}Te are reported. The magnetic moment of the 6^+ state in ^{134}Te has been previously measured by Wolf *et al.* [65] and is included in the table for comparison.

Table VII.1: The g-factor measured in this work, as well as previous measurements and calculations.

Nucleus	J^π	τ (ns)	B_{HF}	g	g_{calc} (This work)	g_{calc} (Brown *et al.*)
^{134}Te	4^+	1.96(16)	65.9(6)	$0.44^{+0.34}_{-0.12}$	0.72	0.83
^{134}Te	6^+			0.846(25) [65]	0.72	0.83

Regarding the 4^+ and 6^+ states in ^{134}Te, it is predicted that they have the same g-factor. This is clearly related to the fact that these states, as well as the first excited 2^+ state, are dominated by the same $(\pi g_{7/2})^2$ configuration, with a percentage ranging from 96% to 98%. This result, which was also found in previous calculations [61, 66, 67, 68, 69, 8], is supported by the good agreement found between theory and experiment.

7.4 Conclusions

The knowledge of magnetic moments in nuclei with a few particles outside ^{132}Sn has been extended in this work with the first measurement of g(4^+) in ^{134}Te. A value

consistent with both previous experiment for the 6^+ state and calculations is found within the rather large error bars. The limitations of the IPAC method that introduce this error are discussed in detail. Shell model calculations performed for this work are discussed and compared with previous calculations.

CHAPTER VIII

THE g(2^+)-FACTORS IN ^{140,142}Xe

8.1 Introduction

Systematic trends in g-factors of 2^+ states or higher yrast states can indicate the presence of subshell closures or other structure changes. In this work, the systematics of g-factors in neutron rich, even-even Xe isotopes have been extended. The g-factors of 2_1^+ states in ^{146}Ba and ^{146,148}Ce have been measured and are compared to previous work.

The Xe nuclei with Z=54 and N=86 (88) with two proton pairs above the Z=50 shell closure and two (three) neutron pairs above the N=82 shell closure are transitional between spherical and deformed shapes. Assuming vibrational collectivity is dominant for low energy excitations in ^{140,142}Xe, g-factors in these nuclei are compared with predictions of the IBM-2. Since ^{146}Ba and ^{146,148}Ce show moderate axial quadrupole deformation with $\beta_2 \sim 0.2$ [44], both the IBM-2 and rotation-vibration model with independent proton and neutron deformations [6] are considered in discussion of the results for these nuclei.

The measurements in this work on nuclei (^{140,142}Xe) with only a few proton and neutron bosons above ^{132}Sn provide a test of the accepted parameterization of the boson g-factors in the IBM-2. The result of a fit to both the g-factor measurements from this work and other recent and past measurements is discussed.

8.2 Results

The results of the angular correlations in this work are summarized in table VIII.1, which also gives the hyperfine fields and state lifetimes used to calculate the g-factors. All the lifetimes are taken from the National Nuclear Data Center [35] compilations. The level schemes considered for ^{140,142}Xe are given in figures 8.1 and 8.2, respectively.

The $4^+ \rightarrow 2^+ \rightarrow 0^+$ angular correlation for ^{142}Xe is shown in figure 8.3. As a check on the value of the hyperfine field, the correlation through the 4^+ state in ^{136}Xe was measured and the hyperfine field was calculated by using the g-factor $g(4_1^+)=0.80(15)$ [70]. The result, $B_{HF}(\mathrm{Xe})=87(30)$ T, is consistent with the value $B_{HF}(\mathrm{Xe})=73(8)$ T given in Ref. [18]. Adopting the latter value, the ^{140,142}Xe 2_1^+ g-factors are found to be 0.35(12) and 0.25(10), respectively.

The measurements of g-factors in ^{140,142}Xe extend the knowledge of systematics for Xe isotopes above ^{132}Sn. While the Ba and Ce isotopes considered here are at least moderately deformed, the Xe isotopes are relatively closer to the double shell closure at ^{132}Sn, and g-factor calculations based on microscopic single-particle theory should also be considered. Brown *et al.* [8] calculated magnetic moments of 2_1^+ states in lighter $^{134-138}$Xe using the shell model with a residual interaction based on the CD-Bonn renormalized G-matrix. These calculations are shown for completeness in this work.

Speidel *et al.* [71] have measured g-factors of 2^+ states in ^{134,136}Xe, and Jakob *et al.* [72] in ^{130,132,134,136}Xe. The results are shown in figure 8.4, along with the present

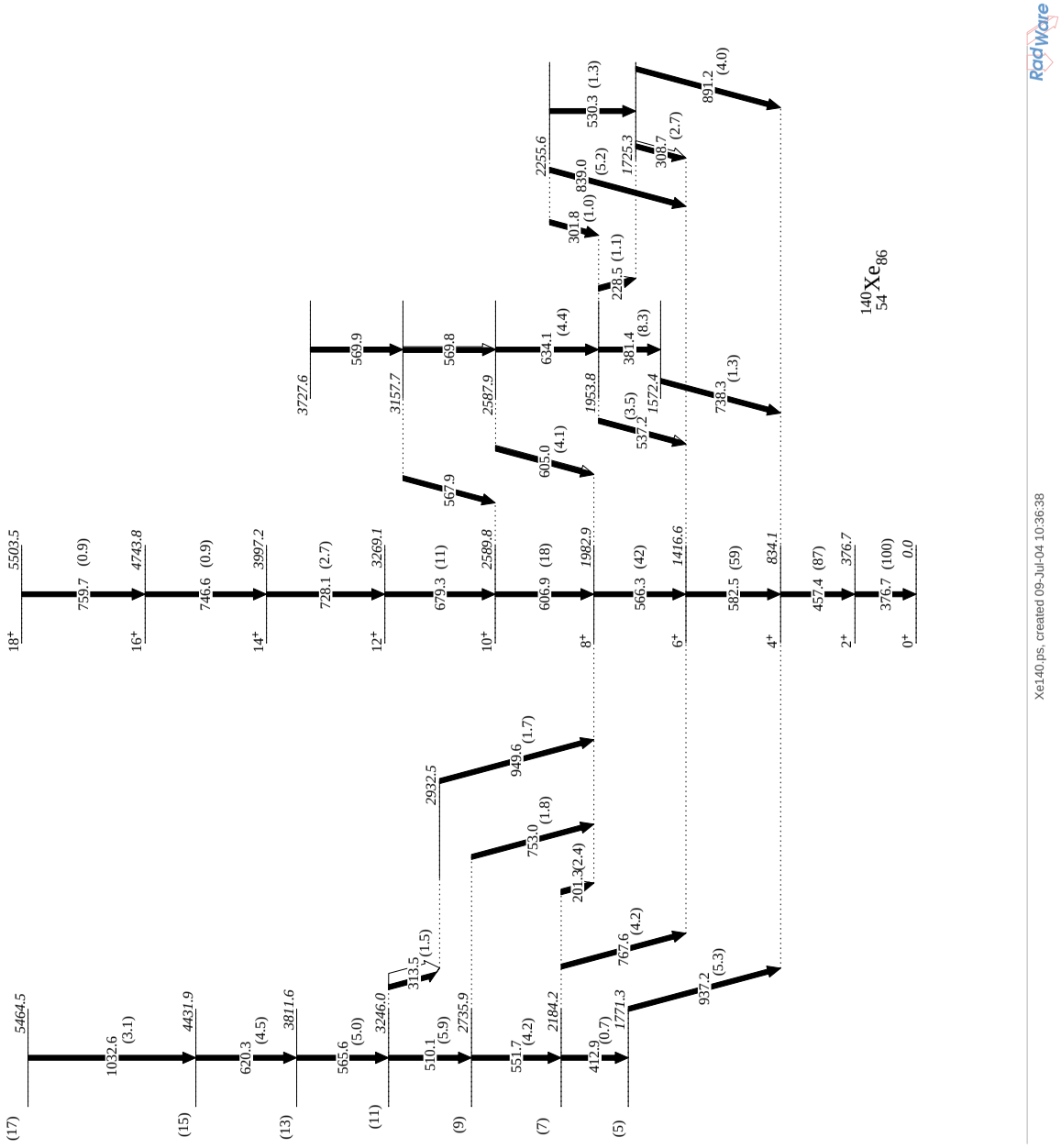

Figure 8.1: The level scheme of ^{140}Xe considered in this work.

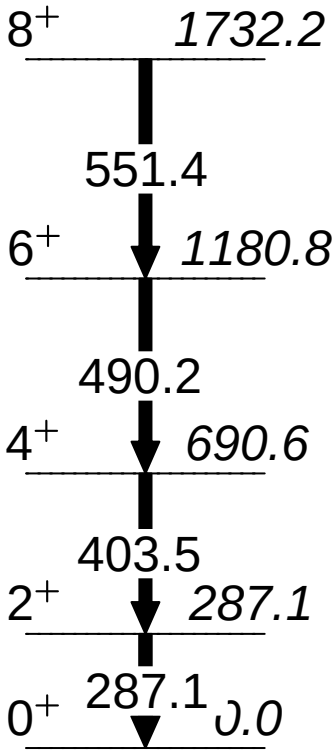

Figure 8.2: The level scheme of ^{142}Xe considered in this work.

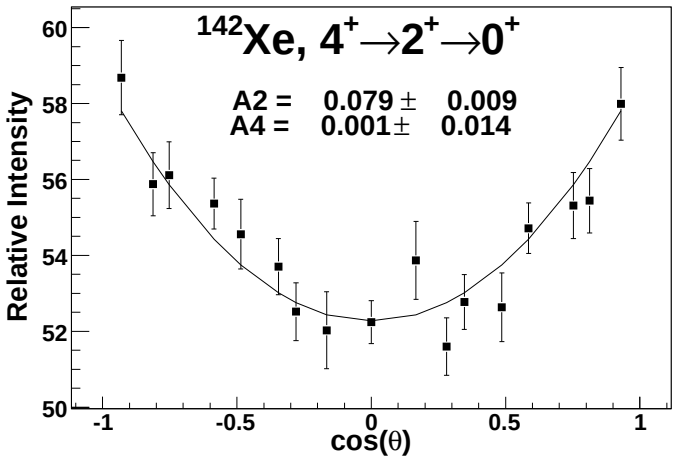

Figure 8.3: The attenuated angular correlation for the $4^+ \rightarrow 2^+ \rightarrow 0^+$ cascade in ^{142}Xe.

measurements for ^{140,142}Xe. The figure reveals almost perfect symmetry about N=82 as a function of neutron number, suggesting very similar make-up of the first 2^+ states below and above the shell closure and symmetry between neutron-hole and neutron-particle excitations. Both shell model [8] and the IBM-2 predictions, also shown in the figure, support this conclusion. The agreement with the IBM-2 model suggests the presence of vibrational collectivity (there is no appreciable axial deformation) in ^{130,132,140,142}Xe ground states. There is also a possibility that the 2^+ states in ^{130,132,140,142}Xe have still significant single-particle component as the g-factors seem to follow smoothly the trend predicted by the shell model when going away from the shell closure.

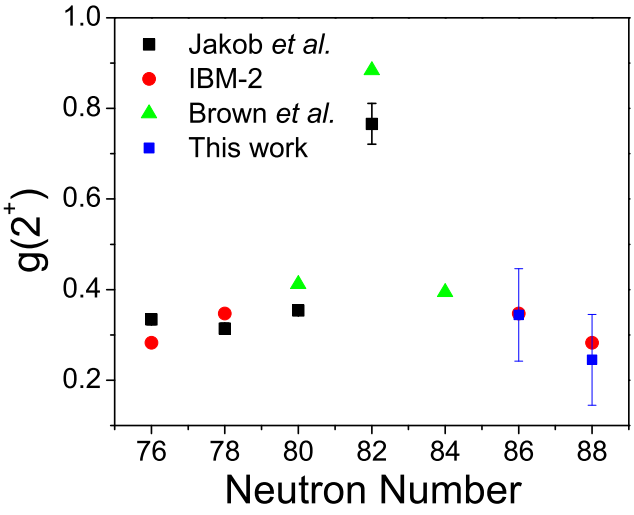

Figure 8.4: The g-factors of the 2^+ states in xenon isotopes near the N=82 shell closure. The green points are from a shell model calculation by Brown *et al.* [8], the black points are from a previous experiment [72], and the red points are an IBM-2 calculation. The blue points are from this work. These data are discussed in the text.

The $4^+ \rightarrow 2^+ \rightarrow 0^+$ angular correlation for ^{146}Ba is shown in figure 8.5. The g-factor of the 2^+ state in ^{146}Ba is found to be 0.27(10). For this measurement, the hyperfine field was calibrated by using the observed attenuation in ^{144}Ba with its known g-factor $g(2_1^+)$=0.34(5) [73], which gave the value B_{HF}(Ba)=37(6) T. Although this value is much larger than that tabulated in [18], the tabulated value leads to a physically unreasonable result, so the calibrated value is adopted for this work.

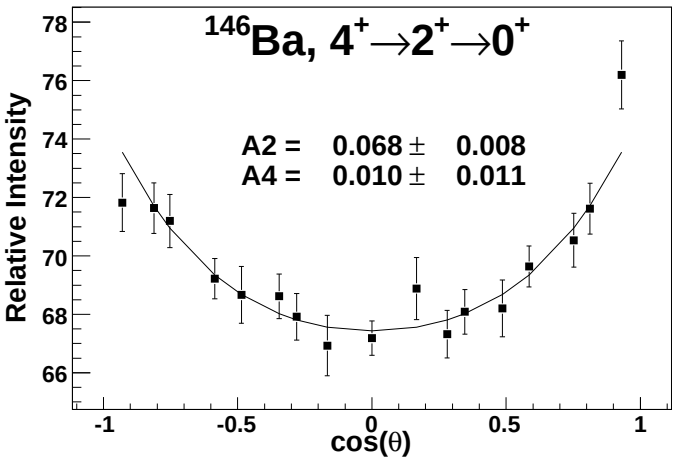

Figure 8.5: The attenuated angular correlation for the $4^+ \rightarrow 2^+ \rightarrow 0^+$ cascade in ^{146}Ba.

The 2^+ state in ^{146}Ba is measured here for comparison and validation of the experimental method. The result, $g(2^+)$=0.27(10) is in good agreement with both [74] and [73], who found $g(2^+)$=0.20(10) and 0.28(7), respectively. Lighter isotopes ^{130,132,134,136}Ba were measured by Brennan *et al.* [75], and ^{134}Ba was earlier measured by Eberhardt *et al.* [76].

The experimental and theoretical g-factors for the first 2^+ state in $^{130-146}$Ba are

shown in Fig. 8.6. Figure 8.6 also shows the predictions of the IBM-2 using the effective boson g-factors determined in this work. The point for N=90, ^{148}Ba is from this work, while the points below N=82 are from Brennan *et al.* [75] The N=82 point is from Bazzacco *et al.* [77], N=86 is from Wolf *et al.* [73], and N=88 is from Smith *et al.* [74]. The remarkable symmetry of the xenon isotopes with respect to N=82 is still present for these barium isotopes, with a possible indication of a lower g-factor at N=90. This lower value could be related to the increased deformation at N=90 as found in Sm nuclei. Again, the good agreement between IBM-2 results and the experimental results is attributed to the presence of vibrational collectivity closer to the shell closure.

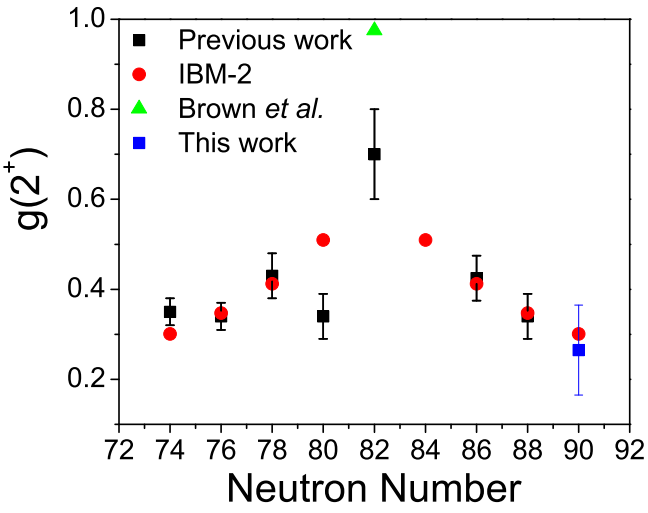

Figure 8.6: The g-factors of the 2^+ states in barium isotopes near the N=82 shell closure. The green points are from a shell model calculation by Brown *et al.* [8], the black points are from previous experiments, and the red points are an IBM-2 calculation. The blue point is the measurement made in this work. These data are discussed in the text.

The $4^+ \rightarrow 2^+ \rightarrow 0^+$ angular correlation for ^{146}Ce is shown in figure 8.7. The g-factors of the 2_1^+ states in ^{146,148}Ce were found to be 0.46(10) and 0.39(8), respectively, taking the hyperfine field to be 41(2) T [18]. The g-factor for ^{146}Ce differs from the Vanderbilt group's previously published value [78] because more restrictive gating conditions were used for the measurement in this work to give cleaner spectra.

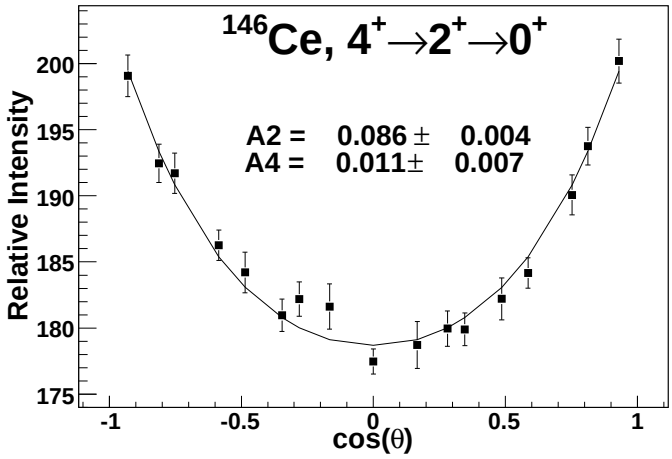

Figure 8.7: The attenuated angular correlation for the $4^+ \rightarrow 2^+ \rightarrow 0^+$ cascade in ^{146}Ce.

The g-factors of the 2^+ states in ^{146,148}Ce measured here are compared with previous results on ^{146,148}Ce [79] and ^{146}Ce [74]. The results of all these measurements are shown in table VIII.2. Agreement of the current result with that of Gill *et al.* [79] for ^{148}Ce is good. However, for ^{146}Ce, while the result of Smith *et al.* [74] is consistent with the more precise value in this work, there is strong disagreement with the result of Gill *et al.* [79], who report a striking difference between the two isotopes. The present results do not confirm this difference. Figure 8.8 shows theses systematics.

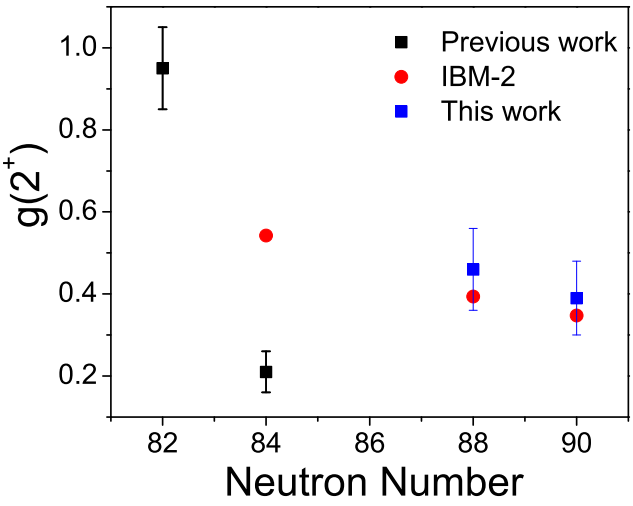

Figure 8.8: The g-factors of the 2^+ states in cerium isotopes near the N=82 shell closure. The green points are from a shell model calculation by Brown *et al.* [8], the black points are from a previous experiment [80], and the red points are an IBM-2 calculation. The blue square points are from this work These data are discussed in the text.

Table VIII.1: Parameters used in the g-factor measurements. The additional gates are either coincident transitions in the isotope of interest or transitions in partner nuclei. For example, for ^{142}Xe, the 242 keV transition is from the fission partner ^{108}Ru. No error is quoted for the A_4 value for ^{136}Xe because the parameter was held fixed at the asymptote. Hyperfine fields are discussed in the text.

Nucleus	τ (ns)	B_{HF} (T)	A_2^{exp}	A_4^{exp}	Additional gates (keV)
^{136}Xe	1.87(25)		0.023(3)	0.001	None
^{140}Xe	0.163(7)	73(8)	0.095(4)	0.010(6)	583,566,607,738,242,423,575,937
^{142}Xe	0.49(14)	73(8)	0.079(9)	0.001(14)	242,270,490,551
^{144}Ba	1.02(3)		0.066(4)	0.008(6)	431,509
^{146}Ba	1.24(4)	37(6)	0.068(8)	0.010(11)	445,524,511,569
^{146}Ce	0.36(4)	41(2)	0.086(4)	0.011(7)	503,565,515,380
^{148}Ce	1.45(9)	41(2)	0.046(6)	0.046(6)	386,451,501,537

Table VIII.2: g-factors of 2^+ states measured in this work and calculated using the parameters in table VIII.1.

Nucleus	g	Previous measurements
^{140}Xe	0.35(12)	
^{142}Xe	0.25(10)	
^{146}Ba	0.27(9)	0.28(7) [73],0.20(10) [74]
^{146}Ce	0.46(10)	0.24(5) [79],0.46(34) [74]
^{148}Ce	0.39(8)	0.37(6) [79]

The results of all measurements are shown in table VIII.2, where they are compared with previous measurements if applicable. The errors quoted include contributions from the attenuation measurements, lifetimes, and hyperfine fields. The results are compared with theory in the following section.

8.3 Discussion

An analysis by Wolf *et al.* [13] of g-factors of neutron rich Ce, Nd, and Sm isotopes in terms of the IBM-2 (see equation 2.10) indicated that effective boson g-factors of g_π=0.63(4) and g_ν=0.05(5) describe the nuclei in this region reasonably well. A later analysis by Gill *et al* [79] for heavy Ba isotopes confirmed this choice of parameters.

In this work, the proton and neutron effective g-factors were extracted from an updated version of the calibration from [13] which includes 2_1^+ g-factors taken from both a recent compilation [81] and the measurements in this paper. In this fit, equation 2.10 is multiplied by N/N_ν, and the values of g_π and g_ν are then given by a linear fit to N_π/N_ν *vs* gN/N_ν. The fit, shown in figure 8.9, yields the effective g-factors g_π=0.67(6), g_ν=0.02(7). The data used in this fit are given in table VIII.3. Although these results are consistent with those of [13], they are somewhat closer to the theoretical estimates.

8.4 Conclusion

In this work the g-factors of the first 2^+ states in ^{140,142}Xe, ^{146}Ba, and ^{146,148}Ce found by using new techniques developed for measuring angular correlations with large detector arrays are reported. The g-factors of 2^+ states in ^{140,142}Xe are measured for the first time, while the g-factors in ^{146}Ba and ^{146,148}Ce are found to have good overall agreement with previously measured values, thus confirming the reliability of the experiment and analysis. The experimental results compare well with the predictions of the IBM-2, indicating the presence of vibrational collectivity in the 2^+

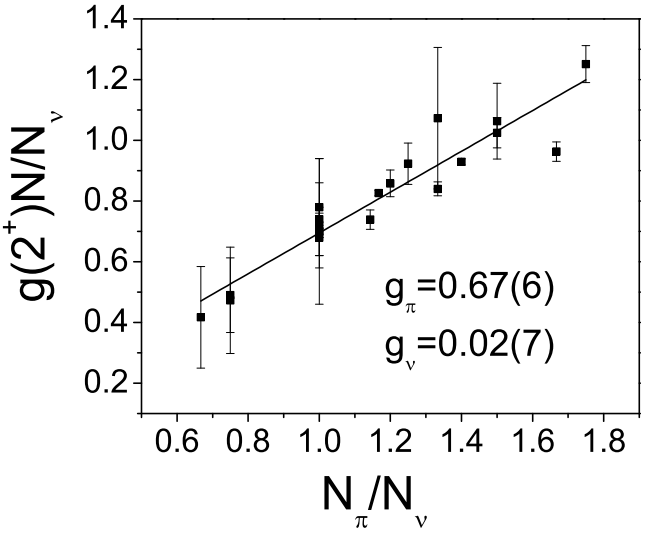

Figure 8.9: Linear fit of the IBM-2 parameters to experimentally measured 2^+ states in nuclei above ^{132}Sn. In this fit, the slope is given by g_π and the intercept by g_ν.

states in ^{140,142}Xe.

Table VIII.3: Experimental g-factors of 2^+ states from this work and previous works.

Nucleus	N_π/N_ν	g_{exp}	Reference
^{140}Xe	1	0.35(12)	This work
^{142}Xe	0.667	0.25(10)	This work
^{142}Ba	1.5	0.425(50)	[81]
^{144}Ba	1	0.34(5)	[81]
^{146}Ba	0.75	0.27(10)	This work
^{146}Ba	0.75	0.28(7)	[81]
^{146}Ce	1.333	0.46(10)	This work
^{148}Ce	1	0.39(8)	This work
^{148}Ce	1	0.37(6)	[79]
^{148}Nd	1.667	0.361(12)	[81] (average)
^{150}Nd	1.25	0.41(3)	[81] (average)
^{152}Sm	1.5	0.41(2)	[81] (average)
^{154}Sm	1.2	0.39(2)	[13]
^{154}Gd	1.75	0.455(22)	[81] (average)
^{156}Gd	1.4	0.387(4)	[81]
^{158}Gd	1.167	0.381(4)	[81]
^{160}Gd	1	0.36(2)	[81]
^{160}Dy	1.333	0.36(1)	[81] (average)
^{162}Dy	1.143	0.345(15)	[81]
^{164}Dy	1	0.35(1)	[81] (average)

CHAPTER IX

CONCLUSIONS

A new method for determining angular correlations of cascades of gamma-rays from high statistics data sets from Gammasphere has been developed. This method has been applied to triple-coincidence data from the fission of ^{252}Cf. A wide range of nuclear properties have been studied in this work, ranging from the proposed doubly-closed subshell nucleus ^{94}Sr to midshell nuclei around A=100 and nuclei above ^{132}Sn. The measured properties include the spins, parities, and magnetic moments of excited states, and the mixing ratios of transitions between states.

The spins and parities of levels in ^{93,94,95}Sr have been determined through angular correlations. The previously proposed 3^- level in ^{94}Sr is determined to be 3^+. The single particle band in ^{95}Sr built on the g7/2[404] neutron single particle state has been confirmed.

The magnetic properties of the neutron rich Zr, Mo, Ru, and Pd isotopes have been studied. The single particle states in the odd-N nuclei have been determined through g-factor and mixing ratio measurements, with the result being that the 3/2[411], 5/2[532], 5/2[402], and 7/2[523] orbitals become more important with increasing proton and neutron number. The mixing ratios of gamma-band to ground-band transitions have been measured for the even-even nuclei with A=102-116, with a shift in phase observed around ^{110,112}Ru. This change in phase is interpreted as corresponding to the shift from prolate to oblate shape.

The spins and of levels in proposed chiral bands in ^{108,110,112}Ru have been determined. The spins determined in this work support the interpretation of these nearly degenerate bands as chiral doublets.

The g-factor of the 4^+ state in ^{134}Te is measured for the first time and found to be consistent with theory, which indicates that the g-factor of this level is dominated by the $\pi g7/2^2$ configuration and is similar to that of the 6^+ state.

The g-factors of the first excited states in ^{140,142}Xe are measured for the first time and compared to systematics. These measurements are found to agree with the prediction of the IBM-2 with the standard parameterization of nuclei in this region. With the addition of these data, the systematics for $g(2^+)$ are extended down to $N_\pi/N_\nu<1$, and it is shown that the accepted parameterization of g_π and g_ν is still applicable in this region.

In conclusion, the development of a method for angular correlations with high-statistics triple coincidence Gammasphere data has allowed the study of a wide range of nuclei. Angular correlations have been determined for relatively weak transitions to open the study of more exotic states in these nuclei.

REFERENCES

[1] O. Haxel, J. Jensen, and H. Suess, Physical Review **75**, 1766 (1949).

[2] A. Bohr and B. Mottelson, Physical Review **90**, 717 (1953).

[3] J. Hamilton, P. Hansen, and E. Zganjar, Reports on Progress in Physics **48**, 631 (1985).

[4] J. H. Hamilton, Progress in Particle and Nuclear Physics **35**, (1995).

[5] J. M. Eisenberg and W. Greiner, *Nuclear Models*, 2 ed. (North Holland, New York, NY 10017, 1975), Vol. 1.

[6] W. Greiner, Nuclear Physics **80**, 417 (1966).

[7] R. Machleidt, Physical Review C **63**, 24001 (2001).

[8] B. Brown *et al.*, Physical Review C **71**, 44317 (2005).

[9] R. Orlandi *et al.*, Physical Review C **73**, (2006).

[10] E. Browne and F. Femenia, Nucl. Data, Sect. A **10**, (1971).

[11] S. Nilsson, Kgl. Danske Videnskab. Selskab., Mat.-fys Medd **29**, (1955).

[12] A. Arima and F. Iachello, Ann Phys **99**, 253 (1973).

[13] A. Wolf, D. Warner, and N. Benczer-Koller, Physics Letters B **158**, 7 (1985).

[14] K. Krane and R. Steffen, Physical Review C **2**, 724 (1970).

[15] M. Rotenberg, R. Bivins, N. Metropolis, and J. Wooten, *The 3-j and 6-j symbols* (The Technology Press, Cambridge, Mass, 1959).

[16] P. Ekstrom, DELTA, http://www.nndc.bnl.gov/nndcscr/ensdf_pgm/analysis/delta/.

[17] C. Goodin *et al.*, Physical Review C **74**, 17309 (2006).

[18] G. N. Rao, Hyperfine Interactions **26**, 1119 (1985).

[19] E. Matthias, S. S. Rosenblum, and D. A. Shirley, Physical Review Lettters **14**,

46 (1965).

[20] A. G. Smith *et al.*, Physics Letters B **591**, 55 (2004).

[21] D. Patel *et al.*, Journal of Physics G Nuclear Physics **28**, 649 (2002).

[22] K. Siegbahn, *Alpha-,Beta-, and Gamma-Ray Spectroscopy (Part2)* (North-Holland, Amsterdam, 1968).

[23] G. M. Ter-Akopian *et al.*, Physical Review C **55**, 1146 (1997).

[24] C. L. Lawson and R. J. Hanson, *Solving Least Square Problems* (Prentice-Hall, Englewood Cliffs, NJ, 1974).

[25] J. Wood *et al.*, Physics Reports **215**, 101 (1992).

[26] J. Skalski, S. Mizutori, and W. Nazarewicz, Nuclear Physics A **617**, 282 (1997).

[27] J. Hwang *et al.*, Physical Review C **67**, 14317 (2003).

[28] J. Hwang *et al.*, Physical Review C **69**, 67302 (2004).

[29] G. Jung *et al.*, Phys. Rev. C **22**, 252 (1980).

[30] A. Wolf *et al.*, Phys. Rev. C **40**, 932 (1989).

[31] F. Buchinger *et al.*, Zeitschrift für Physik A Hadrons and Nuclei **327**, 361 (1987).

[32] P. Raghavan, Atomic Data and Nuclear Data Tables **42**, (1989).

[33] J. Hamilton *et al.*, Progress in Particle and Nuclear Physics **35**, 635 (1995).

[34] F. Buchinger *et al.*, Physical Review C **41**, 2883 (1990).

[35] Brookhaven National Laboratory, National Nuclear Data Center, http://www.nndc.bnl.gov/.

[36] K. Kratz *et al.*, Zeitschrift für Physik A Hadrons and Nuclei **312**, 43 (1983).

[37] R. B. Firestone and V. A. Shirley, *Table of Isotopes*, 8 ed. (John Wiley and Sons, New York, 1996), pp. H–3.

[38] H. Mach *et al.*, Physics Letters B **230**, 21 (1989).

[39] C. Wu, H. Hua, and D. Cline, Physical Review C **68**, 34322 (2003).

[40] A. G. Smith *et al.*, Physics Letters B **591**, 55 (2004).

[41] A. Wolf *et al.*, Physics Letters B **97**, 195 (1980).

[42] A. Smith *et al.*, Physical Review Letters **77**, 1711 (1996).

[43] S. J. Zhu *et al.*, European Physical Journal A **25, Supplement 1**, 459 (2005).

[44] P. Möller, J. R. Nix, W. D. Myers, and W. J. Swiatecki, Atomic Data and Nuclear Data Tables **59**, 74 (1995).

[45] H. Hua *et al.*, Physical Review C **69**, 14317 (2004).

[46] W. Urban *et al.*, Physical Review C **72**, 27302 (2005).

[47] J. Hwang *et al.*, Physical Review C **56**, 1344 (1997).

[48] D. Patel *et al.*, Journal of Physics **28**, 649 (2002).

[49] K. Krane, Physical Review C **8**, 1494 (1973).

[50] S. Frauendorf and J. Meng, Nuclear Physics A **617**, 131 (1997).

[51] E. Mergel *et al.*, The European Physical Journal A-Hadrons and Nuclei **15**, 417 (2002).

[52] C. Vaman *et al.*, Physical Review Letters **92**, 032501 (2004).

[53] J. Timár *et al.*, Physics Letters B **598**, 178 (2004).

[54] P. Joshi *et al.*, Physics Letters B **595**, 135 (2004).

[55] P. Joshi *et al.*, Physical Review Letters **98**, 102501 (2007).

[56] S. J. Zhu *et al.*, American Physical Society, Division of Nuclear Physics Fall Meeting, October 30-November 1, 2003, Tucson, Arizona, MEETING ID: DNP03, abstract# GB. 010 (2003).

[57] P. Möller *et al.*, Physical Review Letters **97**, 162502 (2006).

[58] Y. X. Luo *et al.*, European Physical Journal A (Submitted August 2007).

[59] Brookhaven National Laboratory, NNDC, Evaluated Nuclear Structure Data File, http://www.nndc.bnl.gov/ensdf/.

[60] C. Goodin *et al.*, Physical Review C (Submitted June 2008).

[61] F. Andreozzi *et al.*, Physical Review C **56**, 16 (1997).

[62] L. Coraggio, A. Covello, A. Gargano, and N. Itaco, Physical Review C **72**, 57302 (2005).

[63] B. A. Brown, A. Etchegoyen, and W. D. M. Rae, MSU-NSCL, Report No. 534 .

[64] R. Machleidt, F. Sammarruca, and Y. Song, Phys. Rev. C **53**, R1483 (1996).

[65] A. Wolf and E. Cheifetz, Physical Review Letters **36**, 1072 (1976).

[66] C. T. Zhang *et al.*, Physical Review Letters **77**, 3743 (1996).

[67] P. Daly *et al.*, Zeitschrift für Physik A Hadrons and Nuclei **358**, 203 (1997).

[68] S. K. Saha *et al.*, Physical Review C **65**, 17302 (2001).

[69] S. Sarkar and M. Saha Sarkar, Physical Review C **64**, 14312 (2001).

[70] Z. Berant *et al.*, Physical Review C **31**, 570 (1985).

[71] K. H. Speidel *et al.*, Nuclear Physics A **552**, 140 (1993).

[72] G. Jakob *et al.*, Phys. Rev. C **65**, 024316 (2002).

[73] A. Wolf *et al.*, Physical Review C **37**, 1253 (1988).

[74] A. G. Smith *et al.*, AIP Conference Proceedings, Nuclear Structure 98 **453**, 283 (1999).

[75] J. M. Brennan, M. Hass, N. K. B. Shu, and N. Benczer-Koller, Phys. Rev. C **21**, 574 (1980).

[76] J. Eberhardt and K. Dybdal, Hyperfine Interactions **7**, 387 (1979).

[77] D. Bazzacco *et al.*, Zeitschrift für Physik A Hadrons and Nuclei **328**, 275 (1987).

[78] A. V. Daniel *et al.*, Nuclear Instruments and Methods in Physics Research Sec-

tion B **262**, 399 (2007).

[79] R. L. Gill *et al.*, Physical Review C **33**, 1030 (1986).

[80] D. Bazzacco *et al.*, Nuclear Physics A **533**, 541 (1991).

[81] N. J. Stone, Atomic Data and Nuclear Data Tables **90**, 75 (2005).